INVESTIGATION OF THE NEUROKININ-1 RECEPTOR BY FLUORESCENCE TECHNIQUES

THÈSE N^{O} 3272 (2005)

PRÉSENTÉE À LA FACULTÉ SCIENCES DE BASE

Institut de sciences biomoléculaires

SECTION DE CHIMIE ET GÉNIE CHIMIQUE

ÉCOLE POLYTECHNIQUE FÉDÉRALE DE LAUSANNE

POUR L'OBTENTION DU GRADE DE DOCTEUR ÈS SCIENCES

PAR

Bruno MEYER

Diplômé EPF en sciences naturelles de l'environnement
de nationalité suisse et originaire de Knutwil (LU)

acceptée sur proposition du jury:

Prof. H. Vogel, directeur de thèse
Prof. S. Cotecchia, rapporteur
Prof. M. Mutter, rapporteur
Prof. J. Widengren, rapporteur

Lausanne, EPFL
2005

This work was performed in the laboratory of physical chemistry of polymers and membranes (LCPPM) at the Swiss Federal Institute of Technology in Lausanne (Switzerland), under the supervision of Prof. Horst Vogel, between May 2000 and June 2005.

Part of this work has been published or submitted:

Martinez, K.L., B.H. Meyer, R. Hovius, K. Lundstrom, and H. Vogel. 2003. Ligand Binding to G Protein-Coupled Receptors in Tethered Cell Membranes *Langmuir*, **19**, 10925-29.

Cebecauer, M., P. Guillaume, S. Mark, O. Michielin., N. Boucheron, M. Bezard, B.H. Meyer, J.-M. Segura, H. Vogel, and I.F. Luescher. 2005. CD8+ Cytotoxic T Lymphocyte Activation by Soluble Major Histocompatibility Complex-Peptide Dimers. *J Biol Chem*, **280**(25), 23820-28.

Lill, Y., K.L. Martinez, M. Lill, B.H. Meyer, H. Vogel, and B. Hecht. 2005. Kinetics of the Initial Steps of G-Protein Coupled Receptor Mediated Cellular Signaling Revealed by Single Molecule Imaging. *ChemPhysChem*, in press.

Meyer, B.H., K.L. Martinez, J.-M. Segura, R. Hovius, N. George, K. Johnsson, and H. Vogel. 2005. Covalent labelling of cell-surface proteins for in-vivo FRET studies. *to be submitted.*

Meyer, B.H., J.-M. Segura, K.L. Martinez, R. Hovius, N. George, K. Johnsson, and H. Vogel. 2005. FRET Imaging Reveals the Neurokinin-1 Receptor in Microdomains of the Plasma Membrane of a Living Cell. *to be submitted.*

Prummer, M., B.H. Meyer, R. Francini, J.M. Segura, N. George, K. Johnsson, and H. Vogel. 2005. Posttranslational Covalent Labelling Reveals Heterogeneous Mobility of Individual G Protein-Coupled Receptors in Living Cells. *submitted.*

Contents

Abstract

G protein-coupled receptors (GPCR) constitute by far the largest family of transmembrane cell-surface proteins involved in signal transduction and are the most important targets for the development of novel therapeutic compounds. Many processes mediated by GPCR signal transduction are still not well understood at the molecular level and novel methods for their investigation are of general interest. The thesis presented here describes investigations on the neurokinin-1 receptor (NK1R), a member of the GPCR family, using fluorescence techniques.

Fluorescence resonance energy transfer (FRET), the technique of preference in this work, is used to measure ligand-protein and protein-protein interactions in living cells. In order to reach this goal, the NK1R has been labelled with either fluorescent proteins or by using the novel post-translational ACP labelling technique.

A FRET-based method for monitoring specific ligand binding to NK1R is described. In this context, a fluorescent agonist for NK1R was synthesized and characterized. The ACP labelling technique was shown to be superior for this kind of experiments compared to labelling with fluorescent proteins.

The same ACP labelling approach was shown to be ideally suited to study oligomerization of membrane proteins by FRET. It was shown, that the NK1R does not form homo-dimers, as many other GPCRs do. From these experiments we furthermore conclude, that the NK1R is present in small microdomains in the membrane.

Interactions between the NK1R and the different subunits of the heterotrimeric $G\alpha_q\beta1\gamma2$-complex were investigated by FRET using different instrumentation. Proximity of the NK1R and the G protein could be detected, but no change in FRET was observed after activation of the receptor.

Total internal reflection fluorescence (TIRF), was used to develop an assay for studying ligand binding in vitro. Here, the NK1R was immobilized directly on a surface using a cell membrane preparation. This method was shown to be highly sensitive.

Version abrégée

Les récepteurs couplés aux protéines G (RCPG) forment une famille particulièrement riche de protéines transmembranaires essentielles pour la signalisation cellulaire et constituent une des cibles principales pour le développement de nouveaux composés thérapeutiques. Les diverses étapes de la transmission d'un signal de l'extérieur vers l'intérieur de la cellule par activation de la protéine G ne sont généralement pas connues avec précision à l'échelle moléculaire. Le développement de nouvelles méthodes d'investigation est donc nécessaire pour acquérir une meilleure compréhension du fonctionnement intime des RCPG. Cette thèse applique un large éventail de techniques basées sur la fluorescence à l'étude d'un membre important de cette famille de protéines, le récepteur neuroquinine-1 (NK1R).

La technique de transfert d'énergie par fluorescence résonnante (FRET) a été utilisée de manière prépondérante dans ce travail car elle permet la mesure des interactions entre protéines ou entre une protéine et son ligand au sein même d'une cellule vivante. Ce type d'étude requiert un marquage préalable du récepteur soit avec des protéines fluorescentes soit en utilisant une nouvelle technique post-translationnelle basée sur une protéine transporteuse d'acyles (PTA).

Cette thèse établit une méthode basée sur le FRET qui permet de mesurer la liaison spécifique d'un ligand au récepteur NK1R. Un agoniste fluorescent du récepteur NK1R a d'abord été synthétisé et caractérisé. La technique de marquage par PTA s'est imposée dans le cadre de ces expériences.

La technique de marquage par PTA est particulièrement bien adaptée à l'étude de l'oligomérisation des protéines membranaires par FRET. Il a ainsi été démontré que le récepteur NK1R ne forme pas des homodimères contrairement à la plupart des RCPG étudiés précédemment. Cette série d'expériences indique aussi que le récepteur NK1R se trouve dans des domaines microscopiques de la membrane cellulaire.

Les interactions entre le récepteur NK1R et les différentes sous-unités du complexe heterotrimérique $G\alpha_q\beta 1\gamma 2$ ont été étudiées par FRET dans plusieurs configurations

instrumentales. La proximité du NK1R et de la protéine G a pu être détectée mais aucun changement n'a été observé par FRET lors de l'activation du récepteur.

La fluorescence induite par réflexion interne totale (TIRF) est au cœur d'un essai qui quantifie la liaison d'un ligand à son récepteur in vitro. De manière innovante, le récepteur NK1R a été immobilisé sur une surface directement à partir d'une préparation cellulaire. Cette méthode se distingue par sa très haute sensibilité.

Chapter 1

General Introduction to GPCR Signaling

1.1 Transmembrane Signaling

The ability of organisms, or individual cells, to react to external signals is crucial for their survival. These various signals can be either physical (e.g. light, temperature and pressure) or chemical stimuli (e.g. organic odorants, nucleotides, nucleosides, peptides, lipids and proteins). Regardless of the nature of the signal, the target cell responds by means of specific receptors. In most cases, these receptors are transmembrane cell-surface proteins, because the signal has to overcome the plasma membrane separating the extracellular environment from the interior of the cell.

A basic definition of a receptor is that it must recognize a distinct extracellular stimulus and translate that information into an intracellular signal to which the cell can respond. Receptors are typically composed of three domains (Figure 1.1): a signal receiving domain, a transducing domain and an effector domain , which can be either comprised all within a single protein (e.g. ion channels) or separated into different proteins (e.g. G protein-coupled receptors and G proteins).

1.2 Receptor Classification

The three largest classes of cell-surface receptors are ligand-gated ion channels, enzyme-linked receptors and G protein-coupled receptors. They are defined according to the transduction mechanism used [1, 2].

Ligand-gated ion channels are involved in rapid synaptic signaling between electrically excitable cells (Figure 1.2 A). This type of signaling is mediated by a small

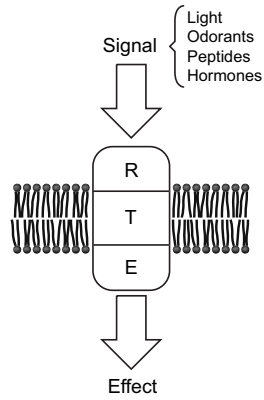

Figure 1.1: Concept of transmembrane signaling. *R, signal receiving domain; T, transducing domain ; E, effector domain.*

number of neurotransmitters released from the presynaptic cell. The neurotransmitters transiently bind to the receptor and thereby open an ion channel formed in the receptor, which in turn briefly changes the ion permeability of the plasma membrane and thereby depolarizes the membrane potential of the postsynaptic cell.

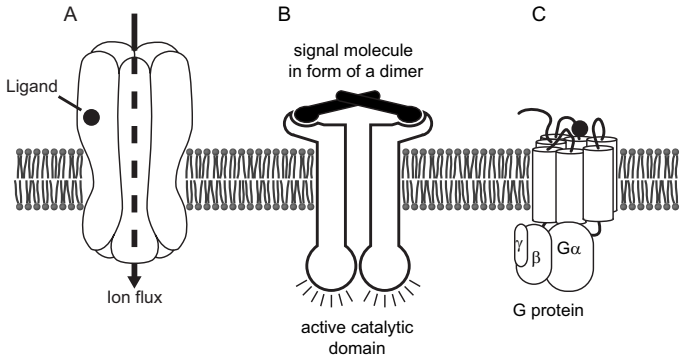

Figure 1.2: Receptor superfamilies. *A, ligand-gated ion channels. B, Enzyme-linked receptors (with an intrinsic enzyme). C, G protein-coupled receptors.*

Enzyme-linked receptors, when activated, either function directly as enzymes or are directly associated with enzymes that they activate (Figure 1.2 B). The great majority of these receptor are protein kinases (e.g. receptor tyrosine kinase) or are associated with protein kinases (e.g. cytokine receptors). Enzyme-linked receptors are involved in growth, proliferation, differentiation, and are important for the survival of the cell.

They have a single transmembrane polypeptide chain and an extracellular ligand-binding domain. The cytosolic domain has either an intrinsic enzyme activity or associates directly with an enzyme.

G protein-coupled receptors (GPCR) act indirectly to regulate the activity of separate effector proteins (Figure 1.2 C). The interaction between the receptor and its effector is mediated by a third protein called the heterotrimeric GTP-binding protein (G protein). The activation of the effector, which can be either an enzyme or an ion channel, can change the concentration of one or more intracellular mediators. These mediators act in turn to alter the behavior of other signaling proteins in the cell.

1.3 GPCRs and Heterotrimeric G Proteins

G protein-coupled receptors constitute by far the largest family of transmembrane cell-surface proteins involved in signal transduction. There are approximately 950 genes in the human genome encoding GPCRs, of which 500 are odorant or taste receptors and 450 are receptors for endogenous ligands [3]. GPCRs recognize signals as diverse as light, odorants, hormones, growth factors and neurotransmitters. They interact with heterotrimeric guanine nucleotide-binding proteins, so-called G proteins, which transmit the receptor signal to different effectors. GPCRs are involved in a wide range of physiological processes and, not astonishingly, are implicated in numerous diseases. This makes GPCRs one of the most important target class of proteins for medicines [4].

1.3.1 Structure of GPCRs

GPCRs are integral plasma membrane proteins with a molecular mass ranging from about 40 to 85 kD. All GPCRs sequenced so far share a common topology illustrated in Figure 1.3, although they do not share any overall sequence homology [5]. They comprise seven transmembrane helices (TM), which are connected by intracellular and extracellular loops. The N-terminus is located on the extracellular side and the C-terminus on the intracellular side of the plasma membrane [6, 7]. Only recently Palczewski et al. [8] solved the crystal structure of the first GPCR, rhodopsin, to 2.8 Å resolution (Figure 1.3 A).

According to sequence homology, GPCRs can be further classified into 3 major families (Figure 1.3 B) [5, 9]. Family A, also named rhodopsin-like family, represents the largest subgroup of these receptors and includes catecholamine, neuropeptides, chemokine, glycoprotein, lipid and nucleotide receptors. The receptors share a set of

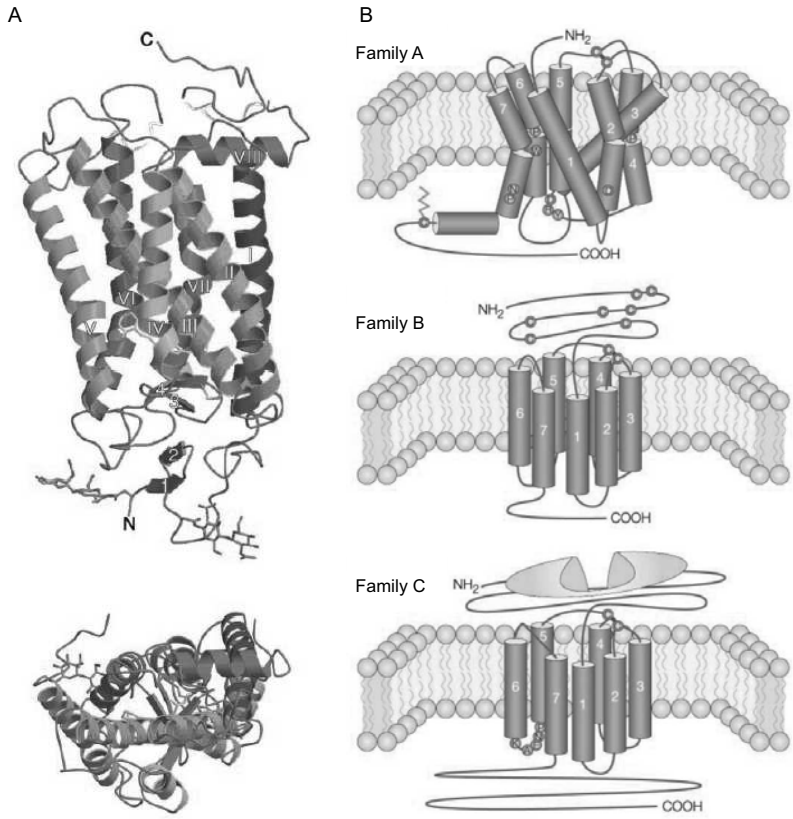

Figure 1.3: Structural properties of GPCRs. *A, 2.8 Å crystal structure of rhodopsin [8]. B, topology model of G protein-coupled receptor families with extracellular N-terminus, 7 transmembrane helices, intracellular C-terminus and the extra- and intracellular loops (from [9]).*

~20 highly conserved amino acids in the cytoplasmic side of the transmembrane core. The high degree of conservation among these residues suggests an essential role for structural and/or functional integrity of the receptors. The ligand binding sites are formed by the extracellular loops and the transmembrane helices. The only residue that is conserved in all family A receptors is the arginine in the Asp-Arg-Tyr (DRY) motif at the cytoplasmic side of TM3. A palmitoylation site follows the last TM helix. The hydrophobic palmitoyl inserts into the intracellular side of the membrane, forming a "fourth" intracellular loop. Family B contains receptors for a large number of peptides such as calcitonin-gene-related peptide (CGRP) and calcitonin. The most prominent characteristics of family B receptors is a large (~100 amino acids) extracellular N-terminus containing several cysteins. It seems to play a key role for ligand binding, although it is not sufficient and additional ligand interaction sites are found on the extracellular loops connecting the TMs. The DRY motif, which is important for family A receptors, is absent in family B receptors. Family C is the metabotropic family comprising the metabotropic glutamate receptors (mGluRs), γ-amino butyric acid receptors ($GABA_B$) and the calcium-sensing receptor. They are characterized by an exceptionally long N-terminus (500-600 amino acids) containing the ligand binding site.

1.3.2 Structure of G proteins

Heterotrimeric GTP binding proteins (G proteins) are peripheral membrane proteins, which are preferentially bound to the cytosolic face of the plasma membrane (Figure 1.4). They consist of an α-subunit and a $\beta\gamma$-complex, which is not dissociable under non-denaturing conditions. Up to now, at least 23 α-subunits derived from 17 different genes have been identified and are classified into four families ($G\alpha_{i/o}$, $G\alpha_s$, $G\alpha_{q/11}$, and $G\alpha_{12}$). Concerning β- and γ-subunits, at least 6 and 12 different molecular species have been described, respectively. The molecular mass of Gα-subunits ranges from 39-52 kD and they consist of two domains: the GTPase domain and the α-helical domain. The GTPase domain contains the GDP/GTP binding site and exhibits a high structural similarity with other small GTPases. The helical domain comprises 6 helices and is believed to increase the affinity for GTP. Furthermore, it seems to participate in effector recognition. Both the N- and C-terminus of the α-subunit are closely located to the plasma membrane and the N-terminus of certain α-subunits is post-translationally modified by lipid groups. The molecular mass of the β- and γ-subunit is about 36 kD and 6-9 kD, respectively. Both β- and γ-subunits are post-translationally modified by lipid groups and thus tether the $\beta\gamma$-complex to the plasma membrane. Several reviews

about heterotrimeric G proteins are found in literature [10–14].

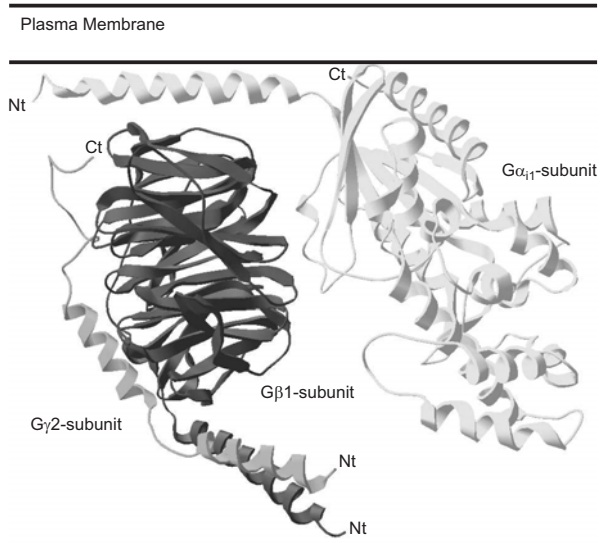

Figure 1.4: Structure of a heterotrimeric G protein. *Crystal structure at 2.3 Å of $G\alpha_{i2}$ complexed with $G\beta1\gamma2$ (PDB:1GG2) [15]. Ct and Nt indicate C-terminus and N-terminus, respectively.*

1.4 Mechanism of GPCR Signal Transduction

1.4.1 Receptor - G protein Interaction

Extensive mutational analysis revealed some interaction sites of GPCRs with G proteins. These include the intracellular loops i2, i3 and, to a lesser extent, i4 [6, 16]. The same G protein subtype can be activated by different receptors containing structurally different intracellular loops, thus, the prediction of the coupling specificity of a GPCR cannot be deduced from its primary structure [17]. The extreme C-terminus of the $G\alpha$ subunit seems to be critical for its interaction with the receptor, especially for the specificity of the receptor-G protein coupling [18, 19]. Also the extreme N-terminus of $G\alpha$ appears to specifically interact with the receptor [20]. This was shown in experiments using chimeric G proteins. Furthermore, there are indications, that the $G\beta\gamma$ subunit takes also part in binding to the receptor, but the structural elements involved in this interaction are less well characterized [21]. There are now several independent lines of

evidence that suggest that G protein activation may require a dimeric GPCR interacting with a single heterotrimeric G protein [22]. It remains still an open question whether receptors are pre-associated with G proteins before ligand binding or if they associate upon receptor activation.

1.4.2 Principles of GPCR-G Protein Activation and Deactivation

The classic paradigm of the GPCR signal transduction is a simple linear model: a ligand-activated receptor protein activates a G protein, which can activate or inhibit a downstream effector protein [23].

The G protein exists in two forms: The inactive, heterotrimeric form, in which the Gα-subunit complexes the nucleotide guanosine diphosphate (GDP) and the active form, in which Gα binds the nucleotide guanosine triphosphate (GTP). Binding of an extracellular ligand to the receptor results in its conformational change, which promotes the Gα-subunit to exchange GDP for GTP. The GTP-complexed and activated Gα dissociates from the $\beta\gamma$-subunit, which then becomes activated as well. Gα and G$\beta\gamma$ then interact with several different effector proteins, which modulate the intracellular concentration of second messengers, leading to a cellular response. Eventually, GTP hydrolysis occurs on the α-subunit. This step is often accelerated by the binding of another protein, called a regulator of G protein signaling (RGS). The inactivated, GDP-bound α-subunit re-associates with the $\beta\gamma$-complex, thereby turning off other downstream events [24–26].

Recent findings indicate that the classical model of G protein coupling and activation of second-messenger-generating effectors do not fully explain their remarkably diverse biological actions. Among them are GPCR oligomerization [27] and the discovery that many proteins, e.g. chaperons, interact with GPCRs [28]. Also the paradigm of G protein subunit dissociation has been challenged [29–31].

1.4.3 GPCR Activity States

Molecular pharmacology divides ligands into full, partial and inverse agonists as well as neutral antagonists [32]. Full agonists are those ligands, which elicit the maximal observed response upon receptor binding, whereas partial agonists only evoke a partial response. Inverse agonists counteract with an existing basal activity of the free receptor. Neutral antagonists inhibit the action of agonists but do not change the activity state of the receptor. An extensive description of the different allosteric receptor models is found in [33, 34].

The extended ternary complex model

In the ternary complex model a receptor, an agonist and a heterotrimeric G protein form a complex which leads to the activation of the G protein (Figure 1.5 A). This

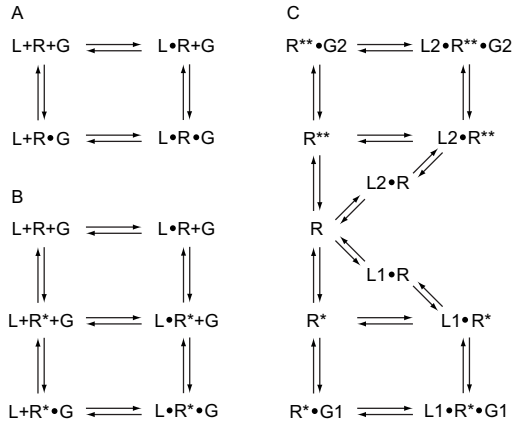

Figure 1.5: Different models for GPCR activation. *A, Ternary complex model, and B, extended ternary complex model, which includes an activated receptor state R* (taken from [35]). C, Taking into account that the potency of agonists acting on one particular receptor depends on the G protein which couples to it, two activated states of the receptor have to be assumed, R* and R** (adapted from [36]).*

model implicitly states that an allosteric transition occurs upon agonist binding which induces G protein activation - otherwise, the receptor would be constitutively active. The discovery of mutations in β-adrenergic receptor which result in constitutive activity, and the subsequent finding that antagonist could counteract these mutations, led to a revised model of receptor activation, the extended ternary complex model (Figure 1.5 B) [35]. In this model, the receptor exists in an equilibrium between an inactive and an active conformation, R and R*. Only the latter can interact with the G protein, but both can interact with ligands. Agonists have a preference for the R* state, i.e. they show higher affinity for the R* than for the R state, thus, their binding leads to a shift of the R $\rightleftarrows$ R* equilibrium to the right, increasing the rate of G protein activation. Inverse agonists have a high affinity for R and shift the equilibrium to R. Partial agonists prefer R* over R, but do not fully shift the equilibrium to the former. Neutral antagonists bind to both, R and R*, and thereby exclude the binding of agonists, but do not change the conformational equilibrium of the receptor.

The extended ternary model can explain why GPCRs often show two different affinities for agonists. According to this theoretical model the receptor exists in equilibrium

between two different conformations, R and R*. Only the latter can interact with the G protein, but both can interact with ligands. Agonists show higher affinity for the R* than for the R state. In native membranes, only the higher affinity is observed. In vitro in absence of G proteins, or if the system is treated with GTPγS (irreversibly activating G proteins), only the low affinity state is observed. Thus, G proteins can also induce the R* state of the receptor.

This is of importance for recombinant expression systems [37], because overexpressed GPCRs are generally present in excess in their host cells, and only a small fraction is complexed to G proteins. In these cells and in plasma membranes harvested from them, a bi-phasic isotherm for agonist binding is measured, which is the result of a superposition of the two (high and low affinity) binding curves.

A thermodynamically more complete version of the extended ternary complex model is the cubic ternary complex model [38–40]. It allows non-activated receptors to interact with G proteins to produce non-signaling species. This non-signaling complex is required to complete the system, but might be not relevant physiologically.

Multiple activity states

Leff et al. suggested that the extended ternary model is still too simplified to account for some experimental results (Figure 1.5 C) [36]. Receptors which can couple to different G protein subtypes, i.e. activate different transduction cascades, have been found to show different relative potencies of their agonists, depending on which transduction cascade is available. This is in disagreement with the assumption that the same receptor conformation activates different G proteins. If this is the case, the efficacies to evoke a response for the two pathways would be different for a given agonist, but the relative potencies between the different agonists would be the same, irrespectively which transduction cascade is activated. Therefore, it has been proposed that at least two, if not more, activated forms of a GPCR exist, each of which preferentially interacts with a subset of agonists and the appropriate G protein.

1.5 Signal Transduction Pathways

G proteins act as transducing units and transmit the signal from the receptor to the effector. The α- as well as the $\beta\gamma$-subunits can interact with different effectors and thereby activate different signaling pathways (Table 1.1). In the following a description of the two most important G protein-coupled signaling pathways is presented.

Subunit	Family	Main subtypes	Primary effector
α	α_s	Gα_s, Gα_{olf}	Adenylate cyclase ↑
	$\alpha_{i/o}$	Gα_{i1}, Gα_{i2}, Gα_{i2}	Adenylate cyclase ↓
		Gα_{oA}, Gα_{oB}	K^+ channels ↑
		Gα_{t1}, Gα_{t2}	Ca^2+ channels ↓
		Gα_z	Cyclic GMP phosphodiesterase ↑
	α_q	Gα_q, Gα_{11}, Gα_{14},	Phospholipase C ↑
		Gα_{15}, Gα_{16}	
	α_{12}	Gα_{12}, Gα_{13}	?
β	$\beta_{1\text{-}5\ (6?)}$	Different assemblies	Adenylate cyclase ↑/↓
		of β- and γ-subunits	Phsopholipase ↑
			Phosphatidylinositol 3-kinase ↑
γ	$\gamma_{1\text{-}11\ (12?)}$		Protein kinase C ↑
			Protein kinase D ↑
			GPCR kinases ↑
			Ca^{2+}, K^+ (and Na^+) channels

Table 1.1: Heterotrimeric G proteins and their effectors. *The arrows indicate up- or down regulation of the effector (from [41]).*

1.5.1 The cAMP Pathway

Cyclic AMP (cAMP) is synthesized from ATP by a plasma-membrane-bound enzyme adenylyl cyclase (AC), and is rapidly and continuously degraded by cyclic AMP phosphodiesterases [42]. There are at least 8 isoforms of AC in mammals, most of which are regulated by both G proteins and calcium. The receptors that act through cAMP can either stimulate the AC via a stimulatory G protein (Gα_s or Gα_{olf}) or inhibit it via a inhibitory G protein (Gα_i). But also the $\beta\gamma$-subunit of the heterotrimeric G protein can stimulate or inhibit AC (Table 1.1). Both Gα_s and Gα_i are targets for bacterial toxins. *Cholera toxin* from the bacteria that causes cholera, catalyzes the ADP ribosylation of the Gα_s-subunit and inhibits the hydrolysis of bound GTP. The α-subunit retains its bound GTP and remains in an active state. *Pertussis toxin* from the bacteria that causes pertussis (whooping cough), catalyzes the ADP ribosylation of the Gα_i-subunit and therefore preventing it from interacting with the receptor. The α-subunit retains its bound GDP and remains in an inactive state. Activation of AC leads to a rapid increase of the cAMP level in the cytosol. This directly activates protein kinase A, which in turn phosphorylates a variety of proteins and thereby modulates their activity.

1.5.2 The DAG/IP3 and Calcium Signaling Pathway

Many GPCRs exert their effects via G proteins, mainly Gα_q, that activate the plasma-membrane-bound enzyme phospholipase C-β (PLCβ) [43]. PLCβ cleaves the lipid phosphatidyl-inositol-4,5-bisphosphate into diacylglycerol (DAG) and the cyclic alcohol inositol-trisphosphate (IP3). Both, DAG and IP3, are second messengers. IP3 acts directly on calcium channels in the endoplasmatic reticulum. This leads to a fast increase in the cytosolic calcium concentration. DAG acts via protein kinase C to open L-type calcium channels in the plasma membrane. The inositol phospholipid signaling pathway is illustrated in Figure 1.6.

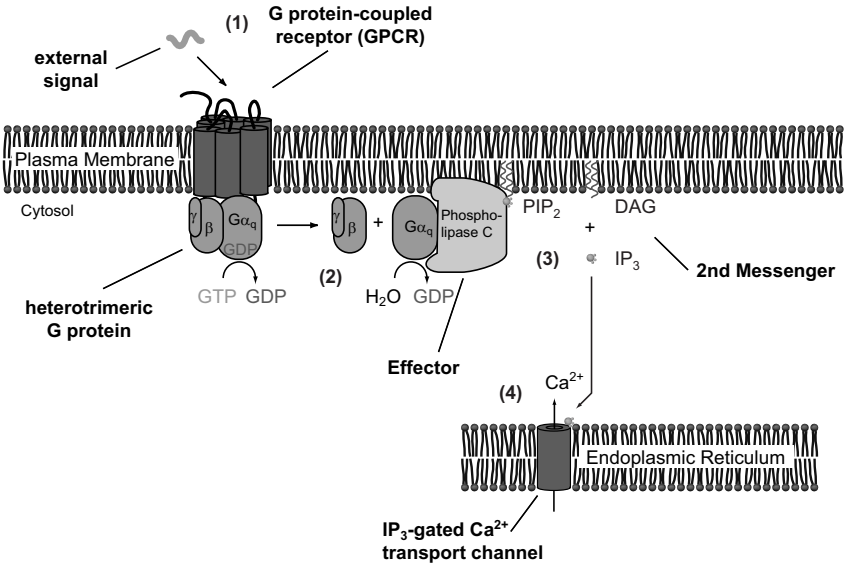

Figure 1.6: Inositol phospholipid signaling pathway through Gα_q. *(1) Receptor activation by external signal. (2) Activation of G protein. (3) Hydrolysation of phosphatidylinositol-4,5-bisphosphate (PIP2) to IP3 and DAG by Phospholipase C (PLC). (4) IP3 acts on calcium channels in the endoplasmic reticulum releasing calcium to the cytosol. (not shown in figure) DAG acts via protein kinase C to open L-type calcium channels in the plasma membrane (adapted from [44]).*

1.5.3 Other Pathways

Some G proteins directly activate or inactivate ion-channels in the plasma membrane (Table 1.1). G protein activated inward rectifier potassium channels (GIRK) are e.g.

found in the heart. The G$\beta\gamma$ subunit has been shown to directly bind to these channels and to gate their pore [45]. Additional effector systems that were classically believed to be activated by growth-factor receptors via tyrosine kinase activation were also shown to be modulated by GPCRs. In particular, the ERK, p38 and mitogen-activated protein kinase (MAPK) signaling pathways were shown to be activated by G proteins of the Gα_{q}, Gα_{i} and Gα_{s} families. In addition, G protein-independent signaling has been documented, such as Na^+/H^+-exchanger regulatory factor (NHERF) or activation of the Janus kinases (JAK) [46, 47].

1.5.4 Diversity, Selectivity and Multiplicity

Complex cell behaviors, such as cell survival and cell proliferation, are generally stimulated by specific combinations of extracellular signals rather than by a single signal acting alone. Therefore it is not surprising that the concept of signal transduction pathways in a linear fashion (one receptor coupling to one G protein that activates one effector) is inadequate to explain all experimental findings.

The same ligand can activate many different receptor family members. The same receptor can couple to different combinations of heterotrimeric G protein subunits and thereby act through different signaling pathways and generate multiple intracellular signals. All this leads to a complex signaling network (reviewed in [7, 16, 24, 41, 48]). The stability and specificity of a receptor-G protein-effector complex could be enhanced by the presence of a scaffolding protein [28].

1.6 GPCR Desensitization

Activation of a GPCR by its agonist also initiates the process of receptor desensitization, a negative feedback reaction to prevent potentially harmful effects due to persistent receptor stimulation.

Desensitization includes the uncoupling of the receptor from the G proteins in response to receptor phosphorylation, the internalization of cell surface receptors to intracellular membranous compartments, and the downregulation of the total cellular complement of receptors due to reduced receptor mRNA and protein synthesis, as well as the lysosomal and plasma membrane degradation of pre-existing receptors. The time frames over which these processes occur range from seconds (phosphorylation) to minutes (endocytosis) and hours (down-regulation). [49]

Phosphorylation occurs at residues within the intracellular loops and C-terminus of the receptor and is mediated by both second messenger-dependent protein kinases and

G protein-coupled receptor kinases (GRKs). Second-messenger dependent kinases, such as protein kinase A and C (PKA, PKC), are activated in response to GPCR-stimulated increases in second-messengers (e.g. calcium, cAMP, and diacylglycerol). Thus, the activation of PKA or PKC can lead to a general desensitization of GPCRs. GRKs selectively phosphorylate agonist-activated receptors, thereby promoting the binding of arrestins, which sterically uncouple the receptor from the G protein. [49, 50]

G protein-coupled receptor internalization is mediated by arrestins [51]. Arrestins are involved in both the physical uncoupling of GPCRs from heterotrimeric G proteins (desensitization) and the targeting of GPCRs to clathrin-coated pits for endocytosis that leads to the loss of the receptor on the cell surface (internalization). Arrestins bind preferentially to agonist-activated and GRK-phosphorylated GPCRs as opposed to second-messenger protein kinase-phosphorylated or non-phosphorylated receptors.

Studies on the translocation of β-arrestin 1 and β-arrestin 2 to GPCRs have shown that GPCRs can be divided into two classes, A and B, on the basis of their internalization properties [52]. Complexes between class A receptors and β-arrestin 1 or β-arrestin 2 are relatively unstable, dissociate at or near the plasma membrane, and the arrestins are excluded from receptor-containing vesicles. Complexes between class B receptors and β-arrestin 1 or β-arrestin 2 are stable and internalize together into endocytic vesicles. Classical and new roles of β-arrestins have been reviewed by Pierce and Lefkowitz [53].

Just as GPCR desensitization provides a mechanism protecting cells against receptor overstimulation, GPCR resensitization protects cells against prolonged receptor desensitization, which would leave a cell unable to respond appropriately to extracellular stimuli. The mechanism by which the resensitization of GPCRs is achieved is thought to be the agonist-stimulated internalization of receptors to an intracellular membrane compartment (endosomes) enriched in a GPCR-specific phosphatase activity. GPCRs, dephosphorylated in endosomes, are subsequently recycled back to the cell surface.

1.7 Oligomerization of GPCRs

GPCRs were for a long time presumed to function as monomers according to the prevailing model: one ligand molecule-one receptor-one G protein [23]. But recently, the existence of dimeric or higher oligomeric structures for some GPCRs has been found by biochemical and biophysical methods (for reviews [9, 22, 46, 54–58]). There is no consensus on the role of GPCR oligomerization, but several potential roles are suggested (Figure1.7).

Oligomerization is seen either between the same receptor subtype (homo-oligomer-

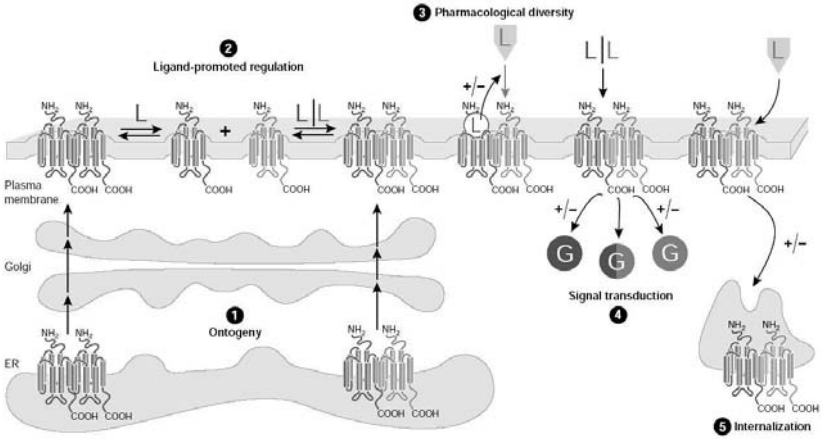

Figure 1.7: Potential roles of GPCR dimerization during GPCR life cycle. *(1) In some cases, dimerization has been shown to have a primary role in receptor maturation and allows the correct transport of GPCRs from the endoplasmic reticulum (ER) to the cell surface. (2) Once at the plasma membrane, dimers might become the target for dynamic regulation by ligand binding. (3) It has been proposed that GPCR hetero-dimerization leads to both positive (+) and negative (-) ligand binding cooperativity, as well as (4) potentiating (+)/attenuating (-) signaling or changing G-protein selectivity. (5) Hetero-dimerization can promote the co-internalization of two receptors after the stimulation of only one protomer. Alternatively, the presence of a protomer that is resistant to agonist-promoted endocytosis, within a heterodimer, can inhibit the internalization of the complex (from [27]).*

ization) or between different receptor subtypes (hetero-oligomerization). Furthermore, one can distinguish between constitutive oligomerization and ligand-dependent oligomerization. Preformed oligomers of some GPCRs may serve as a signaling platform that retains its multimeric status throughout the GPCR life cycle. Other GPCRs may cycle through monomeric and multimeric states in a ligand-regulated process that itself is part of the signaling pathway. GPCR hetero-dimerization can result in altered ligand selectivities and distinctive coupling to signal transduction pathways, providing an additional source of complexity and richness for the fine-tuning of cellular signaling.

1.8 Neurokinin-1 Receptor

In this thesis we will focus on the G protein-coupled receptor neurokinin-1 (Substance P receptor or NK1 receptor, NK1R). The human NK1 receptor consists of 407 amino acids and has a calculated relative molecular mass of 46 kD. Like all GPCRs it comprises 7 predicted transmembrane helices with an extracellular N-terminus and an cytosolic C-terminus. It is a neuropeptide receptor and belongs to the tachykinin receptor subfamily, which are family A or rhodopsin-like receptors. Other members of the tachykinin receptor subfamily are the neurokinin 2 (NK2R) and neurokinin 3 (NK3R) receptors. All three receptors bind the three most abundant tachykinins, which they distinguish with only moderate selectivity; substance P (SP) is preferred by the NK1R whereas the NK2R and NK3R have a higher association constant for neurokinin A (NKA) and neurokinin B (NKB), respectively. The affinities are in the low nanomolar range. [59]

Tachykinin receptors are found in central and peripheral nervous system [60, 61]. The NK1 receptor is involved in a variety of different processes, e.g. neural signal transmission, regulation of the intestine, hematopoiesis, nociception and neurogenic inflammation, and is therefore an important pharmacological target [62].

Tachykinins, the naturally occurring agonists for the neurokinin receptors are small peptides, which share a common C-terminal sequence (Phe-X-Gly-Leu-Met-NH2) and a similar spectrum of biological activities [63–65]. The classical natural agonist with highest affinity for the NK1 receptor is the undecapeptide SP. The existence of SP was described as early as 1931 by Von Euler and Gaddum [66]. The three classical members of the mammalian tachykinin family SP, NKA and NKB are encoded by the two genes preprotachykinin 1 ($TAC1$) and preprotachykinin 2 ($TAC2$) [64]. Recently, a third mammalian tachykinin gene ($TAC4$) has been discovered coding for hemokinins and endokinins [67,68]. Structure-activity studies have led to the development of several peptide and non-peptide ligands for the NK1 receptor [59], some of which are commer-

cially available.

The interaction of SP with the NK1 receptor mainly activates the G protein $G\alpha_q$, leading to the activation of phospholipase C, the increase of the intracellular concentration of IP3 and DAG, and finally calcium [69]. Furthermore, NK1R can interact with $G\alpha_s$ and act via the cAMP pathway [70] and there is evidence that it interacts also with $G\alpha_o$ [71]. Studies on NK1R $G\alpha_q$ and $G\alpha_s$ fusion proteins revealed two active molecular phenotypes, representing complexes with either $G\alpha_q$ or $G\alpha_s$ [72]. The authors proposed that these molecular forms do not interchange readily, which could be due to the presence of microdomains within the cell membrane. Very recently, Monastyrskaya et al. [73] showed localization of NK1R in plasma membrane microdomains by biochemical methods, and that its functionality depends on these microdomains, supporting the previous findings.

Activation of NK1R stimulates translocation of GRKs and β-arrestins from the cytosol to the membrane within seconds. GRKs phosphorylate NK1Rs and β-arrestins then interact with the GRK-phosphorylated receptors [74, 75]. This leads to desensitization and internalization of NK1R, which was shown to take place within 3 minutes of SP incubation at 37°C [76], but also occurred within minutes after SP application at 18°C [77]. The internalization can be prevented by C-terminal truncation of NK1R [78]. Martini et al. [79] fused β-arrestin 1 to the C-terminus of NK1R. The fusion protein was almost totally silenced with respect to agonist-induced signaling through $G\alpha_{q/11}$ and $G\alpha_o$ pathways. The NK1R-βarr1 fusion bound non-peptide antagonist with increased affinity, but surprisingly also bound agonists, SP and NKA, with high, normal affinity.

Furthermore, it was shown that the NK1R belongs to the class B receptors, because (i) it forms stable complexes with β-arrestin 1 or β-arrestin 2 and (ii) they internalize together into endocytic vesicles [52]. Recently, Bennett et al. [80] suggested that NK1R internalization is not required for desensitization but is important in resensitization. Interestingly, the pathway of internalization seems to be SP concentration dependent [81]. High SP concentration (>10nM) leads to translocation of NK1R into perinuclear acidified endosomes, where they remain for several hours. Low SP concentration (1 nM) leads to translocation into early endosomes and rapid recycling.

Also the oligomerization of NK1R was investigated, but so far only hetero-dimerization with the μ-opioid receptor was shown [82]. Until now, there is no evidence for homo-dimerization.

Chapter 2

Aim and Scope of this Thesis

The aim of this thesis is to investigate by fluorescence (microscopic) techniques the function of the NK1 receptor in whole cells. We focus on observing ligand-activated biochemical interactions between the NK1 receptor and corresponding components of its signal cascade. The chosen system serves as an example for developing methods to monitor complex biochemical networks under physiological conditions, which might be the basis for novel screening assays.

Chapter 4 describes the FRET methodology used throughout this thesis. FRET occurs when an excited donor fluorophore transfers its excitation energy non-radiatively to an acceptor fluorophore with an efficiency that depends strongly on their relative distance. Therefore, FRET can quantify molecular association. Here, two ways to determine FRET are used: The first method is based on the evaluation of spectra recorded either from cell suspensions using a common photospectrometer or from single cells using a microscope equipped with a CDD camera coupled to a spectrometer. The second method is based on fluorescence micrographs of single cells recorded with a laser scanning confocal microscope (FRET imaging).

Chapter 5 deals with the fluorescence labelling of NK1R for investigations in living cells. The NK1R is labelled with either fluorescent proteins (e.g. EGFP) or by using the novel ACP labelling technique. The design and cloning of the NK1R fusion constructs and the confirmation of functionality of the NK1R fusion proteins by means of calcium signaling are described.

Chapter 6 deals with the synthesis and characterization of fluorescent derivatives of NK1R agonists to act as acceptors for the donor-labelled NK1R. Preliminary investigation of specific ligand binding using a FRET-based approach are presented.

In Chapter 7 the ACP labelling method is used to simultaneously label the NK1R with donor and acceptor in a well defined ratio. FRET imaging is applied to investigate the oligomerization degree and compartmentalization of NK1Rs.

Chapter 8 deals with the fluorescence labelling of the heterotrimeric G protein and FRET-based studies to investigate interactions between receptor and G protein subunits or between Gα- and G$\beta\gamma$-subunits.

In Chapter 9, a novel approach to immobilize minute amounts of recombinant, biotinylated membrane receptor proteins in a uniform orientation on streptavidin-coated sensor surfaces is described. Very sensitive total internal reflection fluorescence (TIRF) is used to investigate ligand binding on immobilized NK1Rs.

Chapter 3

Experimental Techniques and Procedures

This chapter deals with the materials and general methods used throughout this work unless otherwise stated. It includes the standard techniques for cell cultures, transient and stable expression, calcium ion signaling, fluorescence confocal microscopy, and ACP labelling.

3.1 Materials

Dulbecco's modified Eagle's medium (DMEM), fetal calf serum (FCS) and Dulbecco phosphate-buffered saline (D-PBS) were from Invitrogen (Breda, NL); hygromycin B was from Calbiochem (Darmstadt, D); bovine serum albumin (BSA) and EDTA was from Fluka (Buchs, CH); Substance P was from K. Servis (UNIL, Lausanne, CH); bacitracin was from Serva; CoA-Cy3, CoA-Cy5 and AcpS from were a kind gift from Nathalie George and Kai Johnsson of the Institute of Chemical Sciences and Engineering, Lausanne, Switzerland; tetramethylrhodamine-conjugated substance P (SP-TMR) was from Molecular Probes (Eugene, OR, USA); NK1R antagonist L-732,138 was from Tocris Cookson (Langford, UK).

3.2 Cell Cultures

Adherent human embryonic kidney cells (HEK293 cells) and $G_{q/11}$-deficient mouse fibroblasts were cultured in Dulbecco's modified Eagle medium (DMEM) supplemented with 2.5% and 10% fetal calf serum (FCS), respectively, in a humidified 5% CO_2 atmosphere at 37°C. Cells were sub-cultivated twice a week at ratios between 1:10 and

1:100. For confocal microscopy HEK293 cells were seeded ($1 \cdot 10^{15}$ cells/ml) into 8-well plates (Nalge Nunc International, UK) or into 6-well plates (TPP, Trasadingen, CH) containing a 25 mm diameter glass coverslip (Assistent, D), in 200 μl and 2 ml culture medium, respectively.

3.3 Transient and Stable Expression

HEK293 cells (45-75% confluent) were transfected 16 to 20 hours after splitting, with calcium phosphate-precipitated DNA as described [83]. Per 1 ml of medium 2.5 μg of plasmid DNA was diluted in 50 μl calcium buffer (250 mM $CaCl_2$) and was added to 50 μl phosphate buffer (140 mM NaCl, 1.4 mM Na_2HPO_4, 50 mM HEPES, pH 7.05 at 23°C). After 1 minute incubation at room temperature the transfection solution was added to the cell culture medium. After 4 hours incubation at 37°C, the transfection solution was replaced by fresh medium. Experiments were performed 24-55 hours after transfection. Stable HEK293 cell lines were produced from cells transiently transfected with the desired constructs in pCEP4 expression vectors by selection with 200 μg/ml hygromycin B.

3.4 Calcium Ion Signaling

Activation of NK1R leads to the releases of calcium from internal stores and thereby increases the intracellular calcium concentration. This increase can be monitored with calcium-sensitive dyes. The increase of the intracellular calcium concentration is related to the increase in fluorescence of the calcium-sensitive dye and can be measured on a FLEX station.

HEK293 cells stably expressing wtNK1R, ACP-NK1R or NK1R-ECFP were seeded into a 96 well plate (Greiner) in DMEM supplemented with 2.5% FCS and incubated at 37°C and 5% CO_2. After 24 hours the cells were loaded with a calcium-sensitive dye (Calcium 3 assay kit, Molecular Devices) during 30 minutes at 37°C. The change in fluorescence intensity of the calcium dye upon addition of SP in buffer (50 mM Tris-HCl pH 7.5, 150 mM NaCl, 5 mM $MnCl_2$, 0.1% BSA (w/v), 100 μg/ml Bacitracin) was recorded on a FLEX station (Molecular Devices) with excitation at 485 ± 4.5 nm and fluorescence detection at 525 ± 4.5 nm. The final concentration of SP was 0.003-10 nM. The amplitude of the “calcium peak" versus log[SP] was fitted with the Hill-equation:

$$E_{\mathrm{L}} = E_0 + \frac{E_{\max} - E_0}{1 + 10^{(logEC_{50} - log[L]) \cdot n_{\mathrm{H}}}} \tag{3.1}$$

where E_{L} is the amplitude of the intensity increase (effect) for a given ligand concentration [L]; $log[L]$ is the logarithm of the ligand concentration; $logEC_{50}$ is the logarithm of the EC_{50} value (concentration that produces 50% of the maximal possible effect); E_0 is the baseline; E_{max} is the maximal response or effect; and n_{H} is the Hill coefficient.

3.5 Fluorescence Confocal Microscopy

Laser-scanning confocal micrographs were recorded by using a 453/488nm Ar-Kr laser line or a 543 or 633 nm He-Ne laser line on a Zeiss LSM 510 microscope (Zeiss) with an 63x water (1.2 numerical aperture) objective. Detection and distinction of fluorescence signals was achieved by appropriate filter sets using a multi-tracking mode. Table 3.1 lists the filter sets when using one fluorophore in single-tracking mode and Table 3.2 lists the filter sets when using two fluorophores in multi-tracking mode. If possible, an additional dichroic mirror has been used for the multi-tracking mode to split emission into two channels.

	Excitation Line	Dichroic Mirror	Emission Filter
ECFP	458nm	HFT 458	LP 475
EGFP, EYFP	488nm	HFT 488	LP 505
TMR, Cy3	543nm	HFT 543	LP 560
Cy5	633nm	HFT 633	LP 650

Table 3.1: Filter sets for one fluorophore and single-tracking mode.

	Excitation Line	Dichroic Mirror (HFT)	Beam Splitter (NFT)	Emission Filter
Cy3 and Cy5	543nm 633nm	UV/488/543/633	635 vis	BP 560-615 LP 650
ECFP and EYFP	458nm 488nm	458 488	- -	BP 465-495 BP 510-560
EGFP and TMR	488nm 543nm	488/543	545	BP 505-550 LP 560

Table 3.2: Filter sets for two fluorophores and multi-tracking mode.

3.6 ACP labelling

Before labelling the cells were washed once with D-PBS. The labelling was performed in D-PBS with 10 mM $MgCl_2$, 1 μM AcpS and 5 μM CoA substrate. For double labelling with Cy3 and Cy5 the substrates, CoA-Cy3 and CoA-Cy5, were mixed beforehand at a desired ratios to a total concentration of 5 μM. The labelling was performed at 19-23°C for 40 minutes. After incubation the cells were washed three times with D-PBS.

Chapter 4

Fluorescence Resonance Energy Transfer (FRET)

Fluorescence resonance energy transfer (FRET) has been described first theoretically by Perrin in 1932 [84] and was fully elucidated by Förster in 1948 [85]. Since then it has been used as a method to investigate various physical and biological systems. A good introduction to FRET and fluorescence spectroscopy in general can be found in *Principles of fluorescence spectroscopy* by Lakowicz [86].

In this chapter we give a short overview of the physical principles of FRET (Section 4.1), of the different methods to measure the FRET efficiency (Section 4.2), and of some biological applications of FRET mainly with respect to signal transduction (Section 4.3). Furthermore, FRET spectroscopy and microscopy are explained in more detail and how it was used within this work (Chap. 4.4).

4.1 FRET Theory for a Donor-Acceptor Pair

FRET denotes a process by which the excited-state energy from a excited donor molecule (D) is transferred to an acceptor molecule (A). FRET occurs when the emission spectrum of the donor overlaps with the absorption spectrum of the acceptor, and when donor and acceptor are in close distance (typically 10-100 Å). FRET does not involve emission of light by the donor, but the energy of a photon absorbed by the donor molecule is transferred non-radiatively to the acceptor molecule by a dipole-dipole interaction. The Energy level diagram (Jabłonski diagram) in Figure 4.1 shows the transitions which influence FRET measurements.

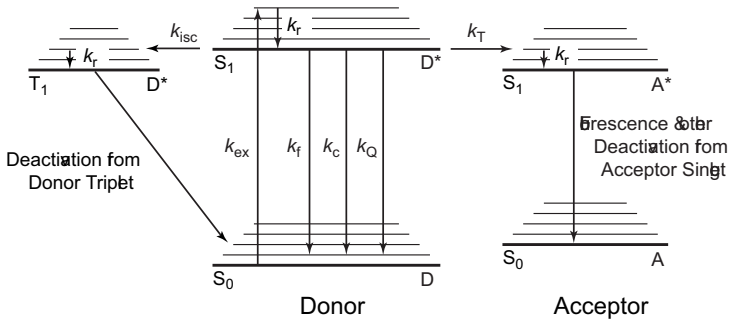

Figure 4.1: Jabłonski diagram showing the transitions which influence FRET. *The thick lines are the lowest vibrational levels of the particular molecular energy states, and the thin lines represent the corresponding higher vibrational levels. S_0, S_1, and T_1 refer to the ground and first excited singlet states and the first excited triplet state, respectively. The donor is excited (k_{ex}) by a photon into higher vibrational levels of the first singlet state S_1 of the donor D^*. Following vibrational relaxation (k_r) to the lowest vibrational state of D^*, the excitation energy is lost spontaneously by one of the following conversions: (1) non-radiative internal conversion k_c, (2) intersystem crossing to the triplet state k_{isc}, (3) collisional quenching k_Q, (4) long-range resonance dipole energy transfer k_T to an acceptor molecule close to the excited donor molecule, and (5) radiative decay k_f to the ground state; k always denotes the rate constant of the indicated process (adapted from Clegg [87]).*

The donor is excited by a photon into a higher energy level and the decay lifetimes of the excited donor in presence (τ_{DA}) or absence (τ_D) of acceptor are given by

$$\tau_{DA}^{-1} = k_c + k_{isc} + k_Q + k_T + k_f \tag{4.1}$$

and

$$\tau_D^{-1} = k_c + k_{isc} + k_Q + k_f, \tag{4.2}$$

where the rate constants (k) are explained in Figure 4.1.

Noting that the quantum yield of any spectroscopic process is the ratio of the rate constant of this process, divided by the sum of the rate constant of all processes occurring from this state, then the quantum yield of energy transfer from the donor (Φ_T^D) is

$$\Phi_T^D = k_T/(k_c + k_{isc} + k_Q + k_T + k_f) = k_T \tau_{DA}. \tag{4.3}$$

The quantum yield of energy transfer from the donor (Φ_T^D) is the experimental variable usually determined in FRET experiments, and can be defined as the efficiency of energy

transfer ($E \equiv \Phi_{\mathrm{T}}^{\mathrm{D}}$). By using Eqs. 4.1 and 4.2, Eq. 4.3 can be written as

$$E = 1 - \frac{\tau_{\mathrm{DA}}}{\tau_{\mathrm{D}}}, \tag{4.4}$$

where E is defined as the quantum yield of energy transfer from the donor ($\Phi_{\mathrm{T}}^{\mathrm{D}}$), or in other words, the fraction of donor molecules de-excited via energy transfer to the acceptor. It is obvious from Eq. 4.3 that this can be done only if the decay rates other than k_{T} are unaffected by the presence of the acceptor, and if the energy levels remain the same in both circumstances. Another way to write Eq. 4.4 is in terms of fluorescence intensities of the donor:

$$E = 1 - \frac{F_{\mathrm{DA}}}{F_{\mathrm{D}}}, \tag{4.5}$$

where F_{DA} is the fluorescence intensity of the donor in the presence of acceptor and F_{D} is the fluorescence intensity of the donor in the absence of acceptor.

As mentioned before, the acceptor must absorb light at donor emission wavelengths for FRET to occur, but it does not need to be fluorescent. However, fluorescent acceptors are often used in FRET experiments. In these cases, light absorbed by the donor and transferred to the acceptor appears as sensitized (or enhanced) acceptor emission and the energy transfer efficiency is

$$E = \left(\frac{F_{\mathrm{AD}}}{F_{\mathrm{A}}} - 1\right)\left(\frac{\varepsilon_{\mathrm{A}}}{\varepsilon_{\mathrm{D}}}\right), \tag{4.6}$$

where F_{AD} is the emission of the acceptor in the presence of the donor (consisting of fluorescence arising from energy transfer and from direct excitation of the acceptor) and F_{A} is the fluorescence of the acceptor-only labelled sample (direct excitation of acceptor only); ε_{A} and ε_{D} are the molar extinction coefficients of the acceptor and donor, respectively, at the wavelength of excitation. Calculation of E from the sensitized acceptor emission requires careful consideration of all interrelated intensities as will be described in more detail in Section 4.4.

In 1948, Förster described a theoretical expression for k_{T} in terms of spectroscopic parameters, relating rate of transfer to distance between donor and acceptor [85]. The transfer rate (k_{T}) for a donor-acceptor pair separated by a distance r is given by

$$k_{\mathrm{T}}(r) = \frac{\phi_{\mathrm{D}}\kappa^2}{\tau_{\mathrm{D}} r^6}\left(\frac{9000(\ln 10)}{128\pi^5 N_{\mathrm{A}} n^4}\right) J(\lambda), \tag{4.7}$$

where ϕ_{D} is the quantum yield of the donor in the absence of acceptor; n is the refractive index of the medium, which is typically assumed to be 1.4 for biomolecules in aqueous

solution; N_A is Avogadro's number; τ_D is the lifetime of the donor in the absence of acceptor; κ^2 is a factor describing the relative orientation in space of the transition dipoles of the donor and acceptor and is usually assumed to be 2/3 (discussed in [88]); and $J(\lambda)$ is the spectral overlap of donor emission with the acceptor absorption. The degree of spectral overlap $J(\lambda)$ is given by the overlap integral,

$$J(\lambda) = \int_0^\infty F_D(\lambda)\varepsilon_A(\lambda)\lambda^4 d\lambda \qquad (\mathrm{M^{-1}cm^{-1}nm^4}), \tag{4.8}$$

where $F_D(\lambda)$ is the corrected fluorescence intensity of the donor, with the total intensity (area under the curve) normalized to unity and $\varepsilon_A(\lambda)$ is the extinction coefficient of the acceptor at λ in units of $\mathrm{M^{-1}cm^{-1}}$.

A number often encountered in FRET experiments is the Förster distance (R_0). It is defined as the distance at which the transfer rate (k_T) is equal to the decay rate of the donor in the absence of acceptor (τ_D^{-1}), or in other words, the distance at which FRET is 50% efficient. Using Eq.4.7, R_0 is given by

$$R_0 = 0.211[\kappa^2 n^{-4}\phi_D J(\lambda)]^{1/6} \qquad (\text{in Å}). \tag{4.9}$$

It lies typically in the range of 20-60 Å for standard DA pairs.

Once the Förster radius R_0 is known, one can derive the rate of energy transfer from Eqs. 4.7, 4.8 and 4.9:

$$k_T(r) = \frac{1}{\tau_D}\left(\frac{R_0}{r}\right)^6. \tag{4.10}$$

As mentioned before, the efficiency of energy transfer (E) is the fraction of photons absorbed by the donor that are transferred to the acceptor and, using Eqs. 4.1, 4.2 and 4.3, can be written as

$$E = \frac{k_T}{\tau_D^{-1} + k_T}, \tag{4.11}$$

i.e. as the ratio of the transfer rate to the total decay rate of the donor. Eq. 4.11 can be rearranged to yield

$$E = \frac{R_0^6}{R_0^6 + r^6} = \frac{1}{1 + (r/R_0)^6}. \tag{4.12}$$

Eq. 4.12 shows that the transfer efficiency is strongly dependent on distance when the donor-acceptor distance is near R_0. If r is twice the Förster distance ($r = 2R_0$), then the transfer efficiency drops to 1.6% (Figure 4.2). Any phenomenon that affects the donor-acceptor distance will affect the transfer rate, allowing the phenomenon to be quantified.

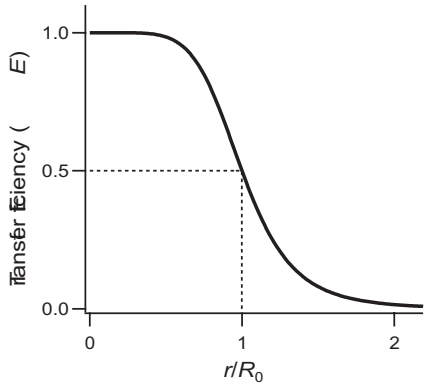

Figure 4.2: Dependence of the energy transfer efficiency (E) on distance r.

It is important to note, that Eqs. 4.4, 4.5 and 4.6 are only applicable when in all DA pairs the donor and the acceptor are separated by a fixed distance. This is a requirement often not matched in biological FRET experiments and it complicates the determination of the energy transfer efficiency. An additional term must be added to take the stoichiometry of donor and acceptor into account

$$E_{\mathrm{app}} = \left(1 - \frac{F_{\mathrm{DA}}}{F_{\mathrm{D}}}\right)\left(\frac{1}{f_{\mathrm{d}}}\right) \tag{4.13a}$$

$$E_{\mathrm{app}} = \left(\frac{F_{\mathrm{AD}}}{F_{\mathrm{A}}} - 1\right)\left(\frac{\varepsilon_{\mathrm{A}}}{\varepsilon_{\mathrm{D}}}\right)\left(\frac{1}{f_{\mathrm{a}}}\right), \tag{4.13b}$$

where E_{app} is the apparent FRET efficiency effectively measured in experiments; f_{d} is the fraction of donor in complex with an acceptor; and f_{a} is the fraction of acceptor in complex with a donor. This will be discussed in more detail in Chapter 7, where the oligomerization states are investigated.

4.2 Methods to Determine E

FRET results in several characteristic changes in the fluorescence of the fluorophores involved. These characteristic changes are based on the three Eqs. 4.4, 4.5, and 4.6

described in Section 4.1,

$$\begin{aligned} E &= 1 - \frac{\tau_{\mathrm{DA}}}{\tau_{\mathrm{D}}}, \\ E &= 1 - \frac{F_{\mathrm{DA}}}{F_{\mathrm{D}}}, \\ E &= \left(\frac{F_{\mathrm{AD}}}{F_{\mathrm{A}}} - 1\right)\left(\frac{\varepsilon_{\mathrm{A}}}{\varepsilon_{\mathrm{D}}}\right), \end{aligned}$$

and can be measured using appropriate methods. In the following a selection of the different methods is given.

First, the FRET efficiency E can be determined by measuring the fluorescence lifetime of the donor in presence or absence of the acceptor (Eq. 4.4). The fluorescence lifetime can be measured in a time-resolved fluorometer [87, 89]. This approach does not depend on the concentration of the donor molecules but requires specialized light sources and detectors capable of quantifying the nanosecond lifetimes. A more sophisticated approach based on donor lifetime with additional spatial resolution is fluorescence lifetime imaging microscopy (FLIM) [90–94]. Another method connected to the fluorescence lifetime of the donor is called donor photobleaching. This method is based on the photobleachability of the donor. The donor photobleaches more slowly if energy transfer to an acceptor is present. The fractional change in the photobleaching time constant caused by energy transfer is the same as the fractional change in the fluorescence lifetime of the donor [90, 95–97]. FRET can also be observed by measuring the anisotropy of the donor fluorescence. The anisotropy depends on the extent of rotational diffusion that the excited molecule undergoes before it emits a photon. Because $\tau_{\mathrm{DA}} < \tau_{\mathrm{D}}$ the anisotropy of the donor usually increases in presence of an acceptor [98].

Second, the FRET efficiency E can be determined by measuring the the fluorescence intensity of the donor in presence or absence of the acceptor (Eq. 4.5). As described before, the donor fluorescence intensity is quenched in the presence of the acceptor. Removal or destruction of the acceptor then leads to donor dequenching. This is usually done by complete photobleaching of the acceptor in a spectrometer [99] or on a microscope [100–102] by exciting the acceptor over a prolonged time.

Third, the FRET efficiency E can be determined by measuring the enhanced fluorescence intensity of the acceptor in presence of the donor (Eq. 4.6). Methods exploiting this effect are often referred to as methods based on sensitized acceptor emission. They are mainly used in microscopy [103–110], but are also applicable on a spectrometer [87], or on a flow cytometer capable of dual wavelength excitation [111].

4.3 Biological Applications of FRET

FRET typically occurs between distances of 10-100 Å. This makes FRET very convenient for the study of macromolecules such as proteins. The technique can be used under physiological conditions with near angstrom resolution and with the sensitivity of fluorescence measurements. With the development of mutants of the green fluorescent protein (GFP) and advances in fluorescence microscopy, FRET has rapidly been gaining importance in the study of biological processes in living cells.

Its main applications include the study of interactions between different proteins tagged with either a donor or an acceptor fluorophore (intermolecular FRET), or the investigation of conformational changes within a single protein labelled with both a donor and an acceptor (intramolecular FRET). The later includes the first FRET-based genetically encoded biochemical sensor using ECFP and EYFP [112]. The so called cameleon undergoes a conformational change upon calcium binding resulting in a dramatic change in FRET.

In the field of GPCRs, intramolecular FRET has been used to monitor GPCR activation [113, 114]. Intermolecular FRET has been applied to investigate different steps in GPCR signaling, including ligand binding [115, 116], GPCR oligomerization [55], receptor-G protein interaction [117], interactions between heterotrimeric G protein subunits [31, 118], GIRK channel activation by G proteins [119], and receptor-arrestin interactions [120, 121].

4.4 Experimental Procedures

FRET has been used as a technique to investigate molecular interactions in this thesis. In the following, the two main experimental methods used are explained in detail. First, FRET spectroscopy, where emission spectra are recorded and the efficiency is determined through sensitized acceptor emission. The method has been used in Chapter 8. Second, FRET microscopy, where the FRET efficiency is calculated from single cell images, also through sensitized acceptor emission. This method has been mainly used in Chapter 7. It is important to note that both methods determine the apparent FRET efficiency, which reflects both the intrinsic FRET for a DA pair and the fraction of acceptor in complex with a donor (Eq. 4.13b).

All data treatment, including curve fitting and image processing, was done with the software `IGOR Pro` (Version 5.02, WaveMetrics Inc.).

4.4.1 Sensitized Acceptor Emission: Spectroscopy

To use a spectrometer is the most straightforward way to measure FRET. Illuminating at a wavelength appropriate to excite the donor results in an emission spectrum containing contributions of the donor emission and acceptor emission. The acceptor emission is then the sum of emission due to direct excitation and due to FRET. To calculate FRET efficiencies it is necessary to separate these three contributions.

Setup and Data Acquisition

Fluorescence spectra can be recorded either from a cell suspension using a conventional spectrometer or from single cells using a microscope equipped with a spectrometer coupled to a CCD camera.

Little instrumentation is needed when working with cell suspensions (∼200'000 - 1'000'000 cells/ml). Here, a SPEX Fluorolog II (Instruments S.A., Stanmore, UK) was used, which contains a monochromator for emission and excitation. The sample was placed in a 1 ml quartz glass cuvette (Hellma, D) with a stirrer to keep cells in suspension.

Measurements in a conventional spectrometer, where cell suspensions are used, cannot reveal cell-by-cell differences, and a contribution from dead cells, cellular debris and unbound, free fluorescent molecules can be present in the signal. Therefore, a home-built setup has been used for recording spectra from single cells (Figure 4.3).

The setup is based on a epiluminescence wide-field microscope (Axiovert 100 TV, Zeiss, D). Circularly polarized light of a diode laser (637 nm) or a tuneable single mode Ar^+ laser (457.9, 488, 514.5 nm) (both Coherent, USA) is directed by a dichroic mirror into a microscope objective (C-Apochromat 63x W Korr, 1.2 NA, Zeiss, D) to illuminate a 22 μm diameter region of the sample. Fluorescence is collected by the same objective, passed through an adequate filter (Table in Figure 4.3) and detected with a CCD camera (LN/CCD-576 EUV, Spectroscopy Instruments GmbH, D) coupled to a spectrometer (CP-140, Spectroscopy Instruments GmbH, D). Spectra are obtained by integrating the fluorescence of the whole cell during 0.5-1 s.

The method to calculate FRET efficiencies using a spectrometer is based on two emission spectra of the same sample recorded at two different excitation wavelengths, regardless of the setup used. First, an emission spectrum extending over the whole range of donor and acceptor fluorescence is acquired by exciting the donor. Second, an emission spectrum of the acceptor is recorded by exciting the acceptor only. In the following equations the subscripts donor and acceptor indicate the spectra taken with

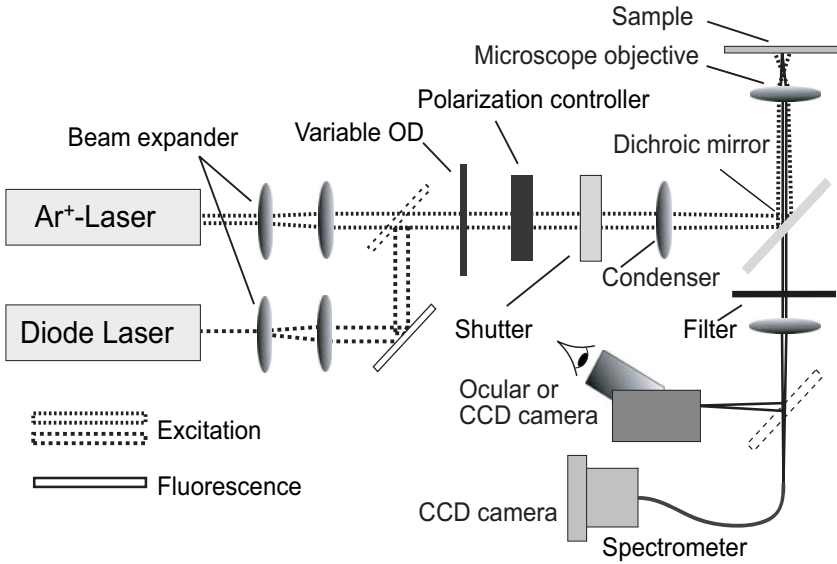

	Excitation Line (nm)	Dicroic Mirror	Emission Filter
Cy3	514.5	FT530	LP550
Cy5	637	Q645LP	HQ710/120
ECFP	457.9	Z458	LP480
EYFP/Citrine	514.5	FT530	HQ570/80M

Figure 4.3: Schematic view of the home-built setup and filter sets.

donor and acceptor excitation, respectively.

ECFP and EYFP were used as DA pair to illustrate the method. The various spectra were recorded with a SPEX Fluorolog II with donor excitation at 430 nm and emission from 440-630 nm, and acceptor excitation at 510 nm and emission from 520-630 nm.

In order to fit the measured spectra from the sample (S) as contributions of donor and acceptor emission and calculate the FRET efficiency, corresponding spectra have to be taken for the buffer only (S_B), a cell suspension without donor and acceptor (S_C), the donor only (S_D), and the acceptor only (S_A) (Figure 4.4). The sample with only cells is required for correction of light scattering and autofluorescence.

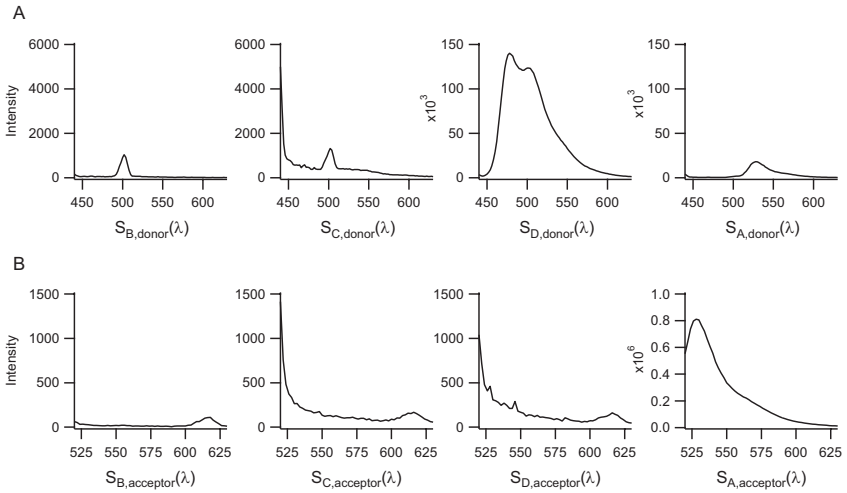

Figure 4.4: Example of spectra used for fitting in FRET spectroscopy. *ECFP and EYFP were used as donor and acceptor, respectively. A, spectra used for fitting of $S_{donor}(\lambda)$ in Figure 4.5 A. Excitation was set at 430 nm. B, spectra used for fitting of $S_{acceptor}(\lambda)$ Figure 4.5 B. Excitation was set at 510 nm.*

Fitting and Calculation of E

As discussed before, the FRET efficiency E can be calculated using Eq. 4.6 for sensitized acceptor emission,

$$E = \left(\frac{F_\mathrm{AD}}{F_\mathrm{A}} - 1\right)\left(\frac{\varepsilon_\mathrm{A}}{\varepsilon_\mathrm{D}}\right),$$

where F_AD is the acceptor emission in presence of donor (consisting of fluorescence arising from energy transfer and from direct excitation of the acceptor) and F_A is the acceptor emission in absence of donor (direct excitation of acceptor only). The ratio

$\varepsilon_A/\varepsilon_D$ depends on the excitation wavelength of the donor and can be estimated from the absorption spectra of donor and acceptor and the molar extinction coefficients found in literature, and is discussed in more detail in Section 4.4.3. The following calculations to obtain the ratio F_{AD}/F_A from the emission spectra are illustrated in Figure 4.5 using an ECFP-EYFP fusion protein.

The first step to obtain F_{AD} and F_A is the decomposition of the spectrum of the sample S into the separate contributions of donor and acceptor. Therefore, S is fitted using the spectrum of the buffer (S_B), of the cells (S_C), of the donor (S_D), of the acceptor (S_A), and an *offset* using

$$S(\lambda) = bS_B(\lambda) + cS_C(\lambda) + dS_D(\lambda) + aS_A(\lambda) + offset, \tag{4.14}$$

where b, c, d, and a are the fit coefficients for the spectrum of buffer, cells, donor, and acceptor, respectively. If the various fitting spectra are well separated the fitting in `IGOR Pro` is very robust and does not depend on the initial values for b, c, d, a and *offset*. A representative example of the fitting is found in Figure 4.5 A and 4.5 B.

The donor and acceptor spectra can have a contribution from the cell autofluorescence. This however did not influence the fitting parameters d and a, for the donor and acceptor, respectively. For the fitting of the acceptor spectra, the fit parameter d could be set to zero, because the donor does not absorb at acceptor excitation. Subtraction of buffer ($bS_B(\lambda)$), cells ($cS_C(\lambda)$) and *offset* from S for both sets of spectra (donor excitation and acceptor excitation) results in

$$S'_{donor}(\lambda) = d_{donor}S_{D,donor}(\lambda) + a_{donor}S_{A,donor}(\lambda) \tag{4.15}$$

and

$$S'_{acceptor}(\lambda) = a_{acceptor}S_{A,acceptor}(\lambda), \tag{4.16}$$

where $S'_{donor}(\lambda)$ is the corrected spectrum of $S_{donor}(\lambda)$ and $S'_{acceptor}(\lambda)$ is the corrected spectrum of $S'_{acceptor}(\lambda)$. The subscripts indicate the excitation used (donor or acceptor).

The term $a_{donor}S_{A,donor}(\lambda)$ in Eq. 4.15 is the emission of the acceptor due to direct excitation and energy transfer. It can be written as

$$a_{donor}S_{A,donor}(\lambda) = (a_{donor,direct} + a_{donor,FRET})S_{A,donor}(\lambda). \tag{4.17}$$

In a sample with acceptor only ($S_A(\lambda)$), the acceptor emission using donor excitation ($S_{A,donor}(\lambda)$) is proportional to the acceptor emission using acceptor excitation ($S_{A,acceptor}(\lambda)$) and depends on instrumental settings. In analogy, in a sample with

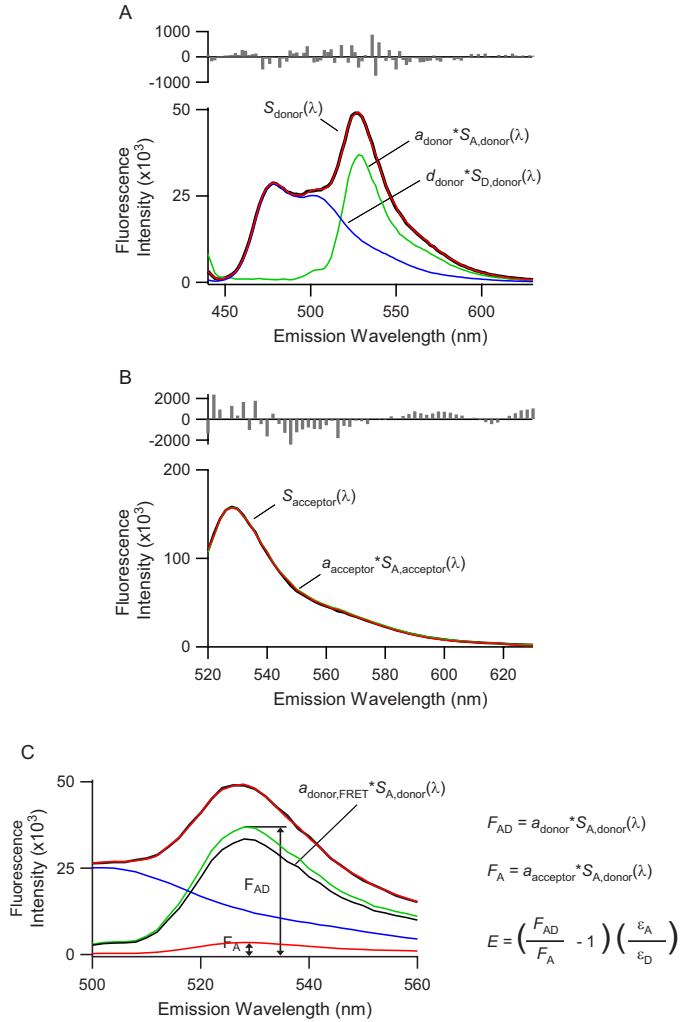

Figure 4.5: Principle of FRET spectroscopy. *Example of FRET spectroscopy for the ECFP-EYFP fusion protein expressed in HEK293 cells. A, spectrum of ECFP-EYFP fusion excited at 430 nm ($S_{donor}(\lambda)$) fitted with the spectra from Figure 4.4 A (residuals of the fit shown above), and the contributions from donor ($d_{donor}\, S_{D,donor}(\lambda)$) and from acceptor ($a_{donor}\, S_{A,donor}(\lambda)$). B, spectrum of ECFP-EYFP fusion excited at 510 nm ($S_{acceptor}(\lambda)$) fitted with the spectra from Figure 4.4 B (residuals of the fit shown above), and the contribution of the acceptor ($a_{acceptor}\, S_{A,acceptor}(\lambda)$). C, enlargement of the spectrum in A, showing the two contributions to F_{AD}, F_A and $a_{donor,FRET}\, S_{A,donor}(\lambda)$. The calculated FRET efficiency for ECFP-EYFP was $E = 0.44$, with $\varepsilon_A/\varepsilon_D = 0.046$.*

donor and acceptor ($S(\lambda)$), the acceptor emission due to direct excitation using donor excitation ($a_{\text{donor,direct}}S_{\text{A,donor}}(\lambda)$) is proportional to the acceptor emission due to direct excitation using acceptor excitation ($a_{\text{acceptor,direct}}S_{\text{A,acceptor}}(\lambda)$) and depends on the same instrumental settings. Because there is not contribution of FRET to the acceptor emission using acceptor excitation, $a_{\text{acceptor,direct}}$ is equal to a_{acceptor}. The unknown is the acceptor emission in $S_{\text{A,donor}}(\lambda)$ due to direct excitation, and can be calculated as

$$a_{\text{donor,direct}}S_{\text{A,donor}}(\lambda) = a_{\text{acceptor}}S_{\text{A,acceptor}}(\lambda)\frac{S_{\text{A,donor}}(\lambda)}{S_{\text{A,acceptor}}(\lambda)}, \tag{4.18}$$

resulting in

$$a_{\text{donor,direct}} = a_{\text{acceptor}}. \tag{4.19}$$

F_{AD} is the fluorescence of the acceptor in presence of the donor. In the spectrum recorded with donor excitation, $S_{\text{donor}}(\lambda)$, F_{AD} is equal to $a_{\text{donor}}S_{\text{A,donor}}(\lambda)$. F_{A} is the fluorescence of the acceptor in absence of the donor. In the spectrum $S_{\text{donor}}(\lambda)$, recorded with donor excitation, F_{A} is equal to the direct excitation of the acceptor, $a_{\text{donor,direct}}S_{\text{A,donor}}(\lambda)$. And therefore, using Eq. 4.19,

$$\frac{F_{\text{AD}}}{F_{\text{A}}} = \frac{a_{\text{donor}}}{a_{\text{acceptor}}}. \tag{4.20}$$

Thus, the apparent FRET efficiency E can be obtained directly from the acceptor fitting parameters a_{donor} and a_{acceptor} (Figure 4.5 C).

Advantages, Disadvantages, Problems

The determination of FRET efficiency using cell suspensions can be limited by the expression level of the protein of interest and more importantly the transfection efficiency. If only a small percentage of cells are expressing the protein of interest, high cell concentrations (>1'000'000 cells/ml) are needed to yield a good fluorescence intensity. The signal to noise ratio can decrease dramatically due to light scattering and cell autofluorescence This in turn can cause a problem with the fitting procedures to decompose the spectra. Moreover, high overexpression might lead to non-physiological conditions and unwanted protein aggregation. Another disadvantage of cell suspensions is that they require constant stirring to prevent cells from precipitation. Therefore it is often necessary to work with large volumes of about 1 ml. When working with antibodies or other more sophisticated labelling techniques, such as ACP labelling, it is desired to minimize the working volume to reduce the quantities of label reagents.

The determination of FRET efficiencies on single cells allows one to work with low

expression levels at physiological expression levels. The home-built setup is more sensitive and cells can be selected before recording. A disadvantage of this setup is its field of illumination, where the two excitation wavelengths overlap only to a certain extent. This does not cause any problems for single small cells, when they are positioned in the center of the illumination field [122]. But it gets critical for a cell or a group of cells, which is larger than the illumination field ($\sim 20\,\mu$m), leading to high variation in the FRET signal depending on the position of the sample.

With both instruments it is possible to observe kinetics. On the SPEX this is done by using two detectors one for donor emission and one for acceptor emission. On the home-built setup whole spectra can be recorded at about 2-4 Hz. In both cases only changes in FRET can be detected unless the efficiency at the start of the measurement is known.

An advantage of the SPEX over the home-built setup is the choice of excitation and emission wavelength. A disadvantage is the time needed to record one spectrum. It is usually in the order of several seconds to minutes as compared to 0.2-1 s on the home-built setup.

4.4.2 Sensitized Acceptor Emission: Microscopy/Imaging

Sensitized acceptor emission imaging is becoming the most popular approach to FRET imaging, as it can be implemented on widefield and confocal microscopes, it is non-destructive, in contrast to acceptor photobleaching, and it allows measurements of FRET changes in time. The sensitized fluorescence of acceptor is detected through an optical FRET filter set that selects acceptor emission during donor excitation. But the image acquired with the FRET filter set contains several contributions beside the FRET signal, which need to be corrected. These include direct excitation of the acceptor at the donor excitation wavelength (cross talk) and bleed-through of the donor emission into the acceptor emission detection.

Several methods have been published for calculation of FRET from steady-state images and for corrections of bleed-through and cross talk [104–110]. All these methods are based on three filter sets: (1) the donor filter set, where the donor emission is recorded during donor excitation, (2) the acceptor filter set, where the acceptor emission is recorded during acceptor excitation, and (3) the FRET filter set, where acceptor emission is recorded during donor excitation. To calculate correction factors, it is necessary to record the three images not only for the sample with donor and acceptor, but also with donor alone and acceptor alone.

In this Section the data acquisition, background and shading corrections, calculation

of bleed-through and cross talk, and the final calculation of the apparent FRET efficiency is discussed in more detail.

Symbols

The symbols used for the various fluorescence intensities in this and the following chapters are the symbols introduced by Gordon et al. [105]. Two- and three-letter symbols are defined to denote the various signals depending on the type of filter set (Donor, FRET or Acceptor), the fluorophores present in the sample (donor only, acceptor only, or both donor and acceptor) and the origin of the signal from either the donor or the acceptor when both are present in the sample. Each symbol starts with an capital letter representing the filter set, D for the Donor filter set, F for the FRET filter set, and A for the Acceptor filter set. The second letter is lowercase and indicates which fluorophores are present in the specimen, d for donor only, a for acceptor only, and f for both donor and acceptor present (FRET is possible). In the three-letter symbols, the third letter is lowercase and indicates the signal from only one of the fluorophores when both fluorophores are present (Table 4.1). The overline refers to the signal expected for a mixture of donor and acceptor if no FRET were present.

Image Acquisition and Background Correction

Laser-scanning confocal micrographs were recorded on a LSM 510 microscope (Zeiss) with an 63× (1.2 NA, W Korr, Zeiss) objective by using a 458/488 nm Ar^+ laser, and 543 nm and 633 nm HeNe lasers. Detection and distinction of fluorescence signals was achieved by appropriate filter sets using a multitracking mode. The excitation wavelength and the filter set used for the DA pairs are given in Table 4.2. Under these conditions each image was taken separately. Depending on the filters and dichroic mirrors of the instrument, the donor and FRET image could also be taken at the same time, since they are excited with the same wavelength. In the case of Cy3/Cy5 as DA pair, the sample was excited at 543 nm and the emission beam was split with a NFT 635 Vis dichroic mirror on two detectors with a BP 560-615 and a LP 650 filter, respectively. This way the image acquisition gets faster, because the donor and the FRET image are recorded at the same time.

The filter sets were chosen according to the filters available in the instrument and to minimize bleed-through and cross talk. The donor filter set selects donor emission during donor excitation, the acceptor filter set selects acceptor emission during acceptor excitation, and the FRET filter set selects acceptor emission during donor excitation.

Two-letter Symbol	Filter Set	Fluorochromes Present	Meaning
Dd	Donor	donor	The signal from a donor-only sample using the Donor filter set
Ad	Acceptor	donor	The signal from a donor-only sample using the Acceptor filter set
Fd	FRET	donor	The signal from a donor-only sample using the FRET filter set
Da	Donor	acceptor	The signal from a acceptor-only sample using the Donor filter set
Aa	Acceptor	acceptor	The signal from a acceptor-only sample using the Acceptor filter set
Fa	FRET	acceptor	The signal from a acceptor-only sample using the FRET filter set
Df	Donor	donor and acceptor	The signal from a donor-acceptor sample using the Donor filter set
Af	Acceptor	donor and acceptor	The signal from a donor-acceptor sample using the Acceptor filter set
Ff	FRET	donor and acceptor	The signal from a donor-acceptor sample using the FRET filter set
Three-letter Symbol	**Filter Set**	**Fluorochromes Present**	**Meaning**
Dfd	Donor	donor and acceptor	Refers to the donor signal only when both donor and acceptor are present
Dfa	Donor	donor and acceptor	Refers to the acceptor signal only when both donor and acceptor are present
Ffd	FRET	donor and acceptor	Refers to the donor signal only when both donor and acceptor are present
Ffa	FRET	donor and acceptor	Refers to the acceptor signal only when both donor and acceptor are present
Afa	Acceptor	donor and acceptor	Refers to the donor signal only when both donor and acceptor are present
Afd	Acceptor	donor and acceptor	Refers to the acceptor signal only when both donor and acceptor are present
$\overline{Dfd}$	Donor	donor and acceptor	Refers to the donor signal that would have been if no acceptor were present and therefore no FRET occured
$\overline{Afa}$	Acceptor	donor and acceptor	Refers to the donor signal that would have been if no donor were present and therefore no FRET occured

Table 4.1: Two- and three-letter Symbols. *The symbols used for the various fluorescence intensities in FRET imaging and their interpretation (Adapted from Gordon et al. [105]).*

		ECFP-EYFP	Cy3-Cy5
Donor Channel	Excitation	458 nm	543 nm
(Track 1)	Dichroic	HFT 458	HFT 543
	Emission	BP 465-495	BP 560-615
Acceptor Channel	Excitation	488 nm	633 nm
(Track 2)	Dichroic	HFT 488	HFT 633
	Emission	BP 510-560	LP 650
FRET Channel	Excitation	458 nm	543 nm
(Track 3)	Dichroic	HFT 458	HFT 543
	Emission	BP 510-560	LP 650

Table 4.2: *Filter sets used for FRET imaging with the DA pairs ECFP-EYFP and Cy3-Cy5. The settings for ECFP-EYFP were also used for ECFP-Citrine.*

Figure 4.6 illustrates the three filter sets for the ECFP/EYFP FRET pair, the images required to calculate correction factors and finally the FRET efficiency.

The images were recorded as 12-bit images to get a higher dynamic range for the intensities. The laser power for the excitation and the gain of the detectors for the emission were adjusted for each experiment to yield an image with a good signal to noise ratio. The pinhole was set at the same value for all filter sets. Scan speed, averaging of images and image size were usually set at 1.6 μs, 2 and 512x512 pixels, respectively, but could be changed depending on required image quality. The amplifier offset was set to zero. Higher laser powers allow lower amplifier gains. Together with averaging of images and open pinholes, it increases the signal-to-noise ratio, but on the cost of more photobleaching, longer imaging time and lower resolution.

In addition to the DA sample it is necessary to record images with exactly the same settings for the donor, acceptor and FRET channel, of background (buffer or cells), donor alone and acceptor alone. These images are used for background, bleed-through and cross talk corrections.

The background of each image originates from the dark noise of the detector or the CCD camera and the background fluorescence from the buffer and the cells (autofluorescence). Usually the background fluorescence from buffer or cells was very small compared to the dark noise. The background intensities were determined by recording an image with all three filter sets (donor, acceptor, FRET) and the average intensity was determined. In the case of cell autofluorescence the average intensity in a ROI within the cell was taken as the background intensity. The average for the background was then subtracted from all images taken with the same filter set. The background had to be determined for all different settings used.

The effect of shading or non-homogenous illumination can be seen by taking an image

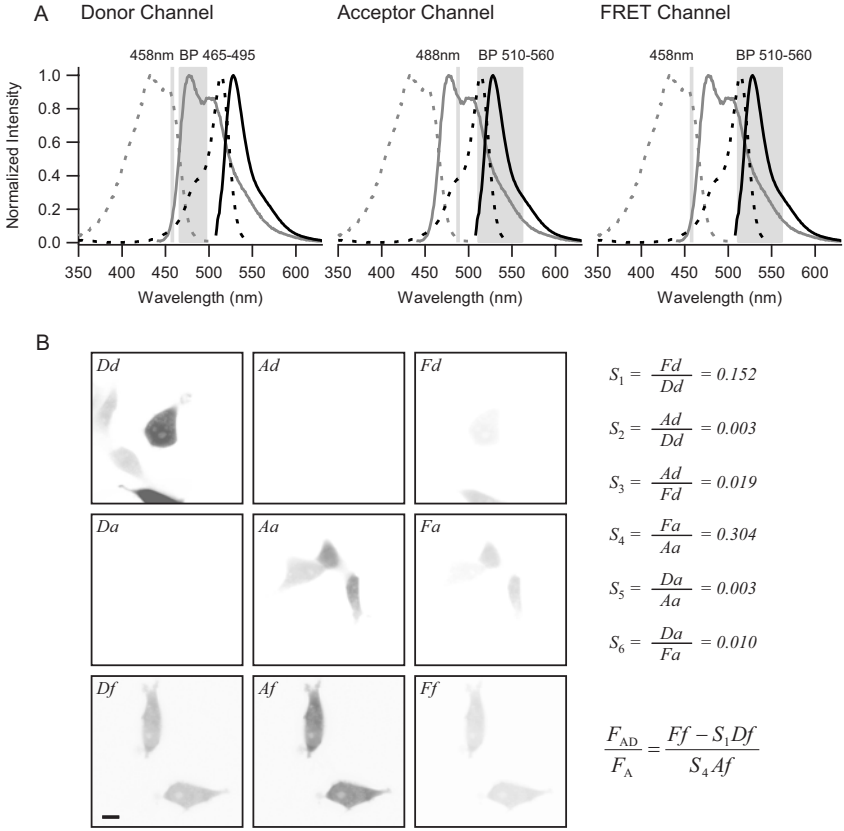

Figure 4.6: Principle of FRET microscopy. *A, absorption (dashed) and emission (solid) spectra of ECFP (grey) and EYFP (black) with indicated excitation wavelength and emission band pass filters for donor, acceptor and FRET channel (Table 4.2). B, the confocal micrographs for Dd, Ad, Fd, Da, Aa, Fa, Df, Af, and Ff required for calculating FRET efficiency E. Colors in the micrographs are inverted to make the low intensities in Fd and Fa visible. Scale bar represents 10 µm.*

of a solution with donor or acceptor fluorophores. With the Zeiss LSM 510 microscope the intensity distribution was uniform over the whole image. No corrections for shading were needed. In case of a widefield microscope the illumination is not homogenous and shading corrections have to be done.

Calculation of the FRET efficiency

With every particular filter set one has more or less cross talk and bleed-through. The acquired images are composite images that consist of multiple terms and have to be corrected to find the real FRET values. We separate three terms of emission intensities: donor emission (quenched), direct acceptor emission and acceptor emission due to FRET: $Intensity = D_{\text{quenched}} + A_{\text{direct}} + A_{FRET}$. The intensities in the images Df, Af and Ff are thus given as

$$\begin{aligned} Df &= (\overline{Dfd} - FRET1) + S_5\ \overline{Afa} + S_6\ G \cdot FRET1 && (4.21a)\\ Ff &= S_1\ (\overline{Dfd} - FRET1) + S_4\ \overline{Afa} + G \cdot FRET1 && (4.21b)\\ Af &= S_2\ (\overline{Dfd} - FRET1) + \overline{Afa} + S_3\ G \cdot FRET1 && (4.21c) \end{aligned}$$

as described by Gordon et al. [105]. For all three equations, the first term, $\overline{Dfd} - FRET1$, is the donor emission that would be in the absence of FRET, minus the loss of emission due to FRET; the second term, $\overline{Afa}$, describes the direct emission of the acceptor; and the third term, $G \cdot FRET1$, describes the emission of the acceptor due to FRET. S_1 to S_6 correspond to the factors due to cross talk and bleed-through and are defined as

$$\begin{aligned} S_1 = \frac{Fd}{Dd} \quad , \qquad S_2 = \frac{Ad}{Dd} \quad , \qquad S_3 = \frac{Ad}{Fd} \\ S_4 = \frac{Fa}{Aa} \quad , \qquad S_5 = \frac{Da}{Aa} \quad , \qquad S_6 = \frac{Da}{Fa} \end{aligned} \tag{4.22}$$

G is a factor relating the loss of donor emission due to FRET in the Donor filter set to the gain of acceptor emission due to FRET in the FRET filter set (see [105]).

The solution of the three unknowns $\overline{Dfd}$, $FRET1$ and $\overline{Afa}$ is given by

$$\begin{aligned} \overline{Afa} &= \frac{Af - S_3 Ff}{1 - S_3 S_4} && (4.23a)\\ FRET1 &= \frac{Ff - S_1 Df - \overline{Afa}[S_4 - S_1 S_5]}{G[1 - S_1 S_6]} && (4.23b)\\ \overline{Dfd} &= Df + FRET1\,[1 - G\,S_5] - S_5 \overline{Afa} && (4.23c) \end{aligned}$$

The FRET ratio ($FR = F_{\mathrm{AD}}/F_{\mathrm{A}}$) is the value to be determined using sensitized acceptor emission (Eq. 4.6). FR is equal to the fractional increase in acceptor emission due to FRET:

$$FR = \frac{F_{\mathrm{AD}}}{F_{\mathrm{A}}} = \frac{F_{\mathrm{A,direct}} + F_{\mathrm{A,FRET}}}{F_{\mathrm{A,direct}}}, \tag{4.24}$$

where the numerator is the emission of the acceptor in the presence of donor (consisting of fluorescence through the FRET filter set arising from direct excitation of the acceptor, $F_{\mathrm{A,direct}}$, and from energy transfer, $F_{\mathrm{A,FRET}}$), and the denominator is the emission of the acceptor in absence of the donor (direct excitation of acceptor, $F_{\mathrm{A,direct}}$). Noting that $F_{\mathrm{A,direct}} = \overline{Afa}$ and $F_{\mathrm{A,FRET}} = G \cdot FRET1$ the FRET ratio FR becomes

$$FR = 1 + \frac{G \cdot FRET1}{S_4\overline{Afa}}. \tag{4.25}$$

Substituting $\overline{Afa}$ and $FRET1$ from Eqs. 4.23a and 4.23b in Eq. 4.25, and noting that $S_2 = S_1S_3$ and $S_5 = S_4S_6$, gives a general equation accounting for all possible cross talk and bleed-through

$$FR = \frac{Ff(1 - S_3S_4) - Df(S_1 - S_2S_4)}{Af(S_4 - S_1S_5) - Ff(S_3S_4 - S_2S_5)}. \tag{4.26}$$

Choosing the right DA pair with appropriate filter sets and excitation wavelengths, Ad and Da become zero and the correction factors S_2, S_3, S_5 and S_6 can be neglected. Therefore, Eq. 4.26 can be simplified to

$$FR = \frac{Ff - S_1Df}{S_4Af}. \tag{4.27}$$

Masking and *FR* Histogram

The following steps, masking and FR histogram, are important mainly when the protein of interest is a membrane protein. Membrane proteins are restricted to a small part of the cell, the plasma membrane, and the intensity levels are usually not evenly distributed. Figure 4.7 A illustrates the process to calculate the FR value from the original images of membrane proteins.

A threshold is applied before background subtraction on the Df or Af image and is set high enough to select the membrane. All pixels below the threshold value are removed from further calculations. The threshold was usually set at about twice the background intensity. The threshold should not be applied on the Ff image, because the intensity depends on FRET. Pixels with higher FRET ratios would be selected, which can lead to overestimated FR values. With low donor and acceptor intensities,

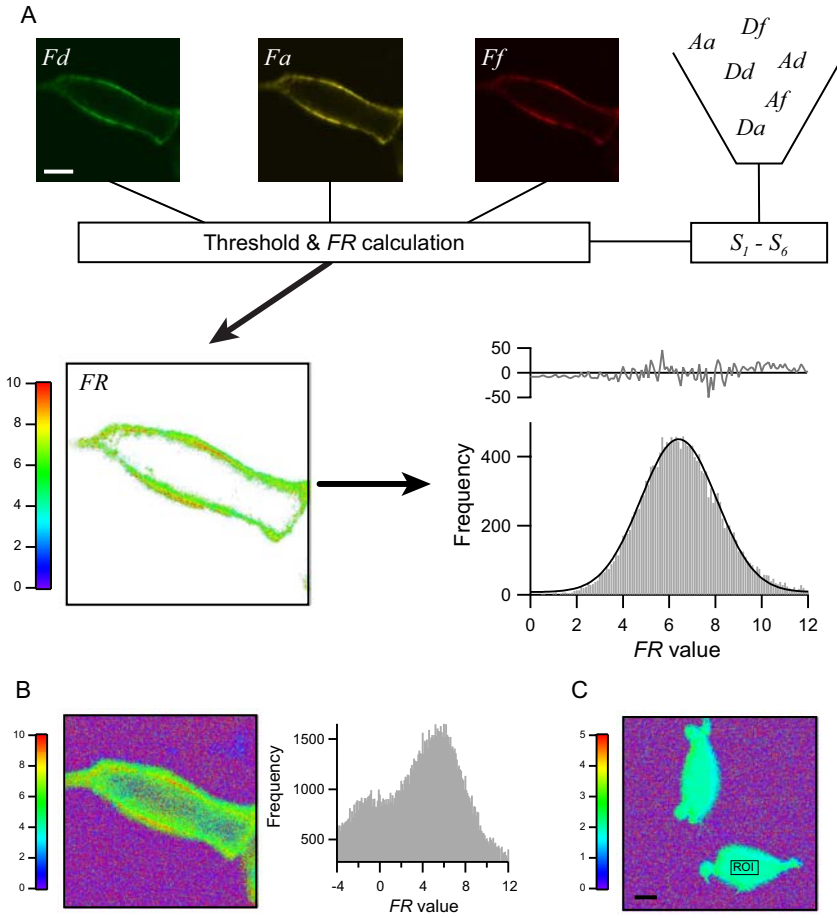

Figure 4.7: Masking and *FR* histogram. *A, scheme of the process for determination of the FR value. The correction factors S_1 to S_6 are calculated from background subtracted images Dd, Da, Ad, Aa, Fd and Fa. A threshold is then applied on the Df or Af image to mask the membrane. The FR value is calculated on a pixel-by-pixel basis according to Eq. 4.26 or to the simplified Eq. 4.27, resulting in the FR image. The histogram over all FR values is created and fitted with a Gaussian to determine the average value for FR. B, FR image and histogram was calculated with the same correction factors but without applying a threshold to the original Df, Af and Ff images. C, FR image of HEK293 cells expressing ECFP-EYFP fusion protein. Scale bars represent 10 μm.*

the threshold can be set only slightly above the background intensity, because otherwise most pixels are removed. In this case, a threshold of about 105% of the background intensity is applied to both images. This removes most of the background signal. Some pixels in the background remain, because of the noise around the average background. But because they will not be at the same position in all the three images and because any pixel removed in one of the three images is not taken into account for further calculations, the background is completely removed in the resulting *FR* image. This process increases the quality of the resulting *FR* image.

To determine the *FR* value from the *FR* image, a histogram over all remaining pixels is calculated. The histogram is then fitted with a Gaussian. This procedure minimizes the artifacts due to the threshold at low *FR* values and gives a better estimation of the real *FR*.

Figure 4.7 B illustrates the effect of not applying a threshold before the calculation of the *FR* image and histogram. In this case, the true *FR* value can still be found by fitting the second peak with a Gaussian. But if the total number of non-background pixels is much smaller than the number of background pixels (eg. small cells or protein expression in a small area) and the *FR* value is close to one, it will become almost impossible to separate the true *FR* values from the background.

For soluble proteins, which are distributed all over the cell (eg. ECFP-EYFP fusion protein) the application of a threshold is not necessary. A region of interest (ROI) within the cell can be selected and the average of *FR* is determined (Figure 4.7 C).

Misfocusing Deviations

As the calculation of FRET involves mathematical operations based on three raw images, it is of importance that these channels spatially overlap, both in lateral and axial directions. The donor and acceptor images are effectively taken from slightly different planes in the cell causing pixels with extreme high and low FRET. Source for misfocusing deviations are chromatic aberrations and differences in the collimation of the laser beams. Chromatic aberrations are due to the wavelength dependency of the refractive index of the optical glasses (Table 4.3). In general, DA pairs with higher excitation wavelengths are preferred.

4.4.3 The Factor $\varepsilon_{\mathbf{A}}/\varepsilon_{\mathbf{D}}$

When calculating E by sensitized acceptor emission (Eq. 4.6), the factor $\varepsilon_{\mathrm{A}}/\varepsilon_{\mathrm{D}}$ directly influences the dynamic range of the *FR* ratio. Assuming a 1:1 DA stoichiometry and an

Laser line pair (nm)	Distance (μm)
458/514	0.30
488/568	0.17
514/633	0.04

Table 4.3: Misfocusing deviations. *Differences in focus distance between commonly used laser line pairs using a standard 63x, 1.32 NA oil immersion objective (from [109]).*

energy transfer of 100%, the maximal possible FRET ratio ($FR_{\max}$) can be calculated by $FR_{\max} = (\varepsilon_A/\varepsilon_D)^{-1} + 1$. This means that a small $\varepsilon_A/\varepsilon_D$-ratio results in a larger dynamic range for *FR*. With longer excitation wavelength, the direct excitation of acceptor relative to the FRET is too high. Furthermore, it is difficult to discriminate the spectra. With shorter excitation wavelength the donor is hardly excited anymore.

The factor $\varepsilon_A/\varepsilon_D$ is calculated from the absorption spectra of donor and acceptor normalized to the molar extinction coefficient of the fluorescent dye. Figure 4.8 illustrates the $\varepsilon_A/\varepsilon_D$-ratio for the FRET pairs ECFP-EYFP and Cy3-Cy5. In the case of ECFP-EYFP the $\varepsilon_A/\varepsilon_D$-ratio for excitation at 430 nm is much better than at 457 nm. But this is often restricted by the instrument, especially when using laser excitation.

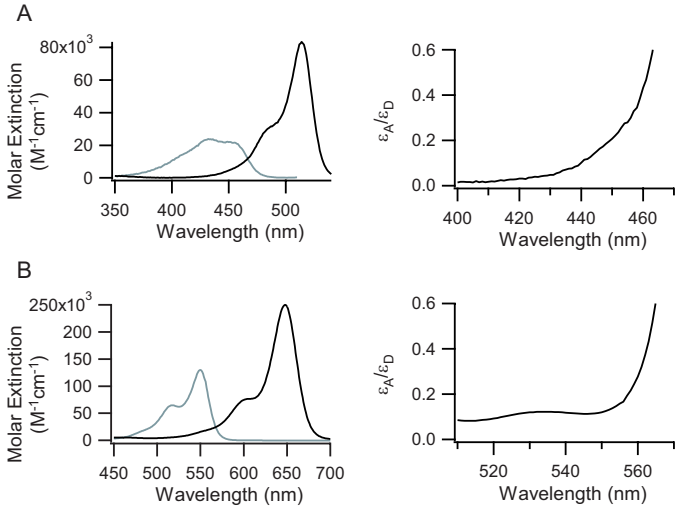

FRET pair	excitation	$\varepsilon_A/\varepsilon_D$	FR_{max}
ECFP-EYFP	430nm	0.048	21.8
	458nm	0.34	3.9
ECFP-Cit	430nm	0.042	24.8
	458nm	0.30	4.3
Cy3-Cy5	543nm	0.11	10.1

Figure 4.8: Molar extinction and $\varepsilon_A/\varepsilon_D$ factor. *Molar extinction of the fluorophores ECFP and EYFP (A), and Cy3 and Cy5 (B) ($\varepsilon_{max,ECFP} = 23'900$, $\varepsilon_{max,EYFP} = 83'400$ from [123]; $\varepsilon_{max,Cy3} = 130'000$, $\varepsilon_{max,Cy5} = 250'000$ from Amersham), and corresponding $\varepsilon_A/\varepsilon_D$ factor, which defines the dynamic range of the measurable FRET ratio. Table: the $\varepsilon_A/\varepsilon_D$ factor for a given DA pair and excitation wavelength. FR_{max} is the maximal possible FRET ratio assuming 1:1 DA stoichiometry and 100% transfer efficiency.*

Chapter 5

Fluorescence Labelling of NK1R

5.1 Introduction

The main goal of this thesis was the investigation of processes involved in GPCR signal transduction in living cells using fluorescent techniques. The NK1R, a prominent member of the GPCR family and an important pharmaceutical target, was chosen for this purpose. Was it for the investigation of ligand binding, receptor oligomerization or receptor G protein interactions, in every case, it was of importance to construct a functional, fluorescently labelled receptor.

The classical way of protein labelling in living cells is by means of antibodies. In recent years however, new techniques have been developed, e.g. incorporation of nonnatural fluorescent amino acids [124] or fusion to green fluorescent proteins [125]. Even more recently, post-translational *in vivo* labelling has been introduced, where the fluorescent label is covalently or non-covalently attached to a fusion tag or fusion protein [126–132].

In the field of GPCR research EGFP has been used to study GPCR localization and trafficking [133]. Vollmer et al. [115] investigated ligand binding kinetics to EGFP labelled NK2R by FRET between a fluorescent ligand and the EGFP. GPCR fusions with variants of green fluorescent protein or *Renilla* luciferase (RLuc) led to new advances in the understanding of GPCR oligomerization [55]. Incorporating fluorescent nonnatural amino acids at specific sites was used to investigate structure and function of NK2R [124]. A combination of ECFP and EYFP or FlAsh has been used for a FRET assay to determine GPCR activation in living cells [113, 114].

In this work two approaches were chosen for labelling of NK1R in living cells: (i) mutants of EGFP and (ii) the acyl carrier protein (ACP) for post-translational labelling. In both cases a protein (EGFP or ACP) was genetically fused to either the N- or C-terminus of the NK1R.

This Chapter deals with the design and cloning of the NK1R fusion constructs and the confirmation of functionality of the NK1R fusion proteins by means of calcium signaling. Furthermore, it explains the basics of the ACP labelling technique.

5.2 Experimental Procedures

5.2.1 Materials

pSFV1::NK1R-his was a gift from Kenneth Lundstrom (BioXtal, CH); CoA-Cy3, CoA-Cy5 and AcpS were a kind gift from Nathalie George and Kai Johnsson (LIP-ISIC, EPFL, CH); the vectors encoding for EGFP, ECFP, and EYFP were from Clontech (Palo Alto, CA, USA); pCEP4 expression vector and Dulbecco's phosphate-buffered saline (D-PBS) were from Invitrogen (Breda, NL); pBluescript II KS+ was from Stratagene (La Jolla, CA, USA); the synthetic oligo-nucleotides (primers) were from MWG-Biotech (Ebersberg, D); L-723,138 was from Tocris Cookson (Langford, UK); EDTA was from Sigma (Buchs, CH).

Cell culturing, cell transfection and preparation, calcium ion signaling, ACP labelling, and fluorescence confocal microscopy were performed as described in Chapter 3.

5.2.2 Saturation of ACP Labelling

The ACP labelling saturation curve was obtained from HEK293 cells stably expressing ACP-NK1R. The cells were grown in 24-well plates and labelled with Cy5 (200 μl D-PBS, 10 mM $MgCl_2$, 5 μM CoA-Cy5, 1 μM AcpS). After 5, 10, 20, 40 and 60 minutes the cells were washed three times with D-PBS and detached with D-PBS supplemented with 5 mM EDTA, pelleted for 2 min at 1000 g and resuspended in 1 ml D-PBS. Fluorescence intensity of Cy5 was measured on a SPEX Fluorolog II (Instruments S.A., Stanmore, UK) with excitation and emission at 620 ± 1.8 nm and 664 ± 2.7 nm, respectively, and quantified using a CoA-Cy5 standard of known concentration determined by absorbance ($\varepsilon = 250'000\,\mathrm{M^{-1}cm^{-1}}$). Total protein content for the same sample was determined using the Bradford protein assay system (Pierce, Rockford, Il, USA) with BSA as standard.

5.3 cDNA Constructs of Neurokinin-1 Receptor

Polymerase chain reaction (PCR), DNA agarose gel preparation (analytic and preparative), restriction digest, ligation, DNA purification, plasmid amplification in *E.coli* XL1

blue strain, bacterial medium (2TY), were done according to standard protocols described in *Molecular cloning, a laboratory manual* [134]. The plasmid constructs were confirmed by restriction mapping and DNA sequencing.

Several NK1R fusion proteins were designed for different purposes, which are explained in more detail in the corresponding Chapters. Three types of genetic NK1R fusion constructs have been constructed. First, the gene encoding for ECFP or EYFP was fused to the intracellular C-terminus of NK1R. These constructs were mainly used to investigate interactions of NK1R with fluorescently labelled heterotrimeric G proteins by means of FRET (Chapter 8). Second, the gene encoding for EGFP was fused to the extracellular N-terminus of the NK1R. As EGFP is not secreted by cells, the N-terminal end of EGFP was further fused to the first 32 amino acids of the mouse serotonin receptor type 3A comprising a signal peptide to promote translocation of the N-terminal domain to the extracellular space. Different subtypes were constructed, where either EGFP or NK1R or both were truncated. This construct was used to investigate specific binding of a fluorescent ligand (Chapter 6). Third, the gene encoding for ACP was fused to the extracellular N-terminus of the NK1R in the same way as EGFP. This construct has been used to investigate specific ligand binding (Chapter 6) and oligomerization of NK1R (Chapter 7). Both, the EGFP-NK1R and ACP-NK1R carry in addition a FLAG- and a 10xHis-tag at their C-terminus. The wildtype NK1R (wtNK1R) was used as a reference for the different NK1R fusion constructs. Figure 5.1 illustrates the different NK1R constructs used in this thesis.

In the following we give a detailed description of the cloning steps to obtain the different NK1R plasmids used for this thesis. The original plasmid used for cloning was a pSFV1 Semliki Forest virus vector containing the human neurokinin 1 receptor cDNA with a C-terminal FLAG and 6xHis tag (pSFV1::NK1R-his). The primers used for cloning are found in Table 5.1.

wtNK1R

The gene encoding for the human NK1R was amplified by PCR on the template pSFV1::NK1R-his using the forward primer *fw-NheI-NK1R* and the reverse primer *rv-BamHI-NK1R* introducing a *NheI* restriction site and a Kozak sequence [135] at the 5' end, and a STOP codon and a *BamHI* restriction site at the 3' end of the hNK1R gene. The *NheI*/*BamHI* cut and purified fragment was ligated into the *NheI*/*BamHI* cut pCEP4 expression vector yielding pCEP4::wtNK1R.

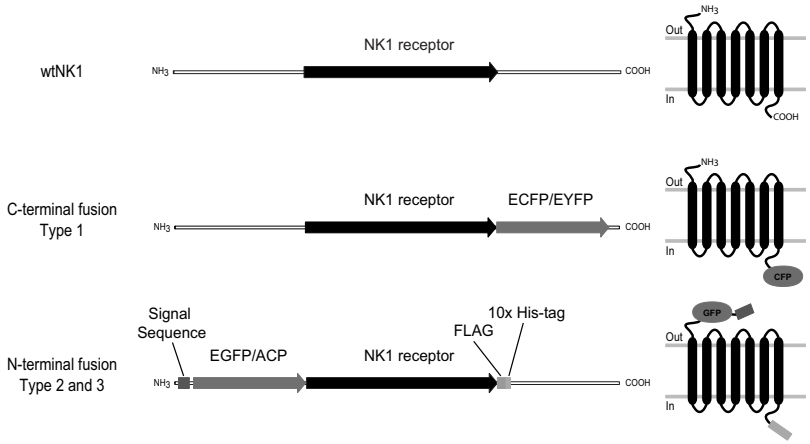

Figure 5.1: Overview of genetic constructs of NK1R. *wtNK1R, wildtype human NK1R; Type 1, NK1R with C-terminal ECFP or EYFP (representing NK1R-ECFP and NK1R-EYFP); Type 2 and 3, NK1R with N-terminal 5HT3 signal sequence and EGFP or ACP and C-terminal FLAG- and 10xHis-tag (representing the four different EGFP-NK1R constructs and ACP-NK1R).*

Primer	Sequence
fw-NheI-NK1R	5'-G GCC GGG CTA GCC ACC ATG GAT AAC GTC CTC CCG GTG G-3'
fw-SpeI-NK1R	5'-GCG CGG ACT AGT ATG GAT AAC GTC CTC CCG GTG-3'
fw-SpeI-d15NK1R	5'-GCG CGG ACT AGT TCC ACT AAC ACC TCG GAA CCC-3'
fw-EagI-ssGFP	5'-CCG CGG CCG ATG CGG CTC TGC ATC CCG-3'
fw-NheI-ssGFP	5'-G GCC GGG CTA GCC ACC ATG CGG CTC TGC ATC CCG-3'
fw-EagI-NK1R	5'-GGG CGG CCG ATG GAT AAC GTC CTC CCG G-3'
fw-SpeI-EGFP	5'-CGC GGC ACT AGT GGA GGT GGA GGA ATG GTG AGC AAG GGC GAG-3'
rv-BamHI-NK1R	5'-CCG CCG GGA TCC CTA GGA GAG CAC ATT GGA GGA GAA G-3'
rv-BamHI-his	5'-CCG CGC GGA TCC TTA ATG GTG ATG GTG ATG ATG ATG ATG ATG ATG GCT GCT GC-3'
rv-SpeI-EGFP	5'-GCG CCG ACT AGT CTT GTA CAG CTC GTC CAT GCC G-3'
rv-SpeI-trEGFP	5'-GCG CCG ACT AGT GAT CCC GGC GGC GGT CAC GAA CTC C-3'
rv-SpeI-NK1R(dS)	5'-CCG CCG ACT AGT GGA GAG CAC ATT GGA GGA GAA G-3'
rv-BamHI-EGFP	5'-GCC GCG GGA TCC TTA CTT GTA CAG CTC GTC CAT GC-3'

Table 5.1: Primers. *Primers used for the cloning of NK1R constructs. Restriction sites are underlined.*

EGFP-NK1R and Truncated Versions

The strategy was to use different restriction sites on both ends for correct orientation and to do the first cloning steps in the pBluescript II KS+ cloning vector with a multiple cloning site (MCS) containing *EagI-SpeI-BamHI*. First, four histidines were added to the C-terminal end of the NK1R-his to enlarge the 6xHis-tag to a 10xHis-tag. The resulting construct was inserted between the *SpeI* and *BamHI* site. In a second step the EGFP was inserted between the *EagI* and *SpeI* site. In a third and last step the EGFP-NK1R was amplified by PCR and inserted into the pCEP4 expression vector.

Furthermore, in some constructs the NK1R and/or the EGFP were truncated at the N-terminal and C-terminal end, respectively, yielding EGFP-NK1R, EGFP-d15NK1R, trEGFP-NK1R and trEGFP-d15NK1R (Figure 5.2). In trEGFP (truncated EGFP) the

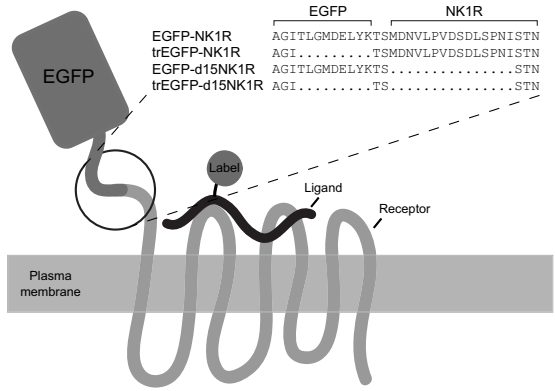

Figure 5.2: Truncated EGFP-NK1R and Ligand. *Schematic representation of EGFP-NK1R fusion proteins with fluorescently labelled ligand.*

last 9 C-terminal amino acids were deleted. In d15NK1R the first 15 amino acids of the NK1R were deleted. All 4 constructs have as a signal sequence the first 32 amino acids of the mouse serotonin receptor type 3A (5HT3) in front of the EGFP and a FLAG and 10xHis tag after the NK1R gene. The plasmid that served as a template for the signal sequence fused to EGFP (pBS::ssGFP) was made during the diploma work of Erwin Illegems. In the following EGFP-NK1R stands also for EGFP-d15NK1R, trEGFP-NK1R and trEGFP-d15NK1R.

In the first step the gene encoding for human NK1R with a C-terminal FLAG and 6xHis tag was amplified by PCR on the template pSFV1::NK1R-his using the forward primer *fw-SpeI-NK1R* (or *fw-SpeI-d15NK1R* for the truncated NK1R (d15NK1R)) and the reverse primer *rv-BamHI-his* introducing a *SpeI* restriction site at the 5' end, and

four histidines, a STOP codon and a *BamHI* restriction site at the 3' end of NK1R-his. The *SpeI*/*BamHI* cut and purified fragment was ligated into the *SpeI*/*BamHI* cut pBluescript II KS+ cloning vector yielding pBS::NK1R (or pBS::d15NK1R).

In the second step the gene encoding for signal sequence fused to the N-terminal end of EGFP (ssGFP) was amplified by PCR on the template pBS::ssGFP using the forward primer *fw-EagI-ssGFP* and the reverse primer *rv-SpeI-EGFP* (or *rv-SpeI-trEGFP* for the truncated EGFP (trEGFP)) introducing a *EagI* restriction site at the 5' end, and a *SpeI* restriction site at the 3' end. The *EagI*/*SpeI* cut and purified fragment was ligated into the *EagI*/*SpeI* cut pBS::NK1R (or pBS::d15NK1R) plasmid yielding pBS::EGFP-NK1R.

In the third step the gene encoding for EGFP-NK1R (and truncated versions), including the N-terminal signal sequence and the C-terminal FLAG and 10xHis tag, was amplified by PCR on the template pBS::EGFP-NK1R using the forward primer *fw-NheI-ssGFP* and the reverse primer *rv-BamHI-his* introducing a *NheI* restriction site and the Kozak sequence [135] at the 5' end, and a *BamHI* restriction site at the 3' end. The purified fragment was ligated into the *NheI*/*BamHI* cut pCEP4 expression vector yielding pCEP4::EGFP-NK1R.

NK1R-ECFP and NK1R-EYFP

The strategy was to use different restriction sites on both ends for correct orientation and to do the first two cloning steps in the pBluescript II KS+ cloning vector with a multiple cloning site (MCS) containing *EagI-SpeI-BamHI*. Since ECFP and EYFP defer only in a few point mutations towards the center of the nucleotide sequence, the same forward and reverse primers could be used.

In the first step the gene encoding for human NK1R was amplified by PCR on the template pSVF1::NK1R-his using the forward primer *fw-EagI-NK1R* and the reverse primer *rv-SpeI-NK1R(dS)* introducing a *EagI* restriction site at the 5' end, and a *SpeI* restriction site at the 3'. The Stop codon of NK1R was removed in the same step. The *EagI*/*SpeI* cut and purified fragment was ligated into the *EagI*/*SpeI* cut pBluescript II KS+ cloning vector yielding pBS::NK1R.

In the second step the gene encoding for ECFP (or EYFP) was amplified by PCR on the template pECFP-N1 (or pEYFP-N1) using the forward primer *fw-SpeI-EGFP* and the reverse primer *rv-BamHI-EGFP* introducing a *SpeI* restriction site and 4 glycine as a spacer at the 5' end, and a STOP codon and a *BamHI* restriction site at the 3' end. The *SpeI*/*BamHI* cut and purified fragment was ligated into the *SpeI*/*BamHI* cut pBS::NK1R plasmid yielding pBS::NK1R-ECFP (or pBS::NK1R-EYFP).

In the third and last step the gene encoding for NK1R-ECFP (or NK1R-EYFP) was amplified by PCR on the template pBS::NK1R-ECFP (or pBS::NK1R-EYFP) using the forward primer *fw-NheI-NK1R* and the reverse primer *rv-BamHI-EGFP* introducing a *NheI* restriction site and the Kozak sequence [135] at the 5' end, and a *BamHI* restriction site at the 3' end. The purified fragment was ligated into the *NheI*/*BamHI* cut pCEP4 expression vector yielding pCEP4::NK1R-ECFP (or pCEP4::NK1R-EYFP).

5.4 Functionality of NK1R constructs

Agonist binding to NK1R leads to the activation of the DAG/IP_3 and calcium signaling pathway (see Section 1.5) and is usually determined by measuring the IP_3 or calcium concentration. Here, the functionality of wtNK1R, NK1R-ECFP, and ACP-NK1R were verified by measuring the increase of intracellular calcium ion concentration upon receptor activation by addition of the agonist SP. Therefore, HEK293 cell lines stably expressing wtNK1R, NK1R-ECFP, or ACP-NK1R were produced and calcium concentration response curves for SP were obtain on a FLEX station and fitted with the Hill equation (Figure 5.3). The pEC_{50} values were the same for all three constructs, wtNK1R, NK1R-ECFP, and ACP-NK1R.

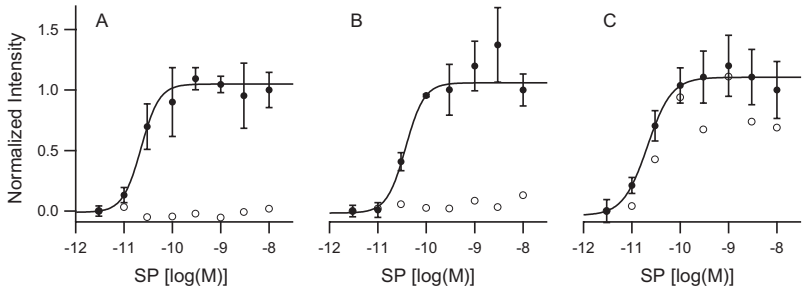

Construct	pEC_{50}
wtNK1R	10.6 ± 0.32
NK1R-ECFP	10.4 ± 0.20
ACP-NK1R	10.7 ± 0.34

Figure 5.3: Concentration response curves with pEC_{50} of SP for different NK1R constructs. *Substance P concentration response curves for wtNK1R (A), NK1R-ECFP (B), and ACP-NK1R (C) in absence (full circles) or in presence of 10 μM antagonist L-723,138 (empty circles). Data are means of 3-4 points ± S.D. in absence and means of 2 points in presence of L-723,138. pEC_{50} values were obtained by fitting with Hill equation (Eq. 3.1) ± 95% confidence interval.*

The pEC_{50} measured here are in agreement with the literature, where variations of one order of magnitude can be found depending on the cells used. Sagan et al. [136] reported a pEC_{50} of 9.2 by measuring the IP_3 accumulation for wtNK1R stably expressed in CHO cells. Dery et al. [137] reported a pEC_{50} of 9.2 by measuring the calcium increase with calcium-sensitive dyes for wtNK1R stably expressed in KNRK cells. Holst et al. [72] reported a pEC_{50} of 10.1 by measuring the IP_3 accumulation for wtNK1R transiently expressed in COS-7 cells. Martini et al. [79] reported a pEC_{50} of 9.4 also by measuring the IP_3 accumulation for wtNK1R transiently expressed in COS-7 cells.

We were not able to measure complete concentration-response curves for EGFP-NK1R, because of high background signals from EGFP. EGFP absorbs and emits in the same range as the calcium-sensitive dye from the Calcium 3 assay kit.

Nevertheless, the functionality of the EGFP-NK1R could be verified by measuring the increase of intracellular calcium ion concentration by using fluorescence confocal microscopy. The same procedures were used for loading the cells with the calcium-sensitive dye as for the experiments on the FLEX station. The fluorescence increase was recorded on single cells expressing the receptors. Figure 5.4 shows a representative time trace of a calcium response for EGFP-NK1R. The fluorescence signal increased

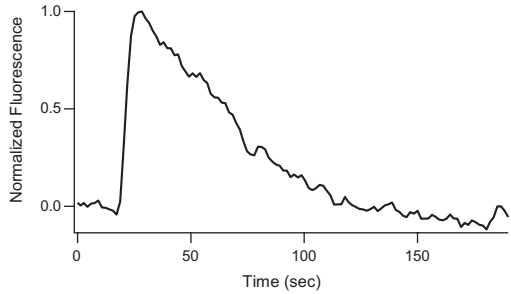

Figure 5.4: Calcium response of EGFP-NK1R. *Time course of the normalized fluorescence intensity of calcium sensitive probes inside the HEK 293 cells after stimulation of NK1R by addition of 3 nM SP (at 20 seconds on the time axis).*

steeply, reflecting an increase of the intracellular calcium ion concentration. These result were not quantitative, because they did not provide an EC_{50} value, but they showed that the EGFP-NK1R fusion protein is functional and able to activate the calcium signaling pathway. The length of the response ($\sim$100 sec) is consistent with literature reports [78, 138].

With respect to binding of antagonist (Figure 5.3, empty circles), there seemed to be

a difference between wtNK1R and ACP-NK1R. Cells expressing ACP-NK1R responded to SP even when preincubated with 10 μM antagonist L-732,138. This indicates either a lower affinity of antagonist for ACP-NK1R as compared to wtNK1R or even a complete loss of antagonist binding. It is insofar surprising, because ACP is fused to the N-terminus of NK1R, which takes part in the binding of the agonist SP but not of the non-peptide antagonist CP-96,345 [139, 140]. The same effect has been observed for EGFP-NK1R and needs further investigation.

5.5 ACP Labelling

Several methods for post-translational labelling of proteins have been developed recently [127–132]. The method used for this work is based on the acyl carrier protein (ACP) and has been described by George et al. [128]. The labelling method makes use of the post-translational modification of ACP by phosphopantetheine transferase (PPTase), leading to the transfer of 4'-phosphopantetheine from coenzyme A (CoA) to a serine residue of ACP (Figure 5.5). The fluorescent dyes Cy3 and Cy5 attached to the phos-

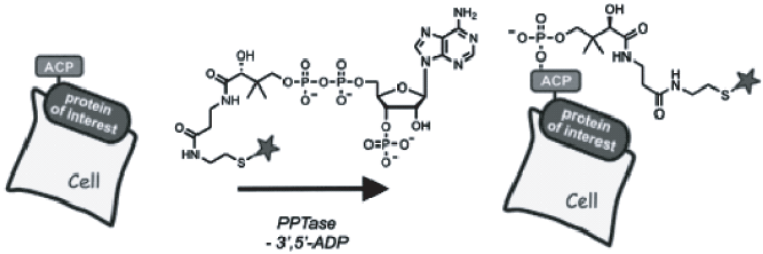

Figure 5.5: ACP labelling technique. *The fluorescent label (star) attached to CoA is transferred together with 4'-phosphopantetheine by PPTase to ACP. The ACP is genetically fused to the extracellular side of the protein of interest (from [128]).*

phopantetheine on CoA are transferred to the ACP together with 4'-phosphopantetheine during the labelling process. The ACP/PPTase pair used here is from *Escherichia coli*. PPTase from *E. coli* (AcpS) can be easily purified and possess a relative narrow substrate specificity with respect to ACP. [128]

The ACP labelling time course with Cy5 (Figure 5.6 A) showed that 40 minutes incubation at 19 °C is sufficient for the labelling of all receptors. Furthermore, the ACP-NK1R could be labelled with Cy3 and Cy5 simultaneously by mixing the substrates in a 1:1 ratio before adding to the cells (Figure 5.6). Only receptors that are

correctly expressed in the plasma membrane are accessible for the labelling, which prevents background fluorescence arising from receptors inside the cells. In addition, all the cells expressing ACP-NK1R were labelled with both fluorophores.

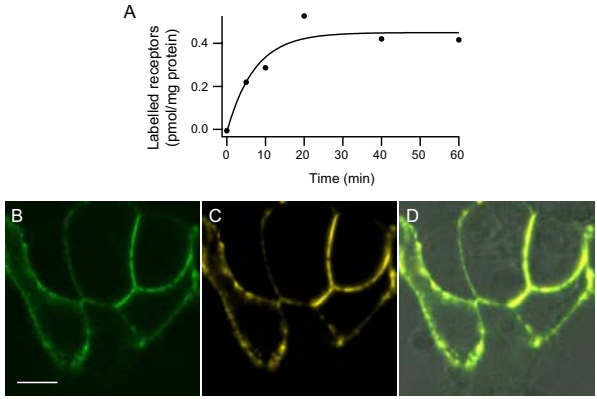

Figure 5.6: Labelling of ACP-NK1R fusion protein on cell surface. *A, time course of labelling with Cy5 on ACP-NK1R stably expressed in HEK293 cells. B-D, fluorescence confocal micrographs showing HEK 293 cells transiently expressing ACP-NK1R labelled with Cy3 (B) and Cy5 (C). D, transmission image of the same area with fluorescence micrographs B and C superimposed. Scale bar represents 10 µm.*

5.6 Conclusion and Outlook

The NK1R has been labelled using two approaches. First, C- or N-terminal fusion of EGFP, and second, N-terminal fusion of ACP and post-translational labelling with Cy3 or Cy5. All fluorescent NK1R constructs were functional with respect to agonist binding and calcium signaling. In the case of N-terminal EGFP and ACP fusions, the affinity of the non-peptide antagonist was changed dramatically or even lost, and further investigation is needed. Nevertheless, the constructs used in this thesis are functional with respect to agonist binding and activation of the calcium signaling pathway. Furthermore, it has been shown that 40 minutes at 19 °C is sufficient for the complete labelling of ACP-NK1R receptors expressed in HEK293 cells and that ACP-NK1R receptors can be labelled simultaneously with at least two different dyes.

The NK1R constructs can be used for several studies such as ligand binding, trafficking, oligomerization, and protein-protein interactions.

Chapter 6

Monitoring Specific Ligand Binding by FRET

6.1 Introduction

GPCR mediated cellular signaling is initiated by the binding of a ligand to its cognate receptor. Since the development of radiolabelled ligands many binding studies have been performed leading to insight in binding affinities, structures of binding pocket, topography models of receptors, and (relatively slow) binding kinetics. Fluorescent ligands have been used for the same kind of studies with the advantage, that they are much more sensitive, that they can be applied to living cells using fluorescence microscopy, and therefore give access to spatial distributions in time, and in addition they allow the detection of fast kinetics [141].

For GPCRs fluorescent ligands have been used to probe binding domains [140,142], to investigate ligand binding by fluorescence anisotropy [143] or on immobilized receptors by TIRF [144] (see Chapter 9), to follow receptor internalization [76,145], and to monitor receptor diffusion by single molecule spectroscopy [146].

The NK1R comprises several binding affinities for SP, which are attributed to different receptor states, depending on the coupling to heterotrimeric G proteins: (1) uncoupled receptors, (2) receptors coupled with $G\alpha_q$, and (3) receptors coupled with $G\alpha_s$ [72, 147–149]. Ligand binding kinetics would give further insight into the different states of the receptor and its functionality.

FRET is a promising method to directly measure specific ligand binding with high time resolution. It has been applied to measure fast kinetics of ligand binding to tachykinin NK2 receptor [115, 116, 150], the chemokine CXCR4 receptor [151] and the

muscarinic M1 receptor [152, 153]. Figure 6.1 shows a scheme of the principle of this method, where a donor is fused to the extracellular end of the receptor and the ligand is labelled with an acceptor. Upon ligand binding the donor-acceptor distance is suffi-

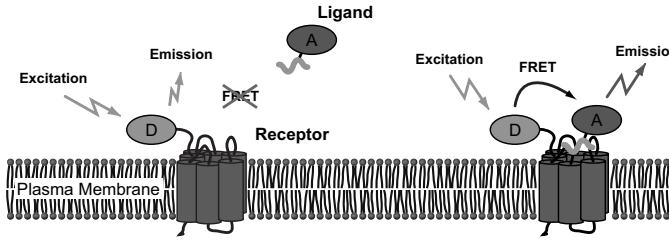

Figure 6.1: FRET between ligand and receptor. *Scheme showing the principle of FRET between a ligand and its receptor. The donor (D) is fused to the N-terminal end of the receptor, and the acceptor (A) is conjugated to the ligand.*

ciently small to quench the donor fluorescence and to sensitize the acceptor emission. By recording the quenching of the donor one can directly measure the specific ligand binding.

Here, we labelled the NK1R at its extracellular N-terminus by either fusion of the fluorescent protein EGFP or the ACP with subsequent labelling by Cy3 (see Chapter 5). This Chapter deals with the synthesis and characterization of fluorescent derivatives of the NK1R agonist (SP) to act as an acceptor for EGFP or Cy3. Preliminary investigation of specific ligand binding, using FRET, revealed the advantages of the ACP labelling over the EGFP labelling.

6.2 Experimental Procedures

Tetramethylrhodamine-labelled substance P (SP-TMR) was from Molecular Probes (Eugene, OR, USA); NK1R antagonist L-732,138 was from Tocris Cookson (Langford, UK); Ac-Substance P (AcSP) was synthesized by K. Servis (UNIL, Lausanne, CH); Cy3B and Cy5 succinimidyl esters were from Amersham Biosciences (Buckinghamshire, UK).

Cell culturing, cell transfection and preparation, calcium ion signaling, ACP labelling, and fluorescence confocal microscopy were performed as described in Chapter 3. The genetic constructs used in this chapter are wtNK1R, NK1R-ECFP, EGFP-NK1R, EGFP-d15NK1R, trEGFP-NK1R, trEGFP-d15NK1R. Detailed description of the molecular cloning and the construction of the plasmids can be found in Chapter 5.

6.2.1 Synthesis of SP-Cy3B and SP-Cy5

2 mg of N-terminally acetylated substance P (AcSP) in 0.5 ml *N*,*N*-dimethylformamide (DMF) and 50-100 μl 100 mM carbonate buffer at pH 8.2 was mixed with a solution of 0.9 molar equivalent of Cy3B or Cy5 succinimidyl esters in 100-500 μl DMF. The reaction was complete (> 90%) after 1 hour at room temperature. The solvents were evaporated by lyophilization. The solid obtained was dissolved in 300 μl of MeOH:H_2O:5 M HCl (85:14:1) and purified by semi-preparative silica gel thin layer chromatography (TLC, 0.25 mm layer thickness), using 5% NH_4OH in MeOH as the mobile phase. The colored band on the top was the non-reacted fluorophore, the large central band was the product and the small other bands were impurities from the fluorophore and side-products. The part of the TLC with the product was detached and extracted three times with MeOH:H_2O:5 M HCl (85:14:1). The final volume was around 3-4 ml. The concentration of SP-Cy3B and SP-Cy5 was measured by absorbance spectroscopy ($\varepsilon_{\text{Cy3B}} = 130'000\,\text{M}^{-1}\text{cm}^{-1}$, $\varepsilon_{\text{Cy5}} = 250'000\,\text{M}^{-1}\text{cm}^{-1}$). The solution with the product was aliquoted, dried and stored at -20°C.

6.3 Results and Discussion

6.3.1 Synthesis of SP-Cy3B and SP-Cy5

The physiological agonist for NK1R is substance P (SP),

H-Arg-Pro-Lys-Pro-Gln-Gln-Phe-Phe-Gly-Leu-Met-NH_2,

a neuropeptide that belongs to the group of tachykinins and consist of 11 amino acids with an amidated C-terminus [64]. C-terminal amidation occurs during biosynthesis. All mammalian tachykinins known up to now share a common C-terminal amino acid sequence (FXGLM-NH_2), which is essential for its binding to the receptors. The N-terminus seems to be less important for ligand binding and is therefore suitable for conjugation of a fluorophore, as was shown by Tota et al. [143] who labelled SP with fluorescein at Lys3 and retained high affinity binding. Dansyl or fluorescein were also attached at residue 1, 3, 8 and 11 of SP, where labelling at residue 3 showed the smallest decrease in affinity as compared to non-labelled SP [140]. Molecular Probes, Inc. (Eugene, OR, USA) offers five fluorophore-conjugated analogs of SP, where the fluorophores Alexa 488, BODIPY Fl, fluorescein, Oregon Green 488 and tetramethylrhodamine were conjugated to the third amino acid of SP, Lys3. Except for SP-Alexa488, all of them were shown to bind to NK1Rs and induce a calcium response in living cells [154]. Also

Cy5 has been conjugated to SP at Lys3 and the resulting derivative retained high affinity for NK1R [155].

The peptide SP has two reactive amino groups, the N-terminal amino group and the ε-amino on the lysine side chain. Both amino groups in SP have a similar pK_a value and could not be selectively labelled with succinimidyl esters of the fluorophores. In order to label SP with one fluorophore only, we used a SP analogue, where the N-terminal amine was replaced by a non reactive acetyl-group. Thus, the fluorophores were attached selectively to the lysine at position 3. Cy3B and Cy5 were chosen as fluorophores to act as acceptor for EGFP and Cy3, respectively (Table 6.1). Although the commercially available tetramethylrhodamine (TMR) conjugated SP would be also suitable as an acceptor for EGFP, the Cy3B was used because it shows a longer Förster distance (R_0).

	Molar Extinction	Absorption Maximum	Emission Maximum	Spectral Overlap	Förster Distance (R_0)
Cy3B	130'000	566	580	$4.14 \cdot 10^{15}$	58.0
Cy5	250'000	646	664	$6.79 \cdot 10^{15}$	50.0
TMR	85'000	560	575	$2.72 \cdot 10^{15}$	54.1

Table 6.1: Properties of the fluorophores conjugated to SP. *Extinction coefficient in $M^{-1}cm^{-1}$ (Cy3B and Cy5 from Amersham, TMR from Molecular Probes), absorption and emission spectra maxima in nm, calculated spectral overlap (in $M^{-1}cm^{-1}nm^4$), and Förster distance R_0 (in Å) for EGFP-Cy3B and Cy3-Cy5, respectively. Donor quantum yields used for the calculation of the spectral overlap were 0.6 and 0.15 for EGFP and Cy3, respectively (from Clontech and Amersham). TMR, tetramethylrhodamine.*

6.3.2 Specific Ligand Binding and Receptor Localization

Studies in Chapter 5 showed that EGFP-NK1R and ACP-NK1R are functional with respect to SP binding and calcium signaling. Next, we wanted to know if the fluorescent SP derivatives also bind to these receptors. Therefore, the different receptors were expressed in HEK293 cells and specific ligand binding was monitored by confocal microscopy.

As shown in Figure 6.2, all four EGFP-NK1R constructs were able to bind fluorescent derivatives of SP selectively, confirmed by (i) removal of fluorescent ligands with an excess of unlabelled SP, and (ii) absence of SP binding on cells not expression EGFP-NK1R. Furthermore, confocal micrographs of the four different EGFP-NK1R fusion constructs showed partial localization of EGFP-NK1R in the plasma membrane with a considerable fraction of immature and incompletely processed proteins inside the cells.

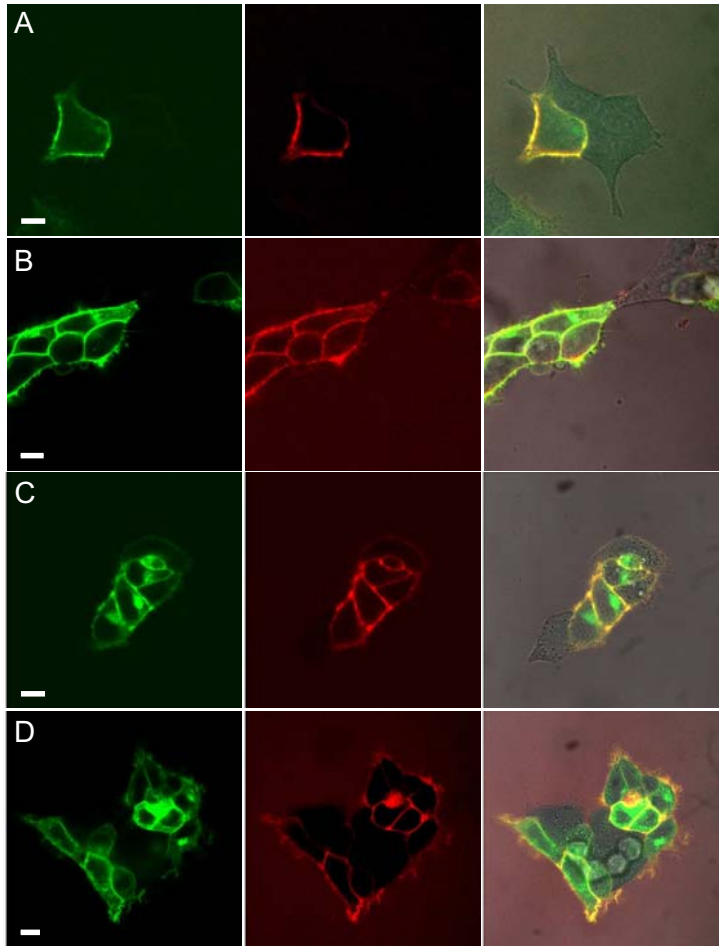

Figure 6.2: Expression of EGFP-NK1R constructs. *Confocal micrographs showing, first column (green), EGFP-NK1R fusion constructs transiently expressed in HEK293 cells. Second column (red), binding of fluorescent SP derivatives. Third column, white light transmission image of the same area with fluorescence images superimposed. A, EGFP-NK1R with 100 nM SP-TMR; B, EGFP-d15NK1R with 100 nM SP-TMR; C, trEGFP-NK1R with 50 nM SP-Cy3B; D, trEGFP-d15NK1R with 50 nM SP-Cy3B. Scale bars represent 10 μm.*

Because the ligand only binds to receptors expressed in the plasma membrane, the fluorescence signal of labelled SP colocalized only with the EGFP signal from receptors in the plasma membrane. This can be seen very well in the micrographs in the third column of Figure 6.2, where the overlay of red and green signal turns yellow. The fraction inside the cells varied from day to day and is probably due to variations of the cell cycle.

In comparision, Figure 6.3 A and B show ligand binding to the Cy3-labelled ACP-NK1R. The colocalization of SP-Cy5 with the labelled receptor indicates that only receptors accessible to SP and therefore located at the cell surface are labelled with the ACP labelling technique. The specific SP-Cy5 binding was further confirmed by competition with excess of unlabelled SP. Furthermore, the ACP-NK1R internalized

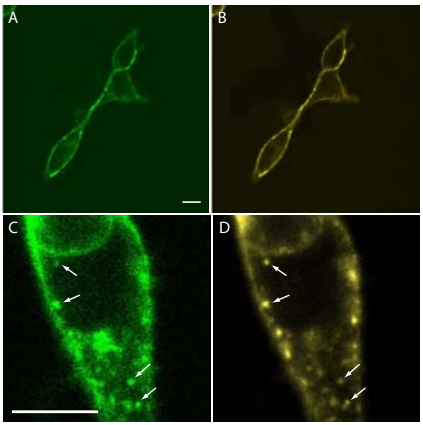

Figure 6.3: Expression of ACP-NK1R in HEK 293. *A-B, fluorescence confocal micrographs showing HEK 293 cells transiently expressing ACP-NK1R labelled with Cy3 (A) and the agonist SP-Cy5 at 100 nM bound to the receptor (B). C-D, fluorescent confocal micrograph showing HEK293 cells stably expressing ACP-NK1R labelled with Cy3 (C) after 15 minutes incubation with 100nM SP-Cy5 (D) at 20° C. Arrows indicate internalized NK1R and SP-Cy5. Scale bars represent 10μm.*

together with SP-Cy5 within 15 minutes after ligand application at room temperature (Figure 6.3 C and D).

Similar to ACP-NK1R and SP-Cy5, internalization of SP-TMR was observed after 30 minutes incubation at room temperature. Surprisingly, hardly any signal arising from the EGFP fused to the receptor could be detected inside the cells, whereas SP-TMR was detectable (Figure 6.4). A reason for this effect could be the acidic environment of early endosomes. It is known that the fluorescence emission of EGFP decreases at low

pH [156–158], and EGFP fused to the extracellular side of the receptor is in the lumen of the early endosomes after internalization.

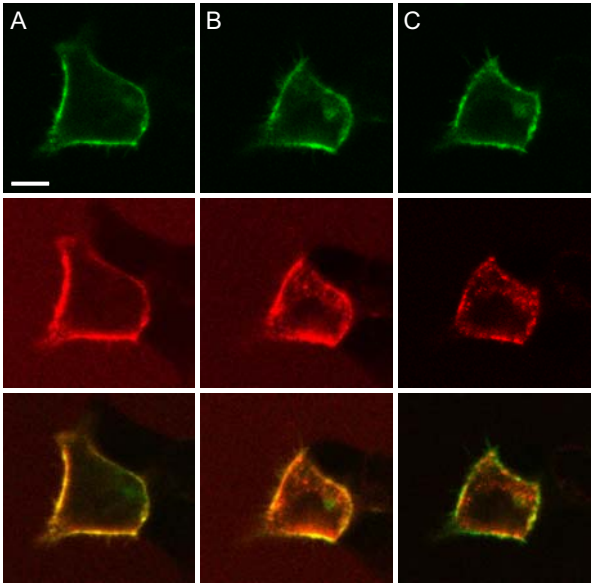

Figure 6.4: EGFP-NK1R internalization. *Confocal micrographs showing EGFP-NK1R expressed in HEK293 cells, 1 (A) and 30 (B) minutes after addition of 100 nM SP-TMR. C, removal of SP-TMR by antagonist L-732,138. First and second row, fluorescent signal from EGFP and SP-TMR in green and red, respectively. Third row, overlay of EGFP and SP-TMR signal. Scale bar represents 10 μm.*

Addition of excess concentration of the antagonist L-732,138 removed partly the SP-TMR on the cell surface. The remaining SP-TMR can be attributed to either ligands with very slow off-rates or ligands bound to internalized receptors present in small vesicles attached to the plasma membrane. SP-bound NK1Rs expressed in KNRK cells internalized at 18°C within minutes into small vesicles beneath the plasma membrane [77].

The observed ligand binding and subsequent receptor internalization show that the fluorescent ligands act as agonists. In the following part detailed cellular calcium response after receptor activation are presented.

6.3.3 Calcium Response of Fluorescent SP Derivatives

As mentioned before, activation of NK1R leads to the releases of calcium ions from internal stores and thereby increases the intracellular calcium ion concentration. This effect can be monitored with calcium-sensitive dyes. The increase of the intracellular calcium ion concentration is related to the increase in fluorescence of the calcium-sensitive dye and can be measured on a FLEX station. A concentration response curve is measured plotting the amplitude of the intensity increase versus the agonist concentration. The data points can be fitted with the Hill equation (Eq. 3.1, Chapter 3).

Such experiments were performed for the newly synthesized fluorescent SP analogues, SP-Cy3B and SP-Cy5, as well as the commercial available SP-TMR. Figure 6.5 shows the concentration response curves and the pEC_{50} values for the ligands SP, SP-Cy3B and SP-TMR, using a HEK293 stably expressing NK1R-ECFP. SP-Cy3B and SP-TMR

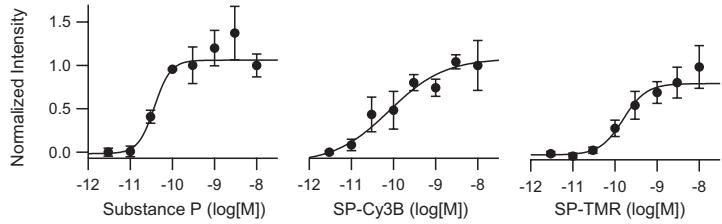

Ligand	pEC_{50}
Substance P	10.4 ± 0.2
SP-Cy3B	10.1 ± 0.9
SP-TMR	9.8 ± 0.5

Figure 6.5: Concentration response curves with pEC_{50} of fluorescent SP derivatives. *Concentration response curves of SP, SP-Cy3B, and SP-TMR on HEK293 cells stably expressing NK1R-ECFP. Data are means of 3-4 points ± S.D. pEC_{50} values were obtained by fitting with the Hill equation ± 95% confidence interval.*

were shown to act as agonists with a pEC_{50} in the same range as SP. As a control, cells preincubated with 10 μM antagonist L-732,138 showed no response at all.

The ability of SP-Cy5 to activate the calcium signaling pathway was also verified, using HEK293 cell lines stably expressing wtNK1R and ACP-NK1R (Figure 6.6). The pEC_{50} for SP on both wtNK1R and ACP-NK1R was the same, 10.6 ± 0.3 and 10.7 ± 0.3, respectively. The pEC_{50} for SP-Cy5 on both wtNK1R and ACP-NK1R was also the same, 9.2 ± 0.6 and 8.9 ± 0.5, respectively, but with about 50 times higher pEC_{50} values.

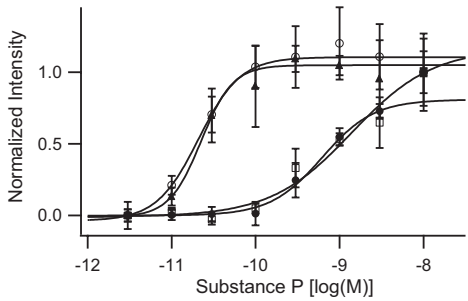

	SP	SP-Cy5
wtNK1R	10.6 ± 0.3	9.2 ± 0.6
ACP-NK1R	10.7 ± 0.3	8.9 ± 0.5

Figure 6.6: Concentration response curves of SP and SP-Cy5 on wtNK1R and ACP-NK1R. *Concentration-response curve for SP on wtNK1R (triangles) and ACP-NK1R (empty circles), and for SP-Cy5 on wild type NK1R (full circles) and ACP-NK1R (empty squares). pEC_{50} values are shown in the Table. Data are means of 3-4 points ± S.D. pEC_{50} values were obtained by fitting with Hill equation (Eq. 3.1) ± 95% confidence interval.*

6.3.4 Quenching of Fluorescently Labelled NK1R

GPCR mediated cellular signaling is initiated by the binding of a ligand to its receptor. Ligand binding kinetics can be monitored in real-time by FRET, where the receptor is labelled with a donor and the ligand carries the acceptor. Upon ligand binding the donor fluorescence is quenched due to FRET. With the fluorescent NK1R constructs and the fluorescent ligands, the tools to investigate specific ligand binding by FRET were available.

Two examples with the first approach, where EGFP has been fused to the NK1R, are shown in Figure 6.7. The best results were achieved with SP-Cy3B as ligand and the two NK1R constructs, where the EGFP is truncated (trEGFP-NK1R and trEGFP-d15NK1R). The time courses of EGFP intensities where calculated from a region of interest (ROI) over a part of the plasma membrane. The intensities were background subtracted and normalized. Selection of the membrane with a ROI was necessary, because of the high intracellular background signal from incompletely processed EGFP-NK1R.

Specific ligand binding could be observed through quenching of EGFP on trEGFP-NK1R and on trEGFP-d15NK1R, confirmed by the increase of the signal after application of excess of non-labelled SP. The quenching was more pronounced for trEGFP-

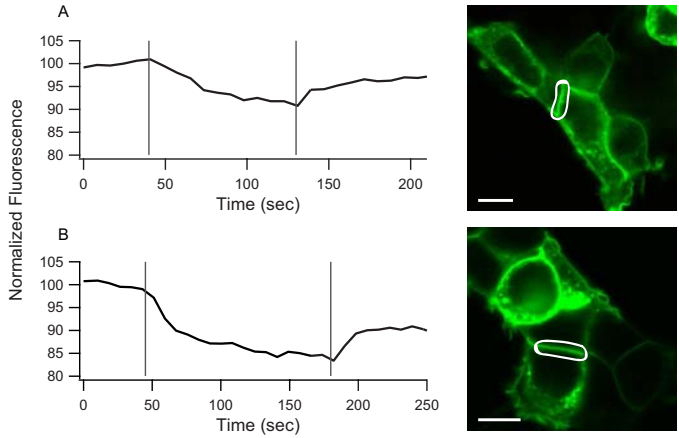

Figure 6.7: Quenching of EGFP-NK1R. *50nM SP-Cy3B were added to HEK293 cells transiently expression either trEGFP-NK1R (A) or trEGFP-d15NK1R (B). Curves are time traces of the normalized fluorescence from EGFP. First vertical line indicates time when SP-Cy3B was applied (40 s and 45 s, respectively). Second vertical line indicates application of excess (2.5 µM) of non-labelled SP (130 s and 180 s). Fluorescence confocal micrographs represent EGFP signal and ROI from which the intensity time curves were calculated. Scale bars represent 10 µm.*

d15NK1R. This is probably due to a shorter distance between donor and acceptor. The reason why the EGFP signal did not recover its intensity as before the quenching is not clear. It could be due to photobleaching, internalization of receptors with agonist still bound, or an additional slow dissociation rate of the agonist.

As mentioned before, the ACP method allows the specific labelling of receptors at the cell surface and therefore does not create intracellular background fluorescence from incompletely processed receptors. In Figure 6.8, SP-Cy5 (116 nM) was applied to HEK293 cells at 19°C stably expressing Cy3-labelled ACP-NK1R. The fluorescence signal of Cy3 decreased simultaneously with the increase of Cy5 fluorescence, indicating specific binding of agonist SP-Cy5 to the receptor.

The mixing time for SP-Cy5 to reach the desired equilibrium concentration is in the range of 3-4 seconds (Figure 6.8, top). The second trace in Figure 6.8 shows fluorescence changes with time constants in the range of 30-40 seconds. It is not obvious if the changes observed in the short time regime is a combination of the mixing time and an additional fast association time for SP-Cy5 to NK1R.

In contrary, the third trace in Figure 6.8 reveals specific binding of SP-Cy5 to Cy3-labelled ACP-NK1R, because only bound ligands are able to quench the Cy3-labelled

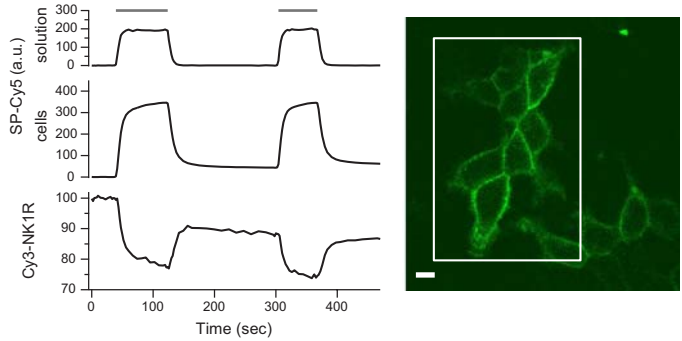

Figure 6.8: Quenching of ACP-NK1R. *116 nM SP-Cy5 was applied with the pipette of a perfusion system a few micrometers away from the cell at 19 °C. Application durations depicted by bars above the curves were 84 s (first) and 63 s (second). Top curve represents fluorescence intensity (a.u.) of SP-Cy5 in the buffer next to the cells. Middle curve represents fluorescence intensity (a.u.) of SP-Cy5 binding to ACP-NK1R. Bottom curve represents the time course of the normalized fluorescence intensity of Cy3-labelled ACP-NK1R over the same region of interest (ROI) as for SP-Cy5 binding. Fluorescence confocal micrograph of HEK293 cells transiently expressing ACP-NK1R labelled with Cy3 with white box indicating the ROI for the middle and bottom curves. Scale bar represents 10 μm.*

ACP-NK1R fluorescence by FRET. Here, we can clearly distinguish two association time constants: a short time constant in the range of 3-5 seconds, which might be influenced by the mixing time, and a long time constant in the range of 30-40 seconds.

From the SP-Cy5 trace alone it is not possible to distinguish between specific and unspecific binding, because this signal is the sum of the intensities of specific and unspecific binding of SP-Cy5, the SP-Cy5 in solution, and internalized SP-Cy5. The internalization of the SP-Cy5 remains in the trace after washing with buffer. However, the quenching of Cy3 shows only the specific binding, since non-bound ligand cannot quench the Cy3 bound to the receptor.

Applying the agonist SP-Cy5 for 84 seconds yielded 23% quenching of the Cy3. After washing with buffer the agonist was only partially removed and Cy3 remained quenched by 9%. After adding the ligand for another 63 seconds and then washing with buffer, 13% of Cy3 remained quenched. We attribute the remaining ligand to a slow dissociation process in the range of hours or internalization to small vesicles, which are bound to the cytoplasmic side of the plasma membrane.

ACP-NK1R, trEGFP-NK1R and trEGFP-d15NK1R showed a similar degree of quenching, considering the concentrations of fluorescent SP added (116 nM and 50 nM for SP-Cy5 and SP-Cy3B, respectively). Comparing the Förster distance (R_0) for the

DA pairs EGFP/Cy3B (58 Å) and Cy3/Cy5 (50 Å), and noting the fact that there was no need for truncation in ACP-NK1R construct, suggest that ACP-NK1R is more suitable for these kind of experiments. Furthermore, there is no need to select part of the membrane to evaluate the quenching, as it was the case for the EGFP-NK1R (micrograph in Figure 6.7). Using the ACP-NK1R, an area including all the cells (micrograph in Figure 6.8) can be selected, because there is no background fluorescence from incompletely processed fluorescent NK1Rs. This is especially advantageous if one wants to work with cell suspensions instead of single cells.

6.4 Conclusions and Outlook

Two fluorescent ligands for the NK1R, SP-Cy3B and SP-Cy5, were synthesized to investigate ligand binding by FRET. The fluorophores were attached to the lysine at position 3 of the peptide, and the resulting SP derivatives bound specifically to the NK1R and were shown to act as agonists.

SP-Cy3B turned out to be better for FRET measurements with EGFP-NK1R than the commercially available SP-TMR. Futhermore, the truncation of EGFP was required to obtain FRET. In the case of other GPCRs the N-terminus had to be truncated as well to achieve good quenching signals [115, 152]. The ACP-NK1R fusion construct, where no truncation was necessary, is a good alternative to EGFP-NK1R. Several donor-acceptor combinations can be used on the same fusion protein, and no tedious and time consuming cloning is required. In addition, the choice of good fluorophores is much larger than of fluorescent proteins.

The tools are now available for further detailed investigations of ligand binding kinetics or endocytosis. It would also be interesting to try the labelling of the ACP-NK1R with fluorophores with a long fluorescence life-time, such as lanthanides, to enhance the signal-to-noise ratio for time-resolved FRET investigations. The internalization could be studied with a FRET-based approach, using the Cy3-labelled ACP-NK1R and CypHer 5 conjugated SP. CypHer 5 is a pH sensitive fluorophore that becomes fluorescent at acidic pH as it is present in intracellular endosomes [145].

Although EGFP-NK1R did not quite fulfil our hopes, it showed to be useful in other studies. Lill et al. [146] used the stable EGFP-NK1R cell line for single molecule experiments, were a reduction of receptor diffusion within the first second after ligand binding was shown. Guignet et al. [129] reversibly quenched the EGFP on the extracellular side by binding NTA-I, a quencher conjugated to NTA, to the 10xHis-tag at the cytoplasmic side of the receptor.

Chapter 7

Oligomerization and Compartmentalization of NK1R

7.1 Abstract

Many G protein-coupled receptors (GPCRs) tend to form dimers or higher oligomers which might be of importance for cellular signalling. Here we investigate the oligomerization state of the neurokinin-1 receptor (NK1R) in single living cells by FRET using an in vivo labelling method recently developed by our laboratories. The NK1R was first expressed in form of a fusion protein with an acyl carrier protein (ACP). Subsequently, small fluorophores were covalently bound to the ACP moiety of the ACP-NK1R. This approach offers several substantial improvements as compared to labelling by classical fluorescent protein derivatives: (i) The practically unlimited free choice of the label molecule makes it possible to use fluorophores optimized for FRET measurements. (ii) Because labelling occurs exclusively at the cell surface, only correctly assembled receptor proteins are accessed; in consequence no intracellular fluorescence background appears yielding yet unreached signal to noise ratios even at low receptor concentrations. (iii) Simultaneous dual color labelling e.g. with donor and acceptor of precisely defined and controlled molar ratios between the two fluorophores can be realized which is prerequisite of reliable and quantitatively evaluable FRET measurements in living cells. Our single cell FRET measurements exclude the presence of dimeric or higher oligomeric NK1Rs but indicate that the NK1Rs tend to concentrate in microdomains.

7.2 Introduction

G protein-coupled receptors (GPCR) were for a long time presumed to function as monomers according to the prevailing model: One ligand molecule - one receptor - one G protein [23]. But recently, dimeric or higher oligomeric structures have been found for several GPCRs using biochemical (co-immunoprecipitation) and biophysical methods (BRET and FRET) [9, 22, 46, 54–58]. Oligomerization can occur between the same receptor subtypes (homo-oligomerization) or between different receptor subtypes (hetero-oligomerization) and can be constitutive or ligand-dependent. Preformed oligomers of some GPCRs may serve as a signaling platform that retains its multimeric status throughout the process. Other GPCRs may cycle through monomeric and multimeric states in a ligand-regulated process [27]. GPCR hetero-dimerization can result in altered ligand selectivities and distinctive coupling to signal transduction pathways, providing an additional source of richness for the fine-tuning of cellular signaling.

BRET and FRET assays are presently often used to investigate GPCR oligomerization [55], because they allow in-vivo measurements. As a particular advantage, FRET and BRET measurements allow quantitative determinations of the presence and amount of oligomerization by investigating the dependency of the BRET or FRET signals on the donor-acceptor ratios and on the overall expression levels. Yet, there is only a few reports on such quantitative cellular studies on GPCRs. Ayoub et al. [159] used BRET competition assays with melatonin receptors to determine that the transfer of energy resulted from the formation of dimers and not of higher oligomers. To investigate β1- and β2-adrenergic receptor homo- and hetero-dimerization Mercier et al. [160] plotted the percent maximal BRET level against the donor-acceptor (DA) ratio to distinguish between dimers and trimers. Similar experiments were done with serotonin 5-HT_{2C} receptors [161] using a FRET assay.

A major limitation for quantitative FRET and BRET measurements is the quality of the signals, which is directly related to the type of fluorophore used. Most studies use fluorescent proteins, respectively luciferase for BRET, which both are accompanied with background signals of incompletely processed proteins inside the cell and from the unfavorable emission wavelengths in a spectral region where the autofluorescence of the cells is high. This and the difficulties to adjust DA ratios complicate quantitative estimations. In contrast, post-translational labelling methods [127–132] are more versatile and offer substantially increased signal-to-noise ratios and control of DA ratios. In particular, we have shown previously the feasibility of ACP labelling [128] in FRET studies and its advantages over labelling using fluorescent proteins: The possibility to choose

fluorophores, an exclusive labelling of the receptors translocated to the membrane and straightforward tunability of the acceptor-donor ratio. ACP labelling is based on the enzymatic transfer of fluorescently labelled 4'-phosphopantetheine from coenzyme A (CoA) to an acyl carrier protein (ACP) fused to the protein of interest [128].

In the present studies we chosen the neurokinin-1 receptor (NK1R) as a prototypical example of a GPCR. The NK1R mediates processes such as nociception, neural inflammation or smooth muscle contraction. NK1R enjoys considerable attention as a drug target for instance for treatments against depression. Therefore, it is of importance to investigate the organization, i.e. oligomerization and localization of the NK1R in cell plasma membrane, and to correlate it with its function. It has been shown previously that the neurokinin-1 receptor can form hetero-dimers with the human μ-opioid receptor [82]. However, to our knowledge, there is no report on whether the NK1R is also able to form homo-dimers. Biochemical studies indicate that the NK1R is most probably localized in rafts microdomains in the cell plasma membrane [73]. This has also been proposed by Holst et al. [72] investigating NK1R $G\alpha_q$ and $G\alpha_s$ fusion proteins.

Here, we made use of the advantages of the ACP labelling technique to investigate whether or not NK1R oligomerizes in living cells using sensitized acceptor emission based FRET microscopy (Chapter 4). The NK1R fused with ACP (ACP-NK1R) was labelled simultaneously with a defined ratio of Cy3 and Cy5 as donor and acceptor, respectively. High FRET efficiencies with a strong dependency on DA ratio were observed for receptor expression levels around 300 receptors/μm^2. The dependency was not linear, excluding that the FRET signals was due to the presence of dimers. It was furthermore possible to rule out the presence of oligomers from the sharp dependency of the FRET signal on the expression level. In general, the FRET data can be explained as resulting from stochastic encounters of the donor and the acceptor assuming that the effective surface density is about 100 times higher as expected as a result of the compartmentalization of the NK1R into microdomains.

7.3 Experimental Procedures

7.3.1 Materials

N,N-diethyl-2-[4-(phenylmethyl) phenoxy] ethanamine labelled with Cy5 (DPPE-Cy5) was a kind gift from Silke Mark of the Ludwig Institute for Cancer Research (Epalinges, CH); 1,2-dioleoyl-*sn*-glycero-3-[phosphor-*rac*-(1-glycerol)] (DOPG) was from Avanti Polar Lipids (Delfzyl, NL); methyl-β-cyclodextrin (MBCD) was from Sigma (Buchs, CH).

Cell culturing, cell transfection and preparation, and ACP labelling were performed as described in Chapter 3. The method to calculate sensitized acceptor emission has been described in Chapter 4. Protein content was determined using the Bradford protein assay (Pierce) with BSA as standard. Image treatment and data analysis were performed using custom programs written in IGOR PRO 5 (Wavemetrics). Unless differently stated, all errors indicated are 95% confidence intervals. Error bars represent standard deviations.

7.3.2 Lipid Vesicles Preparation and Estimation of Receptor Surface Density on Cells

DOPG and DPPE-Cy5 dissolved in chloroform were mixed at a molar ratio of 0.03% and 0.06% DPPE-Cy5 to yield a Cy5 surface concentration of 500 and 1000 molecules/μm^2, respectively, assuming a lipid surface area of 60 Å^2. Lipid mixtures were dried over night and rehydrated with PBS at 37 °C during 3 days. The lipid vesicles were placed on glass coverslips and imaged with the same settings used for FRET imaging. A threshold was applied to the background-subtracted images to select the membrane of the vesicles. The average intensity for each single vesicle was determined and the receptor density, σ_r (receptors/μm^2) calculated according to

$$\sigma_\mathrm{r} = \sigma_{\mathrm{Cy5}} \frac{I_\mathrm{C}}{I_\mathrm{V}} \left(\frac{1}{x_\mathrm{A}} \right), \tag{7.1}$$

where I_C is the average fluorescence intensity of Cy5 on a cell; I_V is the average fluorescence intensity of Cy5 on a vesicle (measured with same instrument settings as I_C); σ_{Cy5} is the surface density of Cy5-DPPE on the vesicle (molecules/μm^2); and x_A is the acceptor mole fraction on the labelled cells.

7.3.3 Confocal FRET Microscopy

Laser-scanning confocal micrographs were recorded on a LSM 510 microscope (Zeiss) equipped with a 63× water objective (1.2 W Korr, Zeiss) either excited at 543 nm or at 633 nm using Helium-Neon lasers. Detection of fluorescence signals of acceptor and donor/FRET was achieved by appropriate filter sets using two tracks. The settings for the acceptor track were (excitation wavelength, dichroic mirror, emission filter): 633 nm, HFT 633, LP 650 (acceptor filter set, denoted as acceptor channel). The donor and the FRET images were recorded simultaneously with excitation at 543 nm and a dichroic mirror HFT 543, the emission beam was split with a NFT 635 Vis mirror onto two

detectors with a BP 560-615 filter for donor emission (donor filter set, denoted as donor channel) and a LP 650 filter for acceptor emission (FRET filter set, denoted as FRET channel), respectively. The laser power for the excitation and the gain of the detectors for the emission were adjusted for each experiment to yield an image with a good signal to noise ratio. Fluorescence intensities on the cell were calibrated using measurements of fluorescence intensities of solutions of the donor or the acceptor at known concentrations at the same experimental settings, allowing to compare expression of various cells and to calculate observed donor mole fractions from $x_{\mathrm{D,obs}} = [D]/([D] + [A])$.

7.4 Theory

7.4.1 Relationship between Donor Dequenching and Sensitized Acceptor Emission

The true FRET efficiency, E, refers to the transfer of energy between a donor and an acceptor molecule in a single DA pair or to the average over a large number of DA pairs, excluding the molecules not contributing to FRET. The apparent efficiency, E_{app}, signifies the efficiency of energy transfer in a large population of donors and acceptors, where only a fraction contributes to FRET. The method to measure the efficiency is based either on donor quenching, $E_{\mathrm{app,dq}} = 1 - (F_{\mathrm{DA}}/F_{\mathrm{D}})$, or on sensitized acceptor emission, $E_{\mathrm{app,se}} = (F_{\mathrm{AD}}/F_{\mathrm{A}} - 1)[\varepsilon_{\mathrm{A}}(\lambda)/\varepsilon_{\mathrm{D}}(\lambda)]$ (see Chapter 4). For a mixture of donor and acceptor molecules, where only a fraction of them performs FRET, $E_{\mathrm{app,dq}}$ and $E_{\mathrm{app,se}}$ are not necessarily identical.

It is possible to derive a simple relation between $E_{\mathrm{app,dq}}$ and $E_{\mathrm{app,se}}$. Energy conservation dictates that the excitations lost by energy transfer from the donor are gained by the acceptor. Excitations directly correspond to detected fluorescence through a proportionality factor comprising the fluorescence quantum yield and the detection efficiency. Using the fluorescence quantum yields, ϕ_{D} and ϕ_{A}, and the detection efficiencies, η_{D} and η_{A}, for donor and acceptor, respectively, one gets

$$\frac{1}{\phi_{\mathrm{D}}\eta_{\mathrm{D}}}(F_{\mathrm{D}} - F_{\mathrm{DA}}) = \frac{1}{\phi_{\mathrm{A}}\eta_{\mathrm{A}}}(F_{\mathrm{AD}} - F_{\mathrm{A}}). \tag{7.2}$$

Fluorescence is proportional to number of molecules, extinction coefficients, fluorescence quantum yields and detection efficiencies: $F_{\mathrm{D}} \propto x_{\mathrm{D}}\varepsilon_{\mathrm{D}}\phi_{\mathrm{D}}\eta_{\mathrm{D}}$ and $F_{\mathrm{A}} \propto x_{\mathrm{A}}\varepsilon_{\mathrm{A}}\phi_{\mathrm{A}}\eta_{\mathrm{A}}$.

$$\frac{F_{\mathrm{A}}}{F_{\mathrm{D}}} = \frac{x_{\mathrm{A}}}{x_{\mathrm{D}}}\frac{\varepsilon_{\mathrm{A}}}{\varepsilon_{\mathrm{D}}}\frac{\phi_{\mathrm{A}}}{\phi_{\mathrm{D}}}\frac{\eta_{\mathrm{A}}}{\eta_{\mathrm{D}}}. \tag{7.3}$$

Combining Eq. 7.2 and Eq. 7.3 gives

$$\frac{\varepsilon_A}{\varepsilon_D}\left(\frac{F_{AD}}{F_A}-1\right)=\left(1-\frac{F_{DA}}{F_D}\right)\frac{x_D}{x_A}, \tag{7.4}$$

or

$$\text{or} \quad E_{app,se}=E_{app,dq}\frac{x_D}{x_A}, \tag{7.5}$$

where $E_{app,se}$ is the apparent efficiency measured by sensitized acceptor emission; $E_{app,dq}$ is the apparent efficiency measured by donor dequenching; x_D and x_A are the donor and acceptor mole fractions.

7.4.2 Determining the Presence of Dimers and Higher Oligomers by FRET

The apparent FRET efficiency (E_{app}) is a function of the true FRET efficiency and the donor or acceptor mole fraction. A model to relate donor dequenching ($E_{app,dq}$) to the true FRET efficiency (E) and the donor mole fraction (x_D) was developed previously [162, 163],

$$1-\frac{F_{DA}}{F_D}=E(1-x_D^{n-1}), \tag{7.6}$$

where n is the number of units in an oligomer. Eq. 7.6 expressed as $E_{app,se}$, using Eq. 7.5 and noting that $x_A + x_D = 1$ gives

$$E_{app,se}=E\frac{x_D}{1-x_D}(1-x_D^{n-1}). \tag{7.7}$$

Incomplete Labelling

Adair and Engelman [162] extended their model for the case of incomplete labelling,

$$1-\frac{F_{DA}}{F_D}=E(1-(x'_{DU})^{n-1}), \tag{7.8}$$

where x'_{DU} is the mole fraction of donor labelled and unlabelled receptors together ($x'_{DU} = x'_D + x'_U$). If x'_D and x'_A are the mole fractions of donor- and acceptor-labelled receptors and x'_U is the mole fraction of unlabelled receptors, then $x'_D = x_D(1 - x'_U)$ and $x'_A = x_A(1 - x'_U)$, where x_D and x_A are the donor and acceptor mole fractions used for labelling. Combining Eq. 7.5 and Eq. 7.8, the apparent efficiency measured by sensitized acceptor emission for incomplete labelling is

$$E_{app,se}=E\frac{x_D}{x_A}(1-(x'_{DU})^{n-1}), \tag{7.9}$$

with $x'_{\mathrm{DU}} = x_{\mathrm{D}}(1 - x'_{\mathrm{U}}) + x'_{\mathrm{U}}$.

Oligomers in Presence of Monomers

If we assume a population of oligomers in the presence of monomers, the apparent efficiency would be reduced, with an increasing fraction of monomers. The equation for $E_{\mathrm{app,dq}}$ with a mixture of monomers and oligomers can be derived by writing $E_{\mathrm{app,dq}}$ in terms of molar fluorescence, f_{DA} and f_{D}:

$$E_{\mathrm{app,dq}} = 1 - \frac{F_{\mathrm{DA}}}{F_{\mathrm{D}}} = 1 - \frac{f_{\mathrm{DA}}}{f_{\mathrm{D}}}. \tag{7.10}$$

The molar fluorescence for donor in presence of acceptor, f_{DA}, can be expressed as the sum of contributions of the molar fraction of monomers, x_{mono}, and the molar fraction of oligomers, x_{oligo}:

$$f_{\mathrm{DA}} = x_{\mathrm{mono}} f_{\mathrm{DA,mono}} + x_{\mathrm{oligo}} f_{\mathrm{DA,oligo}} = x_{\mathrm{mono}} f_{\mathrm{D}} + x_{\mathrm{oligo}} f_{\mathrm{DA,oligo}}\,, \tag{7.11}$$

where, $f_{\mathrm{DA,mono}}$ and $f_{\mathrm{DA,oligo}}$ are the molar fluorescence of donor in presence of acceptor for a monomer and an oligomer, respectively. Because monomers cannot undergo FRET, $f_{\mathrm{DA,mono}} = f_{\mathrm{D,mono}} = f_{\mathrm{D}}$. Substituting Eq. 7.11 in Eq. 7.10 yields:

$$\begin{aligned} E_{\mathrm{app,dq}} &= 1 - \frac{x_{\mathrm{mono}} f_{\mathrm{D}} + x_{\mathrm{oligo}} F_{\mathrm{DA,oligo}}}{f_{\mathrm{D}}} \\ &= x_{\mathrm{oligo}} \left(1 - \frac{f_{\mathrm{DA,oligo}}}{f_{\mathrm{D}}}\right) \\ &= x_{\mathrm{oligo}} \left(1 - \frac{F_{\mathrm{DA}}}{F_{\mathrm{D}}}\right), \end{aligned} \tag{7.12}$$

with $x_{\mathrm{mono}} = 1 - x_{\mathrm{oligo}}$ and $f_{\mathrm{DA,oligo}} = f_{\mathrm{DA}}$, because all changes due to FRET occur in the oligomer. The measured apparent efficiency is proportional to the true efficiency with the proportionality factor x_{oligo}.

7.4.3 FRET for Randomly Distributed Donors and Acceptors

For randomly distributed donors and acceptors in membranes, the energy transfer efficiency (with respect to donor dequenching) is a function of the Förster distance (R_0), the distance of closest potential approach of donor and acceptor (R_{c}), and the surface density of acceptors [164].

Wolber and Hudson [165] derived an analytical approximation for the transfer effi-

ciency for randomly distributed donors and acceptors:

$$\frac{F_{\mathrm{DA}}}{F_{\mathrm{D}}} = A_1 e^{-k_1 c_{\mathrm{A}}} + A_2 e^{-k_2 c_{\mathrm{A}}}, \tag{7.13}$$

where c_{A} is the reduced acceptor concentration (acceptor surface density normalized by R_0^2); $A_{1,2}$ and $k_{1,2}$ are constants which change for different R_{c}/R_0 ratios and given in Wolber and Hudson [165]. It is important to note that this approximation holds only for $0 \leq c_{\mathrm{A}} \leq 0.5$.

We introduced a factor α to account for the fact that the receptors might not be homogenously distributed but concentrated in microdomains. This factor increases the local acceptor density. Using Eq. 7.5 we can relate the approximation in Eq. 7.13 to $E_{\mathrm{app,se}}$ as

$$E_{\mathrm{app,se}} = (1 - (A_1 e^{-k_1 c_{\mathrm{A}} \alpha} + A_2 e^{-k_2 c_{\mathrm{A}} \alpha})) \frac{x_{\mathrm{D}}}{1 - x_{\mathrm{D}}}, \tag{7.14}$$

where $c_{\mathrm{A}} = \sigma_{\mathrm{R}}(1 - x_{\mathrm{D}})R_0^2$.

7.5 Results

7.5.1 Controlled Labelling and FRET Imaging of ACP-NK1R

The NK1R was fused at its N-terminus with ACP for subsequent labelling with fluorescent analogs of Coenzyme A. Previous reports have shown that the fusion protein ACP-NK1R expressed in HEK293 cells can be specifically labelled with Cy3 [128] and keeps its ability to bind the agonist Substance P, eliciting a calcium response at a similar effective concentration than for the wild-type receptor (Chapter 5).

For FRET imaging, ACP-NK1Rs were double labelled with Cy3 (Donor) and Cy5 (Acceptor) by mixing the substrates at define ratios before applying to the cells. Figure 7.1 A-C shows typical donor, acceptor and FRET images of a living cell labelled with a donor (acceptor) mole fraction of 0.67 (0.33), revealing a rather heterogeneous distribution of the NK1R in the cell membrane. Because only receptors correctly translocated to the plasma membrane are accessible for labelling, there is no background fluorescence inside of the cells. The FRET ratio (*FR*) was calculated on a pixel-by-pixel basis from the background-subtracted images after applying a threshold to select only the membranes comprising the labelled ACP-NK1Rs (Figure 7.1 D) and was 6.4 (0.01) yielding a corresponding apparent FRET efficiency, $E_{\mathrm{app,se}}$, of 60% using Eq. 4.6 (in Chapter 4).

For quantitative FRET experiments, it is instrumental that the DA ratios in solution

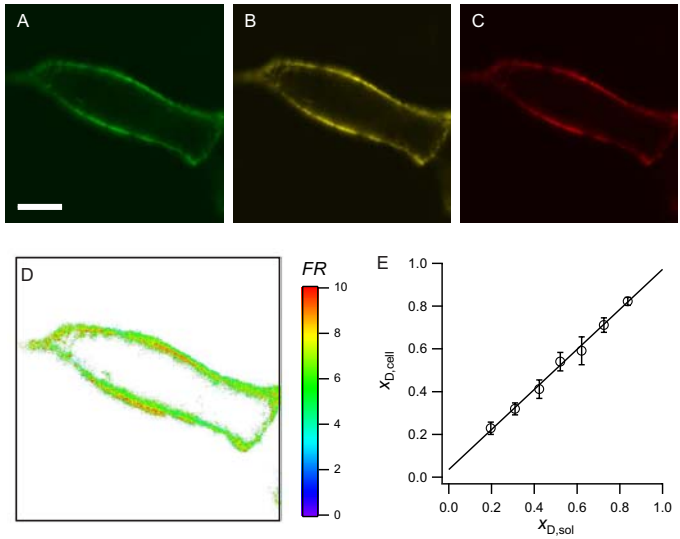

Figure 7.1: Controlled double-labelling and FRET imaging of a living cell. *A-B, Fluorescence confocal micrographs showing a HEK293 cell transiently expressing ACP-NK1R, which was labelled simultaneously with Cy3 and Cy5 at a Cy3 mole fraction (x_D) of 0.67. The cell was imaged with the filter sets for donor (A), acceptor (B) and FRET (C). Scale bar represents 10 μm. D, The micrograph of the FRET ratio (FR) was calculated from images (A), (B) and (C) on a pixel-by-pixel basis. The mean FR value was 6.4 (0.01), corresponding to an apparent FRET efficiency of 60% (see color bar). E, The donor mole fraction, $x_{D,cell}$, observed on the cells as a function of the donor mole fraction in solution, $x_{D,sol}$, used for the labelling. $x_{D,sol}$ is identical to $x_{D,cell}$ within experimental error as shown by a linear regression yielding an intercept of 0.035 ± 0.073 and a slope of 0.94 ± 0.12 ($\pm$ 95% confidence interval). Each point is the mean ($\pm$ S.D.) of 10 cells.*

used for labelling precisely correspond to the real DA ratios obtained on the cells. To test this, we labelled HEK293 cells expressing very low amount of ACP-NK1Rs using donor mole fractions $x_{\mathrm{D,sol}}$ ranging from 0.2-0.8. No FRET occurred at such low expression levels meaning that average fluorescence intensities in the donor and acceptor channels (Df and Af, see Theory) were directly proportional to the respective concentrations. Using a calibration procedure, the observed donor mole fraction $x_{\mathrm{D,cell}}$ was calculated and found to vary linearly with $x_{\mathrm{D,sol}}$ (Figure 7.1 E), confirming that the DA ratio on the receptors after labelling can be directly obtained from the DA ratio used for labelling.

7.5.2 Oligomerization of NK1R

In the following we use the controlled dual color labelling to investigate the oligomerization of the NK1R by FRET imaging. Veatch and Stryer [163] showed that the oligomerization of a membrane protein can be determined from the dependency of the apparent FRET efficiency ($E_{\mathrm{app,dq}}$) on the donor mole fraction (x_{D}, Eq. 7.6). Here, we adapted this model to measure the apparent FRET efficiency using sensitized acceptor emission ($E_{\mathrm{app,se}}$). For dimers ($n = 2$) a linear increase in $E_{\mathrm{app,se}}$ with increasing x_{D} is expected from Eq. 7.7.

ACP-NK1R transiently expressed in HEK293 cells was labelled at various mole fractions of the donor (Figure 7.2, gray circles). Care was taken that all investigated cells showed similar expression levels. A fit of $E_{\mathrm{app,se}}$ as a function of x_{D} using Eq. 7.7 yielded the true FRET efficiency $E = 0.26 \pm 0.09$, and the oligomerization degree $n = 3.75 \pm 1.27$. For the fit, an offset was included in Eq. 7.7, which was found to be -0.022 ± 0.030, i.e. zero within the experimental accuracy.

Remarkably, the number of units n in the oligomer was significantly higher than 2 showing that the NK1R does not form dimers at these expression levels, but rather higher oligomers. From the FRET efficiency, E, and the Förster distance for Cy3 and Cy5 of $R_0 = 50\,\text{Å}$ [164], the average distance R_{c} between donor and acceptor in the oligomer was calculated to be about 60 Å, which is slightly larger than the estimated diameter of a GPCR of 40-50 Å [8, 160].

In order to investigate whether the FRET efficiency varied with the expression level, $E_{\mathrm{app,se}}$ was measured in HEK293 cells stably expressing ACP-NK1R at expression levels 2.5 times lower than for transient expression (Figure 7.2, black circles). Strikingly, such a small concentration difference resulted in the complete loss of FRET. Fitting the data with E fixed to 0.26 yielded an oligomerization degree $n = 1.09 \pm 0.28$ and an $\mathit{offset} = 0.018 \pm 0.047$, meaning that all NK1Rs were present as monomers at this lower expression level. To exclude that this observation was only due to the stable expression of the NK1R, FRET was measured on transiently expressing cells with 2.5 times lower expression levels leading to the same result.

In order to interpret these findings, it is essential to assess the possible influence of unlabelled receptors on the degree of oligomerization. Unlabelled receptors might be present due to (i) incomplete labelling of the ACP-NK1R, (ii) free non-conjugated CoA in the labelling solution, or (iii) presence of wtNK1R or other non-labelled GPCRs forming oligomers with the NK1R. Saturation labelling experiments (Figure 5.6 A in Chapter 5 and [128]) revealed that the labelling efficiency at our conditions is better than 95%, while analysis of the purity of conjugated CoA showed negligible amounts of

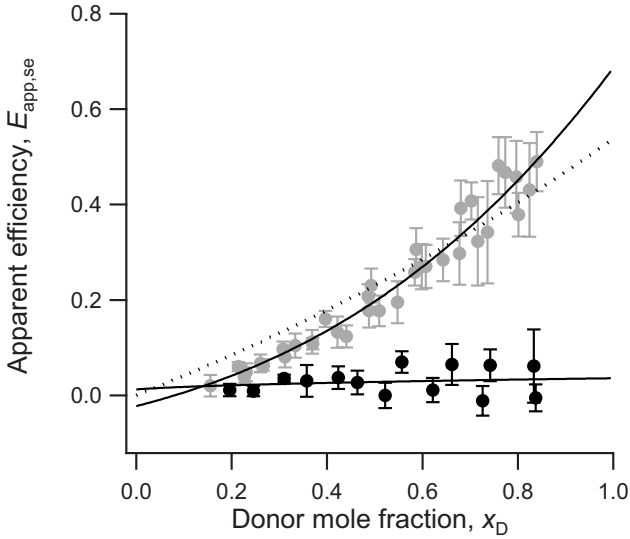

Figure 7.2: FRET between NK1R at different donor mole fraction. *HEK293 cells expressing ACP-NK1Rs were labelled with a mixture of Cy3 and Cy5 fluorophores at different ratios indicated by the donor mole fraction x_D. The apparent FRET efficiency, $E_{app,se}$, is plotted versus x_D, for two populations of cells: The grey circles represent transiently expressing cells while the black circles stem from to stably expressing cells showing a 2.5 times lower expression. Each point is a mean (± S.D.) of 10 cells. Fitting the data with Eq. 7.7 plus an offset (solid curves) yields for the higher expressing cells offset* $= 0.022 \pm 0.030$, $E = 0.26 \pm 0.09$, $n = 3.75 \pm 1.27$, *and for the lower expressing cells with E fixed to 0.26 offset* $= 0.018 \pm 0.047$, $n = 1.09 \pm 0.28$ *(± 95% confidence interval). The dotted curve represents $E_{app,se}$ calculated using Eq. 7.14, with $A_1 = 0.6327$, $k_1 = 1.3686$, $A_2 = 0.3673$, $k_2 = 0.4654$, $\alpha = 81$, $\sigma_R = 256\, R/\mu m^2$ and x_D as an independent variable.*

non-conjugated CoA. HEK293 cells do not express endogenously NK1Rs but it cannot be excluded that other GPCRs present might form hetero-oligomers with NK1R. The effect of unlabelled receptors can be estimated using the oligomerization model from Adair and Engelman [162] adapted for sensitized acceptor emission (Eq. 7.9). Data were fitted using Eq. 7.9 for increasing mole fractions of unlabelled receptor (x'_U). Even assuming x'_U of up to 35% did not noticeably change the resulting FRET efficiency E and the number of units n, which remained within the 95% confidence intervals of the values obtained from the fit at $x'_U = 0$. Furthermore, n increased with x'_U excluding that the presence of unlabelled receptors might explain why n is higher than two. It is worth noting that the possible co-existence of monomers (Eq. 7.12) is also unable to account for n higher than two, as it would only change the apparent efficiency, which

is proportional to the mole fraction of oligomers, and not to the number of units in an oligomer.

Based on these results, we conclude that the NK1R does not form homo-dimers and probably also no higher oligomers unless assuming a dramatic dependency of the oligomer stability on the concentration of receptors. Moreover, such an oligomer would be expected to consist of four NK1Rs, which is mechanistically difficult to conceive.

7.5.3 Influence of the Agonist Substance P

Some GPCRs show an agonist-dependent dimerization [166]. In order to know whether this is also the case for the NK1R, we investigated the stable cell line with lower ACP-NK1R expression levels (450 ± 48 fmol/mg of protein) closer to physiological conditions. Addition of 100 nM SP did not result in a significant increase of the apparent FRET efficiency, indicating that the receptors do not oligomerize upon agonist binding (Figure 7.3).

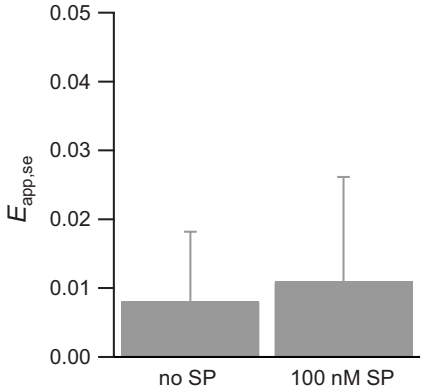

Figure 7.3: Modulation of FRET by SP. *FRET efficiency of cells stably expressing ACP-NK1Rs, labelled with a donor mole fraction of $x_D = 0.6$, before and after addition of 100 nM SP (mean of 7 cells ± S.E.). Data show that the NK1R does not form homo-oligomers upon binding of the agonist.*

7.5.4 Dependence of FRET on the Receptor Density at the Cell Surface

In a next step, we addressed the question, whether FRET at high expression levels might be due to high concentrations of donor and acceptor so that frequent stochastic

encounters due to small average distances between fluorophores (receptors) might allow FRET. Therefore, we transiently expressed ACP-NK1R in HEK293 and labelled the receptors with donor and acceptor at a constant donor mole fraction of 0.67, which is in the range where we measured a high apparent FRET efficiency on cells with high receptor density.

Transiently transfected cells usually provide a wide distribution of receptor expression levels, which in turn allows to measure FRET at different receptor surface densities. Using high detector gains we selected cells with low receptor expression levels. We chose cells with good donor and acceptor signal but no saturation. By gradually decreasing the detector gain we measured the apparent efficiency on cells with increasing expression levels. The expression levels were calibrated as described before. In addition we used lipid vesicles with a defined surface concentration of Cy5 to quantify the receptor concentration on the cell surface.

Figure 7.4 shows $E_{\mathrm{app,se}}$ both as a function of receptor surface density (σ_{R}) and as a function of the concentration of acceptors per R_0^2, $c_{\mathrm{A}} = x_{\mathrm{A}}\sigma_{\mathrm{R}}R_0^2$ (denoted also as reduced acceptor concentration). $E_{\mathrm{app,se}}$ strongly depends on the receptor surface density and reaches saturation at $E_{\mathrm{app,se,max}} = 0.626 \pm 0.042$ (Figure 7.4, fine dotted line). The maximum of the apparent efficiency is expected to be reached when the NK1Rs are closely packed (each receptor surrounded by six neighbors, $n = 7$). Under this condition the true efficiency can be estimated with Eq. 7.7 to be $E = 0.34$, which corresponds to a distance of closest approach $R_{\mathrm{c}} = 55.9\,\text{Å}$, assuming a Förster distance for Cy3 and Cy5 of $R_0 = 50\,\text{Å}$ [164], slightly larger than the estimated diameter of a GPCR of 40-50 Å [8, 160].

Knowing the reduced acceptor concentration c_{A}, the apparent FRET efficiency resulting from stochastic encounters between donors and acceptors can be estimated using Eq. 7.14 (for details see legend of Figure 7.4 and Section 7.4.3). Wolber's formula is an analytical expression containing coefficients which only depend on the ratio of R_{c}/R_0, i.e. 1.1 as obtained from the efficiency at densest packing. As depicted by the bold dotted curve in Figure 7.4 stochastic encounters at low surface density of NK1R cannot account for the experimentally observed high apparent FRET efficiencies.

A possible explanation for this discrepancy would be that the effective density of NK1Rs at the cell surface is higher than the one estimated from the calibration. This would be the case if the NK1R would reside in microdomains. If for example the NK1Rs homogenously distributed over the entire cell surface at a cell surface concentration of $400\,\mathrm{R}/\mu\mathrm{m}^2$ should reach a state of closest packing of $40'000\,\mathrm{R}/\mu\mathrm{m}^2$ at constant receptor number per cell, then the NK1Rs have to be concentrated in only about 1% of the cell

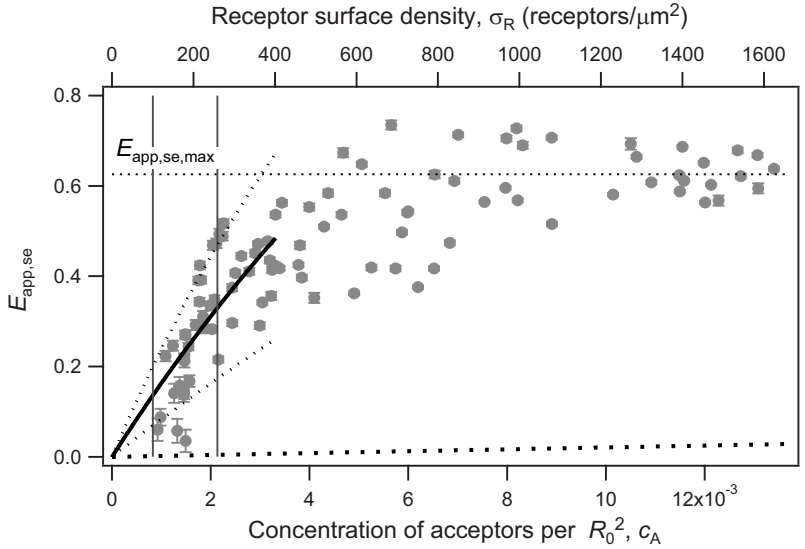

Figure 7.4: FRET dependence on cell surface receptor density. *HEK293 cells transiently expressing the ACP-NK1R were labelled at a donor mole fraction of* $x_D = 0.67$. *The apparent FRET efficiency,* $E_{app,se}$ *(grey circles), was measured and plotted as a function of the reduced acceptor concentration,* c_A *(bottom), and the receptor surface density,* σ_R *(top). Each data point represents an image containing 1-3 cells. The bold dotted curve at the bottom represents* $E_{app,se}$ *calculated with Eq. 7.14 assuming the absence of microdomains (*$\alpha = 1$*; coefficients* $A_{1,2}$ *and* $k_{1,2}$ *from Wolber and Hudson [165] for a* R_c/R_0*-ratio of 1.1;* $A_1 = 0.6327$, $k_1 = 1.3686$, $A_2 = 0.3673$, $k_2 = 0.4654$*). The fine horizontal dotted line represents the maximal apparent efficiency measured by sensitized acceptor emission:* $E_{app,se,max} = 0.626 \pm 0.042$ *(mean of the last 17 points ± S.D.). The two vertical lines represent the receptor surface densities for the data in Figure 7.2. The solid curve represents a fit over the first 47 points using Eq. 7.14 with* α *as the only free parameter:* $\alpha = 81.1 \pm 0.3$ *(± 95% confidence interval). The dotted curves represent the calculated* $E_{app,se}$ *from Eq. 7.14 with* α *factors of* $81.1 \pm 50\%$.

membrane. A more precise estimate can be gained by fitting the initial part of the data in Figure 7.4 using Eq. 7.14 and allowing only one free parameter, the "scaling" factor α to account for the increased effective concentration. The analytical expression in Eq. 7.14 is known to be valid only for a limited range of $c_A = 0 - 0.5$ of the reduced acceptor concentration [165]. The corresponding fit (bold curve in Figure 7.4) yields a scaling factor $\alpha = 81.1 \pm 0.3$. Taking into account the scatter of the data, the variation between cells of the scaling factor can be estimated to be around 50% (dashed curves in Figure 7.4) implying that the receptors are concentrated in microdomains representing only 0.8-2.5% of the total surface area of the plasma membrane. Interestingly, a deviation from the fitting curve can be observed at low apparent FRET efficiency, which might indicate fusion of microdomains. However, it cannot be excluded that this deviation is an artifact of the analysis procedure.

To verify that the model of Wolber can also explain the dependency of $E_{\mathrm{app,se}}$ on x_D (Figure 7.2, black circles) for cells with the same total expression levels, σ_R, of $256\,R/\mu m^2$, we plotted $E_{\mathrm{app,se}}$, calculated with Eq. 7.14 using the parameters obtained previously, as a function of x_D (Figure 7.2, dotted curve). The dotted curve can reproduce the data in a reasonable way besides a deviation at low x_D due to the fact that Wolber's approximation is not anymore valid at these high acceptor densities.

7.5.5 Influence of Cholesterol Depletion

Monastyrskaya et al. [73] recently showed that the NK1R is present in detergent-resistant membrane fractions and that this localization is disrupted by cholesterol extraction with methyl-β-cyclodextrin (MBCD). They further demonstrated that also signaling by the NK1R is abolished upon cholesterol depletion. In order to test whether the microdomains observed by FRET correspond to the detergent-resistant membrane fractions, the dependency of the apparent FRET efficiencies on cholesterol extraction was investigated on transiently expressed ACP-NK1R showing high NK1R densities (Figure 7.5). After incubation with 2% MBCD at RT for 45 minutes (same conditions as [73]), the apparent efficiency decreased significantly ($p \leq 0.005$) by 29% from 0.34 ± 0.048 to 0.24 ± 0.076 (mean of 9 cells $\pm$ S.E.), supporting a model where NK1Rs are localized in microdomains.

7.6 Discussion

Here we have shown the power of the ACP labelling for quantitative FRET measurements in living cells. Although the ACP labelling is limited to membrane proteins

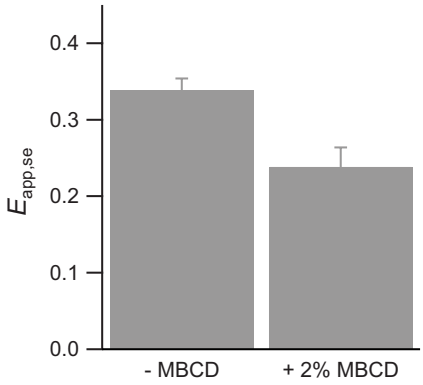

Figure 7.5: Modulation of apparent FRET efficiency by cholesterol extraction. *Apparent FRET efficiency of transiently expressed ACP-NK1Rs before* (0.34 ± 0.048) *and after* (0.24 ± 0.076) *cholesterol extraction (mean of 9 cells ± S.E.). Cholesterol was extracted by incubation with 2% methyl-β-cyclodextrin for 45 minutes at room temperature. ACP-NK1R was labelled with a donor mole fraction of* $x_D = 0.6$.

comprising extracellular fusion of ACP, it has the advantage that only the proteins incorporated into the plasma membrane are labelled, thereby avoiding background signal from incompletely processed receptors. Furthermore, the ACP labelling allows to choose suitable fluorophores for FRET and the control of DA ratios, which is a requirement for precise FRET measurements on membrane proteins where the state of oligomerization is not known.

Physiological NK1R expression levels reported in literature are 550 fmol/mg of membrane protein in rat submaxillary gland membranes [147], 107 fmol/mg of membrane protein in guinea pig lung membranes [167], and 254 fmol/mg of membrane protein in rat brain membranes [168]. In our case, we measured a cell surface concentration of stably expressed ACP-NK1R of 450 fmol/mg of protein. The physiological expression levels from literature were normalized to total membrane protein content. This means that the ACP-NK1R stably expressed in HEK293 shows about 5-10 times higher expression levels than under physiological conditions. Nevertheless, using the stably expressed ACP-NK1R no FRET could be detected, meaning that the NK1R does not form homo-oligomers at physiological expression levels.

At the present state, we cannot exclude that the N-terminus of the NK1R is involved in oligomerization [55] and that the ACP when fused to the N-terminus abolishes oligomerization. But, because the ACP-NK1R is functional with respect to cellular calcium signaling this would mean that homo-oligomerization is not required for func-

tionality of the NK1R.

Investigating SSTR5 homo-oligomerization in CHO cells expressing the receptor at 800 fmol/mg of protein showed significant FRET. Five times lower expression levels showed insignificant FRET, which however increased with increasing agonist concentration [166]. We also investigated the effect of SP on FRET efficiencies for low expression levels and did not measure a significant change of FRET, excluding agonist-dependent oligomerization. From these results we conclude that the NK1R does not form constitutive homo-oligomers and does not oligomerize in an agonist-dependent manner.

BRET and FRET signals were reported to be stable for receptor expression levels ranging from 1.4 to 26.3 pmol/mg of protein for β2-AR receptors [160], from 40 to 100 fmol/mg of membrane protein for CCR5 receptors [169], from 200 to 1000 fmol/mg of membrane protein for opioid receptors [170], and from 580 to 6570 fmol/mg of protein for β2/β3-AR hetero-oligomers [171]. On the other hand we observed a clear dependency of the apparent efficiency on the donor mole fraction by increasing the expression level from about 450 fmol/mg of protein by a factor of 2.5.

Because many GPCRs are reported to form homo- or hetero-dimers [54, 55], and the NK1R is known to form a hetero-dimers with the μ-opioid (MOR) receptor in HEK293 cells [82], it is surprising that the NK1R does not form homo-dimers, and that the FRET measured was in fact strongly concentration dependent.

From the measured receptor density we could exclude FRET originating from high incidence of random collisions. Nevertheless, we measured a strong dependency on receptor density. Because we showed that the NK1R does not form homo-oligomers, we suggest, that the FRET signal is arising from NK1R concentrated in sub-pixel-sized microdomains. Furthermore, cholesterol extraction significantly reduced FRET efficiencies. This is consistent with the observations of Monastyrskaya et al. [73], who reported the presence of NK1R in lipid rafts. Also Holst et al. [72] suggested the existence of NK1R in plasma membrane microdomains based on binding experiments with fusion proteins of NK1R with $G\alpha_q$ and $G\alpha_s$.

Chapter 8

FRET between NK1R and $G_{\alpha\beta\gamma}$ Subunits

8.1 Introduction

A classical model of GPCR signaling states that agonist-activated receptors change their conformation and thereby recruit heterotrimeric G proteins. Upon binding of the G$\alpha\beta\gamma$ complex to the activated receptor, a conformational change leads to the exchange of GDP for GTP in the Gα-subunit, following a disassembly in Gα and G$\beta\gamma$ [1]. Recently, this classical model of GPCR signaling has been challenged [30,47,172,173]. It has been proposed that GPCRs and G proteins exist as persistent multimolecular complexes, where activated G protein subunits do not disassemble from each other. Still little is known about the dynamics of the interaction between receptor and G protein in living cells and whether activated G$\alpha\beta\gamma$-complexes do indeed dissociate.

In vitro approaches using reconstituted model systems, such as surface plasmon resonance [174, 175] or flow cytometry [176] have been developed to measure real-time interactions between GPCRs and their G proteins. These experiments were done in solubilized systems or reconstituted in lipid bilayers and thus do not represent the natural environment. Until very recently there was no report about real-time monitoring of receptor-G protein interactions in living cells [117]. The authors describe a BRET-based assay were they observe a basal BRET signal between receptor and G$\alpha\beta\gamma$ without activation of the receptor. Although they contribute this to constitutive active receptors, the BRET signal increases upon activation and remains constant for several minutes, indicating that activated G proteins do not dissociate from the receptor.

Also the question of the dissociation of G$\beta\gamma$ from activated Gα has recently been addressed in living cells. FRET-based studies in *Dictostelium discoideum* and yeast concluded that GPCR activation leads to the disassembly of the G$\alpha\beta\gamma$-complex [118, 177].

This finding in turn has been challenged by another FRET-based study on mammalian G protein subunits, which led to the conclusion that a rearrangement rather than dissociation occurred in response to receptor activation [31].

This Chapter deals with the experiments to investigate real-time receptor-G protein interactions in living cells using a FRET-based approach. The goal was to detect changes in FRET between NK1R and the $G\alpha_q\beta\gamma$-complex or between the G protein subunits themselves upon activation of the receptor by its agonist. It is also known that G proteins can be activated when the guanine nucleotide binding site of $G\alpha$ is occupied by AlF_4^- which together with GDP mimics the activating effect of GTP [178–180]. Because AlF_4^- is membrane permeable it can be used to directly activate the $G\alpha$ in living cells.

For FRET experiments in living cells a commonly used DA pair is ECFP and EYFP. Unfortunately, high concentrations of fluoride anions in a preparations of AlF_4^- leads to artefacts in FRET, because EYFP is sensitive to halides [181, 182]. Therefore, a point mutation was introduced into EYFP to reduce its halide sensitivity [183] and make it suitable for our experiments. This fluorescent protein, named citrine (Cit), and other derivatives were then fused to the different G protein subunits, and their functionality was investigated. FRET experiments with different combinations of labelled receptor and G protein subunits were performed using three different experimental conditions. FRET could be measured but no changes upon addition of agonist or AlF_4^- was observed.

8.2 Experimental Procedures

8.2.1 Materials

pSFV1::Gq was a gift from Kenneth Lundstrom (BioXtal, CH); pECFP-mem::$G\alpha_{i2}$ was a gift from Andrew Tinker (University College London, UK); vectors containing EGFP, ECFP and EYFP were from Clontech (Palo Alto, CA, USA); pEYFP::$G\beta_1$ (human) and pEYFP::$G\gamma_2$ (bovine) were a gift from Susanna Cotecchia (UNIL, CH); ECFP-EYFP fusion construct was a gift from Régis Grailhe (Institute Pasteur, Paris, F); QuickChange site directed mutagenesis kit was from Stratagene (La Jolla, CA, USA); NaF and $AlCl_3$ were from Fluka (Buchs, CH).

Cell culturing, cell transfection and preparation, calcium ion signaling, and fluorescence confocal microscopy were performed as described in Chapter 3.

8.2.2 cDNAs

Polymerase chain reaction (PCR), DNA agarose gel preparation (analytic and preparative), restriction digest, ligation, DNA purification, plasmid amplification in *E.coli* XL1 blue strain, bacterial medium (2TY), were done according to standard protocols described in *Molecular cloning, a laboratory manual* [134]. The plasmid constructs were confirmed by restriction mapping and DNA sequencing. Following is a detailed description of the cloning steps. The primers used for cloning are found in Table 8.1.

Primer	Sequence
fw-Cit-mut	5'-C GTG ACC ACC TTC GGC TAC GGA TTA ATG TGC TTC GCC CGC TAC CC-3'
rv-Cit-mut	5'-GG GTA GCG GGC GAA GCA CAT TAA TCC GTA GCC GAA GGT GGT CAC G-3'
fw-Gq-mut	5'-CG CTC AAG ATC CCA TAC AAG TAT GGC GCC ATC CAT GGA GAA CAC AAT AAG GCT CAT GC-3'
rv-Gq-mut	5'-GC ATG AGC CTT ATT GTG TTC TCC ATG GAT GGC GCC ATA CTT GTA TGG GAT CTT GAG CG-3'
fw-XFP-mut	5'-C GGG GTG GTG CCC ATA CTA GTC GAG CTG GAC GGC-3'
rv-XFP-mut	5'-GCC GTC CAG CTC GAC TAG TAT GGG CAC CAC CCC G-3'
fw-NheI-Gq	5'-G GCC GGG CTA GCC ACC ATG ACT CTG GAG TCC ATC ATG GC-3'
fw-SpeI-Gq	5'-GCG CGG ACT AGT ATG ACT CTG GAG TCC ATC ATG GCG-3'
fw-BsrGI-Gq	5'-GG CCG GTG TAC AAG ATG ACT CTG GAG TCC ATC ATG GC-3'
fw-KasI-EGFP	5'-G CGG GGC GCC GGT ATG GTG AGC AAG GGC GAG G-3'
fw-SpeI-frCit	5'-G CCC ATA CTA GTC GAG CTG GAC GG-3'
rv-BamHI-Gq	5'-CCG CGC GGA TCC TTA GAC CAG ATT GTA CTC CTT CAG GTT CAG C-3'
rv-NotI-Gq	5'-A TAG TTT AGC GGC CGC TTA GAC CAG ATT GTA CTC CTT CAG GTT CAG-3'
rv-NcoI-EGFP(dS)	5'-CG CGG CCC ATG GCC CTT GTA CAG CTC GTC CAT GCC-3'
rv-BsrGI-frCit	5'-GC GCT GTA CAG CTC GTC CAT GC-3'

Table 8.1: Primers. *Primers used for the $G\alpha_q$-constructs and citrine. Restriction sites are underlined.*

Citrine (Cit)

Citrine is a fluorescent protein derived from EYFP by exchanging glutamine at position 69 for a methionine (Q69M) [183]. To achieve the mutation Q69M two point mutations were introduced into the EYFP gene by site directed mutagenesis using the primers *fw-Cit-mut* and *rv-Cit-mut*. In the same step, an additional *AseI* restriction site was introduced by three further point mutations, where the nucleotide sequence was changed but the amino acid sequence remained the same (silent mutation, Figure 8.1). This

restriction site was used to select positive plasmids by restriction mapping. The Clontech vector pEYFP-C1 was mutagenized yielding pCit-C1.

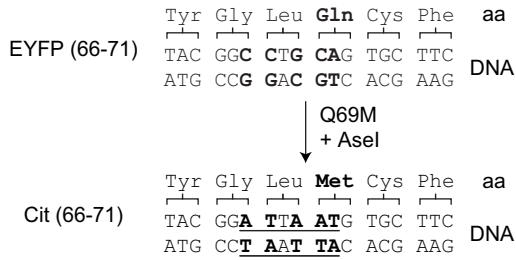

Figure 8.1: Site directed mutagenesis. *Introduction of Q69M mutation and an additional* AseI *restriction site (silent mutation). Bold letters indicate the mutated nucleotides.*

wtGq

The gene encoding for mouse Gα_q was amplified by PCR on the template pSFV1::Gq using the forward primer *fw-NheI-Gq* and the reverse primer *rv-BamHI-Gq* introducing a *NheI* restriction site and a Kozak sequence [135] at the 5' end, and a *BamHI* restriction site at the 3' end of the Gα_q gene. The *NheI*/*BamHI* cut and purified fragment was ligated into the *NheI*/*BamHI* cut pCEP4 expression vector yielding pCEP4::wtGq.

Gq(EGFP)-BM

The gene encoding for mouse Gα_q was amplified by PCR on the template pSFV1::Gq using the forward primer *fw-SpeI-Gq* and the reverse primer *rv-BamHI-Gq* introducing a *SpeI* restriction site at the 5' end, and a *BamHI* restriction site at the 3' end of the mouse Gα_q gene. The *SpeI*/*BamHI* cut and purified fragment was ligated into the *SpeI*/*BamHI* cut pBluescript II KS+ expression vector yielding pBS::Gq.

Two new restriction sites, *KasI* and *NcoI*, were introduced into pBS::Gq between the residues Tyr103 and Glu104 of the wild type mouse Gα_q by site directed mutagenesis resulting in pBS::Gq(mut). The primers were *fw-Gq-mut* and *rv-Gq-mut*.

The gene encoding for EGFP was amplified by PCR using the forward primer *fw-KasI-EGFP* and the reverse primer *rv-NcoI-EGFP(dS)* introducing a *KasI* restriction site at the 5' end, and a *NcoI* restriction site at the 3' end of the EGFP. The STOP codon has been removed. The *KasI*/*NcoI* cut and purified fragment was ligated into

the *KasI*/*NcoI* cut pBS::Gq(mut) plasmid yielding pBS::Gq(EGFP) with a Gly-Ala-Gly spacer in front of and a Gly-His-Gly spacer after EGFP.

In a last step, the gene encoding for Gq(EGFP) was amplified by PCR on the template pBS::Gq(EGFP) using the forward primer *fw-NheI-Gq* and the reverse primer *rv-BamHI-Gq* introducing a *NheI* restriction site and a Kozak sequence [135] at the 5' end, and a *BamHI* restriction site at the 3' end. The *NheI*/*BamHI* cut and purified fragment was ligated into the *NheI*/*BamHI* cut pCEP4 expression vector yielding pCEP4::Gq(EGFP)-BM.

Cit-Gq and ECFP-Gq

The plasmid pECFP-mem::Gα_{i2} is based on the vector pECFP-mem (Clontech) containing the dual palmitoylation signal from GAP43, fused in-frame with ECFP. This in turn is fused at the C-teminus with the Gα_{i2} subunit with a *NotI* site after the STOP codon at the C-terminal end [184]. Fluorescent proteins derived from EGFP contain a native *BsrGI* site at their C-terminal end.

In a first step a *SpeI* site was introduced towards the N-terminus of ECFP (residues 15-17) by site directed mutagenesis using the primers *fw-XFP-mut* and *rv-XFP-mut*. The amino acid sequence of the resulting plasmid, pECFP(SpeI)-Gi2, was not altered by the insertion of the *SpeI* site (silent mutation).

In a second step the the gene encoding for Cit was amplified by PCR using the forward primer *fw-SpeI-frCit* and the reverse primer *rv-BsrGI-frCit* introducing *SpeI* and *BsrGI* restriction sites at the same position as the *SpeI* and *BsrGI* restriction sites in the ECFP of the pECFP(SpeI)-Gi2 plasmid. The *SpeI*/*BsrGI* cut and purified fragment was ligated into the *SpeI*/*BsrGI* cut pECFP(SpeI)-Gi2 plasmid yielding pCit-Gi2.

In a third step, Gα_{i2} was replaced by mouse Gα_{q}. Therefore, the gene encoding for Gα_{q} was was amplified by PCR on the template pSFV1::Gq using the forward primer *fw-BsrGI-Gq* and the reverse primer *rv-NotI-Gq* introducing a *BsrGI* and the last 2 nucleotides of Cit (TGTACAAG) without STOP codon at the 5' end, and a *NotI* restriction site at the 3' end. The *BsrGI*/*NotI* cut and purified fragment was ligated into the *BsrGI*/*NotI* cut pCit-Gi2 plasmid yielding pCit-Gq. To construct pCFP-Gq, the *BsrGI*/*NotI* cut and purified fragment was ligated into the *BsrGI*/*NotI* cut pECFP-mem::Gα_{i2} plasmid.

wtGβ, wtGγ, Cit-Gβ and Cit-Gγ

The *BspEI*/*BamHI* fragments from pEYFP::Gβ_1 and pEYFP::Gγ_2 were cloned into *BspEI*/*BamHI* cut pCit-C1 plasmid yielding Cit-Gβ and Cit-Gγ. The *AgeI*/*BspE1* fragments from pEYFP::Gβ_1 and pEYFP::Gγ_2, containing the Cit-gene fragment, were removed by restriction digest with the corresponding restriction enzymes and the vector was religated (compatible sticky ends) to yield wtGβ and wtGγ, respectively.

8.2.3 Absorption and Emission of Fluorescent Proteins

HEK293 cells expressing cytosolic ECFP, EYFP or Cit were homogenized with a Ultra-Turrax T25 homogenizer (Janke & Kunkel, Staufen, D) to release the cytosolic proteins. Remaining cells end cell fragments were pelleted by centrifugation for 5 min at 14'000 rpm in a 5415D centrifuge (Eppendorf, Hamburg, D). The supernatant with soluble ECFP, EYFP or Cit was stored at -80°C. Optical density at 434 nm for ECFP, and 515 nm for EYFP and Cit was measured on a spectrophotometer DU 640 (Beckman, Fullerton, CA, USA). Emission was measured on a SPEX Fluorolog II (Instruments S.A., Stanmore, UK) with 434 nm excitation and 480 nm emission for ECFP and 510 nm excitation and 530 nm emission for EYFP and Cit. Excitation and emission band pass was 1.8 nm. All measurements were done at room temperature.

AlF_4^- solution is freshly prepared by mixing 800 μl 0.5 mM NaF, 2.4 μl 0.5 mM $AlCl_3$ and 197.6 μl H_2O.

8.2.4 Calcium Response on LSM

G$\alpha_{q/11}$ deficient fibroblast cells were grown in DMEM supplemented with 10% FCS on glass coverslips in 6-well plates. Fibroblasts (60-80% confluent) were transfected using EffecteneTM lipofection (Qiagen, Hilden, D). Transfection solution for one well (2ml medium) contained a total amount of 0.8 μg plasmid DNA in H_2O (1 μg/ml) mixed with 6.4 μl Enhancer in 50 μl EC buffer; it was incubated for 3 minutes at RT. 8 μl Effectene was added, and after 10 minutes incubation at RT, the solution was added to the cells in FCS free DMEM. 24-55 hours after transfection, the cells were loaded with a calcium-sensitive dye (Calcium 3 assay kit, Molecular Devices) in 400 μl during 30 minutes at 37°C. The loading solution was replaced by D-PBS with 0.1% BSA, placed on the Zeiss LSM 510 microscope, and time series were recorded with addition of 100 nM SP.

8.2.5 FRET Spectrometry and Microscopy

For FRET spectroscopy with cell suspensions, HEK293 cells or the stable NK1R-ECFP cell line were transfected according the protocol described in Chapter 3. For FRET between receptor and G protein or between G protein subunits the DNA mixture contained always all three subunits of the heterotrimeric G protein: 10 parts of Gq(Cit) or wtGq, 1 part of wtGβ or wtGγ, and 0.2 part of Cit-Gβ or Cit-Gγ. 48 hours after transfection, cells were washed in PBS and detached from the plates using PBS containing 0.5 mM EDTA. The cells from one 10-cm culture dish were resuspended in isotonic buffer (137.5 mM NaCl, 1.25 mM $MgCl_2$, 1.25 mM $CaCl_2$, 6 mM KCl, 5.6 mM glucose, 10 mM HEPES, 0.4 mM NaH_2PO_4, pH 7.4) to a concentration of about 10^6 cells/ml.

Fluorescence spectra of cell suspensions were recorded on a SPEX Fluorolog II (Instruments S.A., Stanmore, UK). Samples were placed in a $10 \times 4\,\mathrm{mm}^2$ quartz cuvette (Hellma, D) and continuously stirred by a magnetic stirrer. For FRET spectroscopy on single cells and FRET microscopy HEK293 cells were grown on 0.17 mm thick, 25 mm diameter glass coverslips (Assistent, D) deposited in 6-well plates (TPP, CH) and transfected in the same way as described above. Further details and FRET calculations are described in Section 4.4.

The DA molar ratio (r_{DA}) was estimated from corresponding spectra according to

$$r_{\mathrm{DA}} = \frac{\varepsilon_{\mathrm{A}}}{\varepsilon_{\mathrm{D}}} \frac{\phi_{\mathrm{A}}}{\phi_{\mathrm{D}}} \frac{d_{\mathrm{donor}} S_{\mathrm{D,donor}}}{a_{\mathrm{acceptor}} S_{\mathrm{A,donor}}}. \tag{8.1}$$

The molar extinction coefficients at donor excitation wavelength for the acceptor is ε_{A} and for the donor it is ε_{D}. ϕ_{A} and ϕ_{D} are the quantum yields of acceptor and donor,. d_{donor}, a_{acceptor}, $S_{\mathrm{D,donor}}$ and $S_{\mathrm{A,donor}}$ are the fitting coefficients and their corresponding spectra as described in Chapter 4.4. Note that $d_{\mathrm{donor}} S_{\mathrm{D,donor}} = F_{\mathrm{DA}}$ and $a_{\mathrm{acceptor}} S_{\mathrm{A,donor}} = F_{\mathrm{A}}$. F_{DA} is used instead of F_{D}, because the real donor intensity (F_{D}) can not be determined correctly due to quenching by FRET. Therefore, r_{DA} is only a rough estimate of the real DA ratio.

8.3 Results and Discussion

8.3.1 Halide Sensitivity of EYFP and Citrine

In this work, the mutation Q69M has been introduced into EYFP by site directed mutagenesis to yield Citrine (Cit), which is supposed to be less sensitive to fluoride [183] (Figure 8.2 A). Introducing this point mutation was necessary, because a AlF_4^--solution,

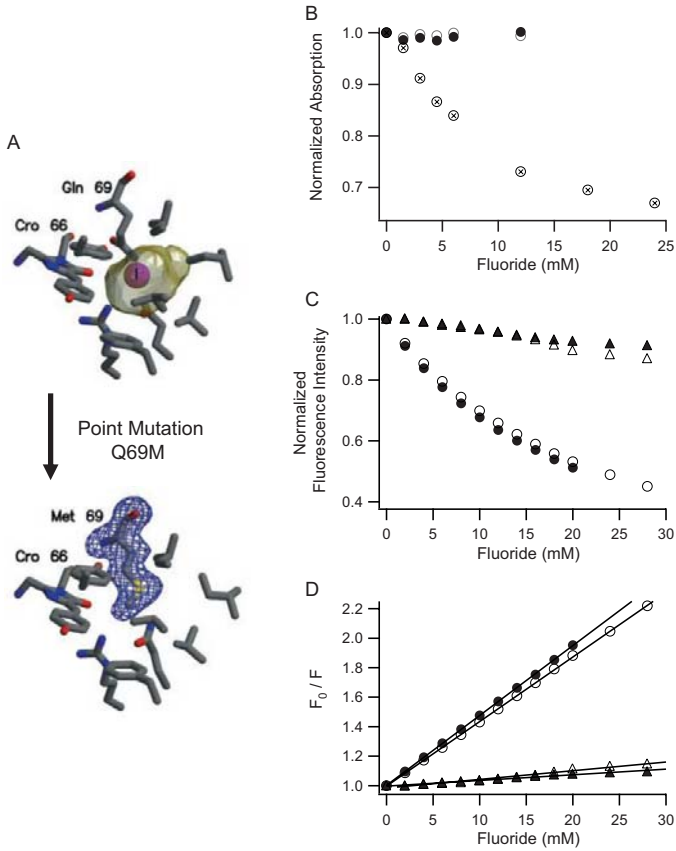

	K_s^{-1} in mM	
	fluoride	AlF_4^--solution
EYFP	21.1 ± 0.1	23.0 ± 0.1
Cit	271 ± 15	201 ± 21

Figure 8.2: Citrine versus EYFP. *A, detailed view of residue 69 and surrounding residues from EYFP and Citrine (Cit) (taken from [183]). The mutation from Gln69 to Met69 reduces the cavity where the halide can bind (here a iodide), and thereby blocks the binding. B, normalized absorption versus fluoride concentration of ECFP (full circles), Cit (empty circles) and EYFP (crossed circles). C and D, normalized fluorescence intensity (C) and Stern-Volmer plot (D) of EYFP and Cit against fluoride and AlF_4^--solution. EYFP vs. fluoride (full circles), EYFP vs. AlF_4^- (empty circles), Cit vs. fluoride (full triangles), and Cit vs. AlF_4^- (empty triangles). The Table represents K_s^{-1} values from the Stern-Volmer plot fitted with Eq. 8.2 (± 95% confidence interval).*

which is used for direct activation of the $G\alpha_q$ contains free fluoride anions, which quench the EYFP fluorescence. Quenching of EYFP further leads to artifacts in the FRET signal and make it impossible to distinguish if changes in FRET are due to quenching or real distance changes.

To compare the effect of fluoride and a AlF_4^--solution on the absorbance and fluorescence emission of ECFP, EYFP and Cit, the soluble FPs were extracted from HEK293 cells transfected with the respective plasmid. The fluorescence emission of EYFP was strongly dependent on the amount of fluoride (NaF) or an AlF_4^--solution (Figure 8.1C). The fluorescence emission of Cit decreased only very little as compared to EYFP. This small decrease might be due to photobleaching. The fluorescence emission of ECFP was not quenched by fluoride (data not shown).

Whether the observed quenching of EYFP is due to dynamic (collisional) or static quenching, can be distinguished by examination of the absorption. Dynamic quenching affects the excited state of the fluorophore and therefore no change in absorption is expected. In contrast, complex formation in static quenching usually results in the perturbation of the absorption spectrum of the fluorophore.

The strong decrease in absorption found for EYFP (Figure 8.1B), indicates static quenching, and the Stern-Volmer equation therefore is

$$F_0/F = 1 + K_s[Q], \tag{8.2}$$

where F and F_0 are the fluorescence intensities of the fluorophore in absence and presence of the quencher, respectively, K_s is the association constant of the quencher and $[Q]$ is the concentration of quencher [86]. K_s^{-1} is the quencher concentration at which $F_0/F = 2$, or 50% of the intensity is quenched. Figure 8.1D represents the Stern-Volmer plot from fluorescence intensity measurements and the corresponding K_s^{-1} values are found in the Table in Figure 8.1.

A K_s^{-1} value of about 20mM was measured for EYFP, which is in agreement with the 6mM reported by Jayaraman et al. [182]. The point mutation Q69M (Cit) led to a 10-fold decrease in fluoride sensitivity. This makes Cit more suitable for FRET measurements when working with AlF_4^- for G protein activation, although on the cost of a lower Förster distance R_0, which was calculated from the absorption and emission spectra and the spectral characteristics of ECFP, EYFP and Cit given in Table 8.2.

	Absorption Maximum	Emission Maximum	Quantum yield	Molar Extinction	R_0 with ECFP
ECFP	434	476	0.42	23'900	-
EYFP	514	527	0.61	83'400	49.2
Citrine	516	529	0.76	77'000	40.5

Table 8.2: Spectral characteristics of ECFP, EYFP and Cit. *Absorption and emission maximum are in nm. Quantum Yield and molar extinction ($M^{-1}cm^{-1}$) for ECFP and EYFP were from [123], and for Cit from [183]. The Förster distance R_0 (Å) with ECFP as donor was calculated from absorption and emission spectra according Eq. 4.8 and 4.9.*

8.3.2 Fluorescent Labelling of NK1R and G Protein Subunits

After having produced the fluoride-insensitive Cit, we constructed the different fusion proteins in order to measure FRET between receptor and G protein in vivo. Therefore, ECFP has been fused to the cytosolic C-terminus of NK1R. This brought the ECFP in closer proximity to the G protein than would have a fusion to the extracellular N-terminus. Construction and characterization of NK1R-ECFP has been described in Chapter 5. The labelling of $G\alpha_q$ turned out to be more difficult. Fusion of a fluorescent protein (FP) to either N-terminus or C-terminus did not yield a functional construct (Susanna Cotecchia, personal communication). Therefore, another approach for the FP fusion had to be found.

Gα-subunits consist of two domains: the GTPase domain containing the GDP/GTP binding site and the helical domain. Little is known about the function of the helical domain of Gα-subunits. It is unique to the heterotrimeric G proteins, whereas the GTPase domain is present in all members of the GTPase superfamily. Among the postulated functions of the helical domain are (1) increasing affinity of GTP binding, (2) acting as a tethered intrinsic GTPase activating protein, (3) participating in effector recognition [13, 185]. Comparison of different mammalian Gα-subunits with the Gα from *Saccharomyces cerevisiae* (Gpa1p) reveals a striking difference within the helical domain (Figure 8.3). Gpa1p has large insertions of 110 amino acids in total, the largest part (∼90aa) being between the helices αA and αB.

As Gpa1p from *Saccharomyces cerevisiae* with an insert of 110 amino acids is functional, there was reason to believe that the FP can be inserted here in the helical domain of $G\alpha_q$ without altering its functionality. In addition, the helical domain seems not to interfere directly with the conserved nucleotide binding motifs in the GTPase domain (G-1 to G-5), the receptor coupling sites at the C- and N-terminus, the palmitoylation sites at the N-terminus, and the PLC interaction sites (Figure 8.4), further supporting

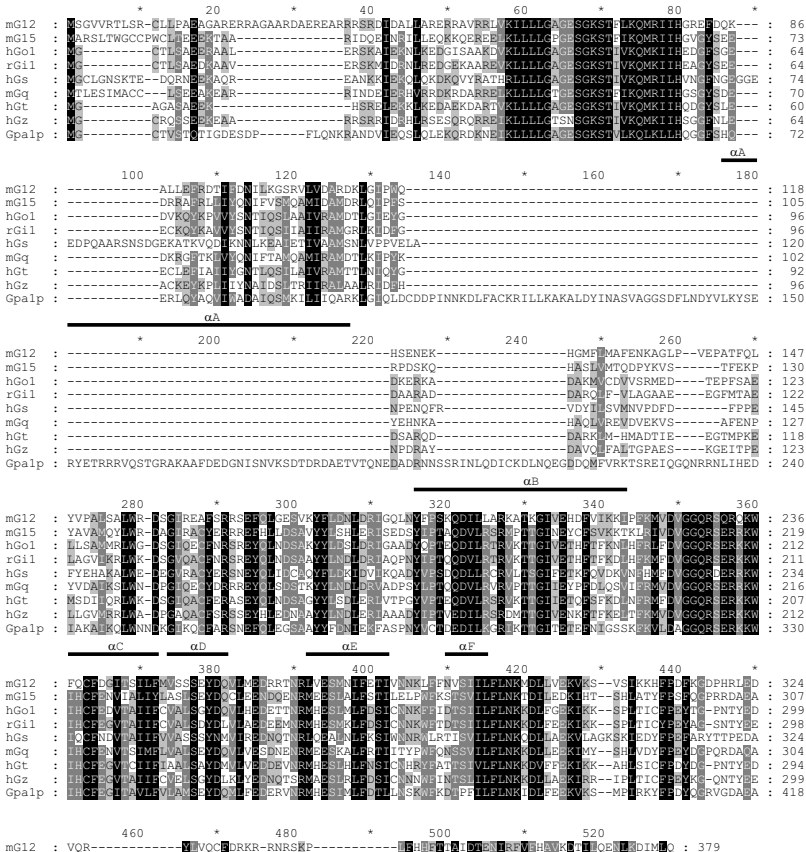

Figure 8.3: Alignment of Gα-subunits. *mG12, mouse Gα_{12} (P27600); mG15, mouse Gα_{15} (P30678); rGi1, rat Gα_{i1} (P10824); hGo1, human Gα_{o1} (P09471); mGq, mouse Gα_q (NP032165); hGs, human Gα_s (P04895); hGt, human Gα_t (P11488); hGz, human Gα_z (P19086); Gpa1p, Gα from* Saccharomyces cerevisiae *(AAB68432). In brackets are the corresponding database accession numbers of the protein sequences. The secondary structure (from αA to αF) corresponding to Gα_t and Gα_{i1} [185] is shown below the aligned sequences. The alignment was done with clustalW (http://www.ebi.ac.uk/clustalw/) using default settings.*

the idea of FP insertion between αA and αB. Therefore, the site between Tyr103 and Glu104 in front of the αB helix (i3 in Figure 8.4) was chosen for insertion. The detailed cloning steps of Gq(EGFP)-BM are described in Section 8.2.

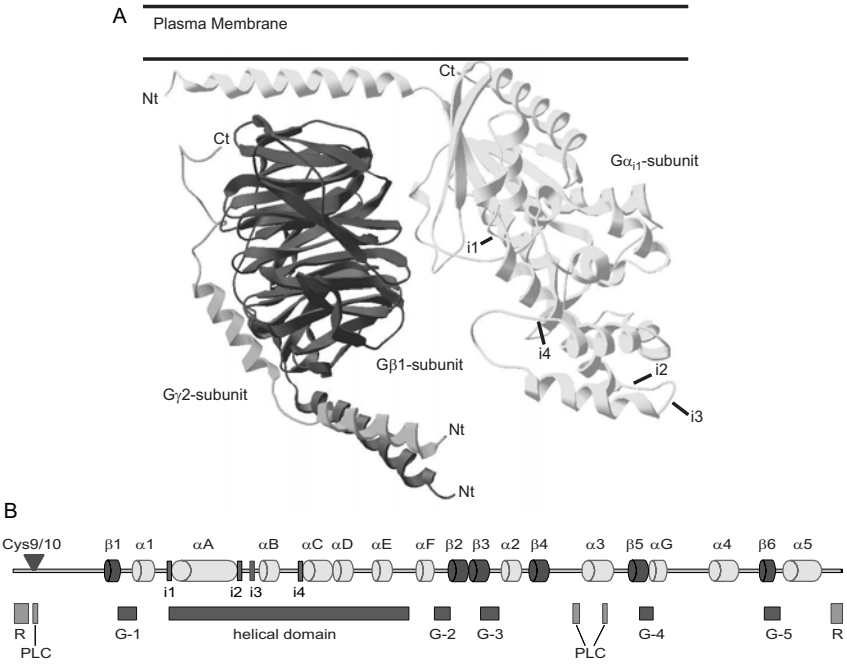

Figure 8.4: Crystal Structure of a G$\alpha\beta\gamma$ and scheme of different domains in mouse Gα_q. *A, crystal structure of Gα_{i2} complexed with Gβ1γ2 (PDB:1GG2) [15]. Ct and Nt indicate C-terminus and N-terminus, respectively. B, Cys9/10, palmitoylation sites [186]; α2 to α5 and αA to αG represent α-helices; β1 to β6 represent β-strands (from alignments with protein sequences with known structures); G-1 to G-5, conserved nucleotide binding motifs [13]; R, receptor coupling sites [20,187]; PLC, domains required for PLC activation [188]. i1, site of FP insertion in Gα_s before helical domain [189]; i2, site of FP insertion in Gα_2 from* D. discodeum *(Lys97 in Gα_q) [118]; i3, site of FP insertion (Tyr103,Glu104) yielding Gq(EGFP)-BM; i4, site of FP insertion (Phe124,Glu125) yielding Gq(ECFP) or Gq(Cit) (same as [190]).*

Although this construct later turned out to be non-functional, the strategy was heading in the right direction. In the meantime, Hughes et al. [190] inserted EGFP between mouse Gα_q residues Phe124 and Glu125, located towards the end of the loop between helices αB and αC (i4 in Figure 8.4). Furthermore, Janetopoulos et al. [118] inserted ECFP towards the beginning of the loop between the helices αA and αB of Gα_2 from *Dictyostelium discoideum*. The insertion site corresponds to residue Lys97 in

mouse $G\alpha_q$ (i2 in Figure 8.4) and is close to our insertion point. Another insertion of EGFP just before the helical domain has been reported for $G\alpha_s$ by Yu et al. [189] (i1 in Figure 8.4).

A different approach for labelling $G\alpha$ was taken by Leaney et al. [184]. They described a functional ECFP fusion to the N-terminus of $G\alpha_{i1\text{-}3}$ and $G\alpha_o$, based on the ECFP-Mem vector (Clontech), which contains the first 20aa of GAP43 as a membrane targeting sequence at the C-terminus of ECFP. The stop codon of ECFP has been removed and the $G\alpha$-subunits were genetically fused to the N-terminus of ECFP.

For further experiments a ECFP (Gq(ECFP)) and EYFP (Gq(EYFP)) fusion with mouse $G\alpha_q$ was constructed in Susanna Cotecchia's lab after the protocol from Hughes et al. [190]. The EYFP in Gq(EYFP) has been further mutated to citrine (Gq(Cit)). Furthermore, the $G\alpha_{i2}$ in pECFP-mem::$G\alpha_{i2}$ (a gift from Andrew Tinker [184]) was exchanged for $G\alpha_q$ yielding ECFP-Gq and Cit-Gq. In addition, the EYFP in the fluorescently labelled subunits EYFP-$G\beta_1$ and EYFP-$G\gamma_2$ (gift from Susanna Cotecchia) was either removed or exchanged for Cit to yield wild type $G\beta_1$ and $G\gamma_2$ and the Cit-labelled subunits, Cit-$G\beta_1$ and Cit-$G\gamma_2$.

8.3.3 Functionality of Fluorescent $G\alpha_q$ and Coupling to NK1R-ECFP

To measure any interactions between NK1R and $G\alpha_q$ it was necessary to know whether the fusion proteins are well expressed and are correctly assembled. Therefore, the new fluorescent $G\alpha$-subunits were expressed in HEK293 cells and confocal micrographs were recorded (Figure 8.5 A-C). Gq(Cit) and Cit-Gq were found to partly localize in the plasma membrane, whereas Gq(EGFP)-BM showed a cytoplasmic localization indicating that this construct, although expressed, might not be functional.

It was shown before, that activation of the NK1R-ECFP led to a calcium response when expressed in HEK293 cells. Because of endogenous $G\alpha_q$ in HEK293 cells, the calcium response resulting from interactions between NK1R-ECFP and fluorescently labelled $G\alpha_q$ had to be measured in a $G\alpha_{q/11}$-deficient fibroblast cell line. Transfection efficiencies of these fibroblast where too low to measure concentration response curves on the FLEX station, as it was done for NK1R-ECFP in HEK293 cells (see Chapter 5). Therefore, calcium response was measured on single cells expressing both the NK1R-ECFP and one of the three $G\alpha_q$ fusion proteins. For Gq(EGFP)-BM no response to SP was observed (data not shown), which we already expected due to the cytoplasmic localization. In contrast, the addition of 100nM SP to cells with Gq(ECFP) or Cit-Gq

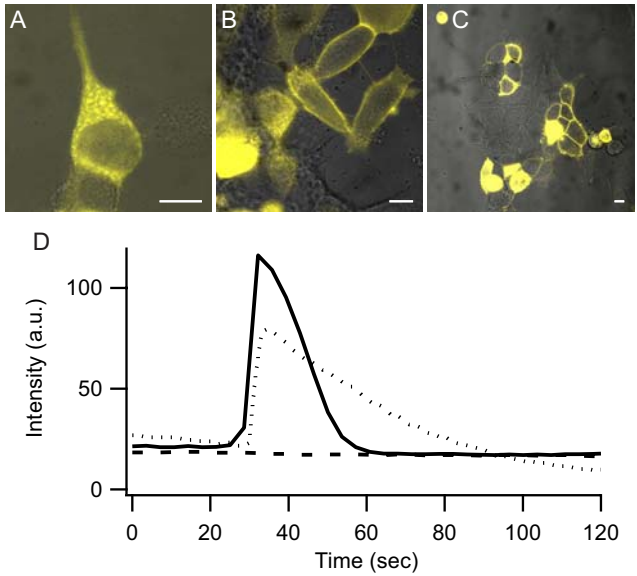

Figure 8.5: Localization of fluorescently labelled $G\alpha_q$ and calcium response. *A-C, confocal micrographs of HEK293 cells expressing Gq(EGFP)-BM (A), Gq(Cit) (B), Cit-Gq (C). Scale bars represent 10μm. D, time course of the fluorescence intensity of calcium sensitive probes inside $G\alpha_{q/11}$-deficient fibroblast cells after SP stimulation of NK1R-ECFP coexpressed with either Gq(Cit) (solid) or Cit-Gq (dotted), and non-transfected cells (dashed). SP concentration used was 100nM. The fluorescence signal increased steeply, reflecting an increase of the intracellular calcium ion concentration.*

resulted in a typical intracellular calcium response (Figure 8.5 D). The response was not detected from non-transfected cells or cells with only NK1R. This confirmed that Gq(Cit) and Cit-Gq were functional with respect to calcium signaling and able to couple to the fluorescently labelled NK1R-ECFP.

It seems that the site of FP insertion into the helical domain of Gα is critical. Insertion of FP between the helices αB and αC yielded a functional Gα_q [190] and insertion of FP between αA and αB also yielded a functional Gα_2-subunit [118]. But the insertion of FP only 6 residues further downstream, still between αA and αB, yielded a non-functional Gα_q-subunit.

Another interesting finding is, that the fusion of FP to the N-terminus of Gα_q was not functional. The reason therefore might be that palmitoylation of Gα_q, required for its functional expression [186], is blocked by the FP fusion. But addition of a membrane targeting sequence with a palmitoylation site targets the fusion construct to the plasma membrane again and restores the functionality.

Although Cit-Gq was functional, we did not use it for FRET studies, because single-molecule experiments performed in our lab (Perez et al., in preparation) showed that Cit-Gq is directly translocated to the plasma membrane without G$\beta\gamma$. Therefore, the protein will mostly be present as a monomer, meaning that it would not interact with the receptor but lead to a high fluorescence background signal in FRET experiments.

For the Gβ- and Gγ-subunits there was no functional assay available in the lab. But because there are several reports of functional Gβ- and Gγ-subunits with a N-terminal fusion of FPs [31,117,118,191,192], we could assume that our constructs are functional as well.

8.3.4 FRET between NK1R and $G_{\alpha\beta\gamma}$ Subunits

With functional fluorescent receptor and G protein subunits tools are now available to measure FRET in whole cells. In a first attempt, FRET was measured in cell suspensions using a spectrometer (see Chapter 4.4). The feasibility of the method was shown with a ECFP-EYFP fusion protein, and by co-expressin ECFP and EYFP in the same cell. Measurements on cells suspensions yielded FRET efficiencies of $45.6\% \pm 0.4$ for the ECFP-EYFP fusion protein and of $4.8\% \pm 1.2$ for co-expressed ECFP/EYFP (mean of 3 samples $\pm$ S.D.). The almost 5% efficiency for the co-expression of ECFP and EYFP is attributed to possible aggregation or high protein expression levels and not an artefact from the method, because a mixture of cells expressing ECFP alone and EYFP alone resulted in 0.9% FRET efficiency.

It is likely that transiently overexpressed fluorescently labelled G protein subunits

are in excess over endogenous free G protein subunits. Because the interaction with G$\beta\gamma$-subunits is required for functionality and membrane targeting of Gα_q [193], the complementary untagged subunits were always co-transfected to promote heterotrimeric complex formation and plasma membrane localization. This meant, that a mixture of three different plasmids had to be used for transient transfection of the stable NK1R-ECFP or wtNK1R cell lines. The DNA ratios of the plasmids for transfection were adjusted to get as close as possible to a 1:1 stoichiometry of expressed donor and acceptor labelled proteins. But even when keeping this DNA ratio constant the estimated DA ratios in the cells varied between different experiments in the range from about 0.1 to 10.

Table 8.3 reflects the range of apparent efficiencies measured in cell suspensions for NK1R-ECFP with Gq(Cit), Cit-Gβ or Cit-Gγ, and for Gq(ECFP) with Cit-Gβ or Cit-Gγ. FRET was detected for all combinations, but for NK1R-ECFP/Cit-Gγ and Gq(ECFP)/Cit-Gγ the apparent efficiencies where rather low and could also be due to overexpression or aggregation of FPs, as it was the case for co-expressed ECFP/EYFP, which showed an apparent efficiency of 5%. In general, the large differences in apparent FRET efficiencies from experiment to experiment were probably due to high variability in transfection efficiencies, expression levels, DA ratios and the fraction of DA complexes. Although FRET could be measured, no changes in FRET could be observed when adding SP or AlF_4^- to activate the NK1R or directly the Gα-subunit, respectively.

	Gq(Cit)	Cit-Gβ	Cit-Gγ
NK1R-ECFP	5-45%	5-20%	1-10%
Gq(ECFP)	-	10-30%	5-10%

Table 8.3: Range of apparent FRET efficiencies of cell suspensions.

The next approach was to use laser scanning confocal microscopy and investigate single cells (see Chapter 4.4). This offers the advantage to select cells of appropriate expression levels and membrane localization of the labelled proteins. Again, the apparent efficiency of the ECFP-EYFP fusion protein and the ECFP/EYFP co-expression was measured and yielded 36%$\pm$1.0 and 1.4%$\pm$3.5, respectively. This showed the feasibility of the approach for cytosolic proteins with a 1:1 DA stoichiometry.

Unfortunately, this approach did not improve the FRET measurements for NK1R and its G proteins. The main reasons were: (i) the excitation of the donor was only possible at 458 nm meaning that the factor $\varepsilon_A/\varepsilon_D$ for ECFP and Cit is 0.3. This leads to high direct excitation of the acceptor and in consequence reduces the dynamic range of the measured *FR* ratio (see Section 4.4.3). (ii) because of misfocusing deviations due

to chromatic aberrations, the donor and acceptor images were effectively taken from slightly different planes in the cells. Therefore, donor and acceptor images did not spatially overlap leading to pixels with extremely high and low FRET.

Because of these problems, we moved to a home-built setup based on a wide-field microscope with a CCD camera coupled to a spectrometer. Here, the deviations due to misfocusing could be avoided by wide-field illumination. Furthermore, the possibility of recording the entire donor and acceptor spectrum should facilitate monitoring FRET changes by simply calculating the ratio between donor and acceptor intensities.

Unfortunately, this approach did not work well either. The main problem here was the field of illumination for the two excitation wavelengths used. Donor and acceptor excitation for a cell or a group of cells of about the size of the illumination field did not overlap, leading to different FRET signals depending on the position of the cells in the field of illumination. Nevertheless, the ECFP-EYFP fusion protein yielded a FRET of $45\% \pm 6.7$, and FRET was also detected between NK1R-ECFP/Gq(Cit), NK1R-ECFP/Cit-Gβ and Gq(ECFP)/Cit-Gβ for some cells, but no changes upon receptor activation were observed.

Taking all this together, we can conclude that there is a FRET signal due to interacting NK1R and G$\alpha\beta\gamma$ and also between Gα_q and G$\beta\gamma$. The reason why no changes could be detected remains unclear. Apart from technical problems, it could also mean, that NK1R and Gα_q form a stable complex, which does not dissociate upon activation. The same could be true for Gα_q and G$\beta\gamma$ as it was seen in the case of Gα_i [31]. This of course is speculation and definite conclusions need further investigations. A setup with wider illumination field and excitation at 430 nm should be used to improve FRET measurements. In addition, the proteins investigated by Bünemann et al. [31] and Gales et al. [117] could be used as a control for receptor-G protein and Gα-G$\beta\gamma$ interaction.

Chapter 9

Ligand Binding to NK1R in Tethered Cell Membranes

9.1 Abstract

G protein-coupled receptors (GPCRs) constitute a large class of seven transmembrane proteins, which bind selectively agonists or antagonists with important consequences for cellular signaling and function. Comprehension of the molecular details of ligand binding is important for the understanding of receptor function and in turn for the design and development of novel therapeutic compounds. Here we show how ligand-receptor interaction can be investigated in situ with high sensitivity on sensor surfaces by total internal reflection fluorescence (TIRF) measurements. A generally applicable method for the surface immobilization of membrane proteins was developed using the prototypic seven transmembrane neurokinin-1 receptor. The receptor was expressed as a biotinylated protein in mammalian cells. Membranes from cell homogenates were selectively immobilized on glass surfaces covered with streptavidin. TIRF measurements showed that a fluorescent agonist binds to the receptor on the sensor surface with similar affinity as to the receptor in live cells. This approach offers the possibility to investigate minute amounts of membrane protein in an active form and in its native environment without purification.

9.2 Introduction

G protein-coupled receptors (GPCRs) play a central role in cellular signaling. Because this class of proteins comprises the most important targets of presently used medicines [194], there is an increasing demand for reliable and fast methods to probe

the function of GPCRs [195] both for investigating the molecular basis of cellular signaling reactions and for developing novel therapeutic compounds [196]. Among the membrane proteins known to belong to the GPCR superfamily, there are only a few with well characterized ligands. Orphan GPCRs, for which no ligands have been identified yet, represent therefore important potential drug targets [197, 198].

Probing the function of large numbers of receptors or libraries of active compounds can be performed either in suspension using microvolume samples [155] or on surfaces, taking advantage of optical surface-sensitive detection, which allows on-line distinction between free and bound molecules without additional separation steps. Typical methods and devices used are infrared spectroscopy [199–201], surface plasmon resonance (SPR) [202–205], reflectometric interference spectroscopy [206], and total internal reflection fluorescence (TIRF) [207, 208]. The detection of molecular interactions of surface-immobilized receptors by fluorescence (either using fluorescent proteins or fluorescent ligands) is in general much more sensitive than by SPR, where variations of effective refractive index at the surface are detected. Although these techniques have been widely used to investigate DNA molecules and water-soluble proteins, they have been rarely applied to membrane proteins, mainly because of difficulties to obtain large amounts of these proteins and to keep them under physiological conditions (whole cells, plasma membranes) in a functionally active form at sensor surfaces.

Surface-sensitive techniques require the immobilization of one of the interacting partners. Apart from chemical cross-linking of the protein to the surface, several surface immobilization strategies have been used based on high affinity interactions between oligohistidine sequences and nitrilotriacetic acid (NTA) [209], glutathion-S-transferease and glutathione, antibody and antigen [210], streptavidin and biotin [202], or complementary oligonucleotides [211]. Presently the combination of biosensing [212] with microarray technology is of great interest in proteomics since it allows highly parallel investigation of many proteins [213].

To probe the function of proteins of low abundance, it is prerequisite to reduce protein consumption to the nano- to picogram region and perform fast, highly sensitive measurements. In the case of membrane proteins, the investigation can be performed under physiological conditions, using either whole cells or plasma membranes, but also on purified samples using detergent-solubilized proteins or reconstituted proteins in artificial lipid membranes [214–216]. Membrane protein purification is generally very time-consuming and not trivial since it requires solubilization without altering the function of the protein.

In this paper,we describe a novel approach to immobilize minute amounts of recombi-

nant, biotinylated membrane receptor proteins in a uniform orientation on streptavidin coated sensor surfaces. Using the very sensitive TIRF technology, we show that it is possible to perform the fluorescent measurements under physiological conditions using non purified cell homogenates. This is demonstrated in the case of the neurokinin-1 receptor (NK1R), a representative GPCR [5, 217], investigating ligand-receptor interactions.

9.3 Experimental Procedures

9.3.1 Materials

Bovine serum albumin (BSA), biotinylated BSA (BSA-biot), and biotin were purchased from Sigma (St. Louis, MO). Fluorescein-labelled BSA (BSA-flu), streptavidin, fluorescein-labelled streptavidin (Strep-flu), and fluorescein-labelled substance P (SP-flu) were purchased from Molecular Probes (Eugene, OR). Competitive antagonist L-732,138 was purchased from Tocris Cookson Ltd. (Langford, UK), and [^{3}H]-SR 140333 from NEN (Boston, MA). Phosphate-buffered saline (PBS) was used (10 mM phosphate, 138 mM NaCl, 2.7 mM KCl, pH 7.4), supplemented with $MgCl_2$ (3 mM) when investigating NK1R-biot.

9.3.2 Neurokinin-1 Receptor

Biotinylated NK1R-biot and wild-type NK1Rs were overexpressed in CHO cells, upon infection with recombinant Semliki Forest virus encoding for the respective proteins as described earlier [218]. NK1R-biot comprises a C-terminal biotin tag. This tagged receptor protein was previously shown to display similar affinity for radioactive substance P ([^{3}H]-SP) as the wild-type protein and to activate calcium signaling as measured by intracellular Ca^{2+} release in Semliki Forest virus infected BHK and CHO cells [218]. Cell pellets were homogenized with a Dounce homogenizer in PBS prior to storage at -80°C. Purified membranes were prepared from cell pellets according to Mazina et al. [219]. The quantity of NK1Rs in the cell membranes was estimated by radioligand binding experiments using NK1R antagonist [^{3}H]-SR 140333.

9.3.3 TIRF Measurements

TIRF measurements were performed using a homemade instrument described elsewhere [208]. Fluorophores at the quartz-water interface were excited by a laser beam of 488 nm and 10 μW (argon-ion laser 163C, Spectra- Physics, Mountain View, CA) at

an angle of incidence of 72° using a quartz prism (Wisag, Zürich, CH) [208] to couple the light into the quartz plate (corresponding penetration depth of the evanescent wave of 100 nm [207]). The prism and plate were kept in optical contact by index matching fluid (Cargille, Cedar Grove, NJ). The emitted fluorescence was collected by a water immersion objective (40×, 0.75 NA,Zeiss, Oberkochen, D) of an inverted Zeiss Axiovert fluorescence microscope, passed a dichroic mirror (510nm) and an emission filter (band-pass 515-565 nm), and was finally measured by a photomultiplier (R928, Hamamatsu, Bridgewater, NJ), using a PC-controlled photoncounting system (System DM3000, Spex, Middlesex, UK). The sample chamber covered 19.6 mm^2 of the total internal reflection glass element and had a volume of 33 μl. It was connected to a peristaltic pump allowing a purge of 500 μl/min fluid.

9.3.4 Surface Modification

Microscope quartz slides (37 × 25 × 1 mm^3, Wisag) were cleaned successively in Hellmanex, water, and ethanol at 60°C for 30 min, followed by 2 min sonication, and finally stored in water. For each experiment, a dried quartz slide was assembled in the TIRF chamber and was incubated for 30 min at room temperature (RT) with a solution of a mixture of BSA/BSA-biot (each 0.05 mg/ml in PBS). The quartz slide sensor surface was then washed with 20 ml of PBS prior to addition of a 10 μg/ml solution of streptavidin, supplemented with 0.5% Strep-flu. After 20 min, the detection chamber was washed with 20 ml of PBS prior to addition of the cellular extracts. The cellular extracts were freshly thawed and sonicated for 3 min at 4°C in a bath sonicator prior to resuspension in PBS supplemented with $MgCl_2$ (3 mM) to reach a final concentration of 9 nM of NK1R-biot. They were then injected into the detection chamber and left for 1 hour at RT prior to washing of the detection cell with 20 ml of buffer.

9.3.5 Estimation of the Protein Density on Surface

The amount of BSA adsorbed on the surface was estimated based on its molecular dimensions [220], assuming a densely packed layer of BSA as expected from the experimental conditions [221, 222]. The solutions of BSA/BSA-biot and streptavidin were supplemented with a defined amount of homologous fluorescently labelled proteins. To prevent self-quenching at the surface, low concentration of labelled proteins were used (2-10% for BSA-flu and 0.5% for Strep-flu). The ratios BSA/streptavidin and streptavidin/SP-flu were estimated by comparison of the respective signals taking into account their respective labelling stoichiometry and fluorescence quantum yields.

9.3.6 Binding of Strep-flu to BSA-biot on Glass Surfaces

Binding of Strep-flu (S) to BSA-biot (B) adsorbed on glass surfaces was measured by TIRF. The TIRF intensities measured at different concentrations of S in the bulk medium are directly proportional to the number of molecules of Strep-flu bound to the BSA-biot, allowing one to establish a binding isotherm. Data were fitted according to the chemical equilibrium $B + \nu S \rightleftarrows BS_\nu$ using a Hill equation, neglecting nonspecific binding and depletion,

$$BS^* = \frac{S_{\mathrm{T}}^\nu}{K_{\mathrm{Sd}}^\nu + S_{\mathrm{T}}^\nu}. \tag{9.1}$$

BS^* is the normalized measured fluorescence intensity of S bound to B and is proportional to the concentration of BS_ν. S_{T} is the total molar concentration of Strep-flu injected, ν is the Hill coefficient, and K_{Sd} is the apparent dissociation constant of the considered complex between Strep-flu and BSA-biot.

9.3.7 Binding of SP-flu to Surface-Immobilized NK1R-biot

TIRF measures total binding (specific plus nonspecific) of SP-flu to immobilized NK1R-biot. The nonspecific binding of SP-flu was estimated using two methods. In the first approach, increasing concentrations of SP-flu were introduced in the flow chamber, always in the presence of the same concentration of non-fluorescent SP (at least a 100-fold excess). The resulting fluorescence signal was shown to be linearly dependent on the SP-flu concentration in the surrounding medium. The second method for estimating the nonspecific binding of SP-flu consisted of an "internal" measurement, which was systematically performed in all binding experiments. The total binding of SP-flu was measured by the stepwise increase of SP-flu concentration. After measuring the fluorescence at the highest concentration of SP-flu (usually 90 nM), an excess of the non-fluorescent competitive antagonist L-732,138 [223] was added to remove the specifically bound SP-flu at this particular concentration, and the nonspecifically bound SP-flu was deduced. Assuming that the nonspecific binding of SP-flu depends linearly on its concentration in the surrounding medium, we calculated the amount of nonspecifically bound SP-flu for each concentration of ligand tested. The two approaches gave similar values.

The intensities measured at different ligand concentrations are directly proportional to the number of molecules of bound SP-flu. The binding curves of SP-flu (L) to NK1R-biot (R) were established on various sensor chips. After normalization of their intensities for 90 nM SP-flu, they were averaged and the average binding isotherm was analyzed

taking into account the reaction $R + L \rightleftarrows RL$, described by

$$RL^* = \frac{L_\mathrm{T}}{K_\mathrm{Ld} + L_\mathrm{T}}. \tag{9.2}$$

RL^*, the measured normalized fluorescence intensity of the ligand bound to surface-immobilized receptor is assumed to be proportional to the molar concentration of the ligand-receptor complex (RL), L_T is the total molar concentration of ligand injected, and K_Ld is the apparent dissociation constant of the complex RL.

9.4 Results and Discussion

9.4.1 Preparation of Sensor Surfaces

Cell membranes comprising GPCRs were immobilized on quartz surfaces as follows. Our method is based on the high affinity of streptavidin for biotin [224,225]. As illustrated in Figure 9.1, the sensor surface is first covered by a mixed layer of BSA/BSA-biot to which an additional layer of streptavidin is bound specifically. This surface acts as a template for the controlled tethering of cell membrane fragments comprising biotinylated GPCRs.

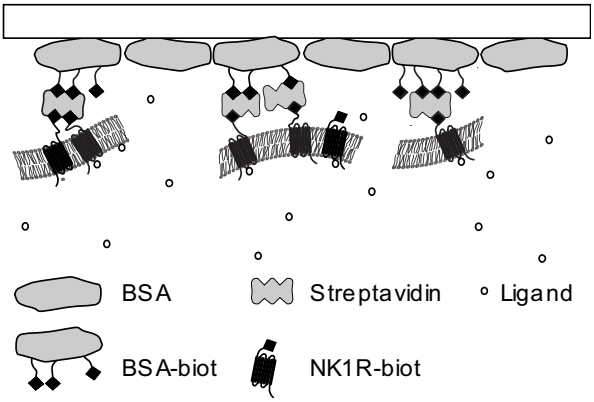

Figure 9.1: Molecular architecture of the functionalized sensor surface. *The quartz slide is first covered with a mixed layer of BSA/BSA-biot. An additional layer of streptavidin is bound specifically to BSA-biot. Cell membrane fragments comprising NK1R-biot are finally assembled on top of the streptavidin layer. Protein concentrations for BSA, streptavidin, and NK1R-biot were estimated to be* $1.8 - 5.5 \times 10^4$, $5 - 15 \times 10^3$, *and* $100 - 400$ *molecules/*μm^2, *respectively.*

Co-adsorption of a 1:1 molar mixture of BSA and BSA-biot to the quartz surface

was monitored by TIRF using BSA-flu as a fluorescent probe (2-10 mol %). At a concentration of 0.1 mg/ml total BSA, the formation of the protein layer was completed within 25 min. 71% of the surface adsorbed layer could not be removed by extensive wash with buffer, which is in agreement with published reports [221, 222].

The functional activity of the surface-immobilized mixed BSA/BSA-biot layer was investigated by quantifying the binding of streptavidin in the presence of 0.5 mol % of Strep-flu by TIRF. A K_{Sd} value of 1.27 ± 0.07 nM (Figure 9.2) was obtained. This value is in agreement with published data for the interaction of streptavidin with protein-coupled biotin (K_{Sd} = 1-10 nM for BSA-biot/streptavidin, depending on the presence or absence of a spacer between the protein and the biotin-tag [225]) and is considerably higher than K_{Sd} values for the interaction of free biotin with streptavidin (typically 10^{-15}M [225]). A molar ratio between streptavidin and BSA-biot of 0.55 ± 0.13 was estimated from the TIRF signals.

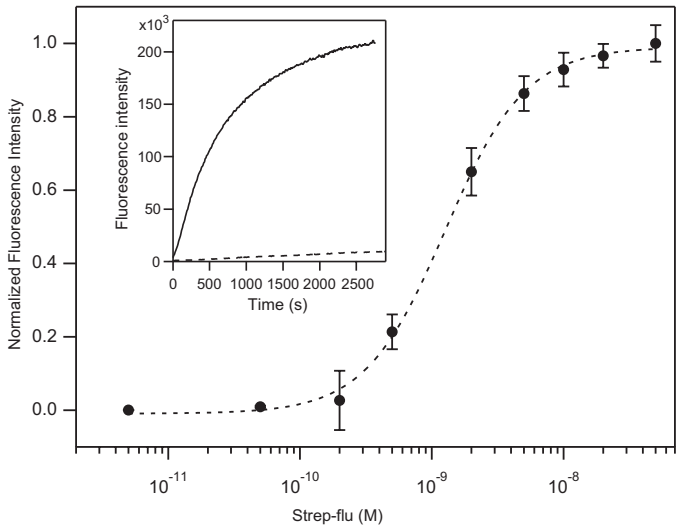

Figure 9.2: Binding of streptavidin to surface-immobilized BSA. *A mixed layer of BSA/BSA-biot (1:1) on the sensor surface was purged with solutions of the indicated concentrations of Strep-flu. Binding of streptavidin to BSA-biot was quantified by measuring the TIRF signal of specifically bound Strep-flu after 30 min of incubation. The insert shows a typical example for the case of 10 nM Strep-flu. The specific binding of Strep-flu (continuous line) is about 16 times higher than the corresponding unspecific binding (dashed line), which was measured after saturating all binding sites accessible on streptavidin by non-fluorescent biotin. Fitting (dashed line) the data (•) with a Hill equation results in a K_{Sd} of 1.27 ± 0.07 nM and a Hill coefficient ν of 1.4 ± 0.1. Data are presented as mean ± standard deviation of three measurements.*

In our experience, the use of a BSA-biot cushion offered a number of advantages over a direct immobilization of streptavidin to the glass surface: (i) Functional activity of streptavidin molecules was improved in a reproducible manner, most probably by preservation of its structure (no direct interaction with the potentially denaturing surface [226]) and by controlling its orientation, that is, its accessibility, and its surface concentration. (ii) Nonspecific binding of proteins and membrane fragments was minimized (data not shown).

9.4.2 Immobilization of NK1R-biot

We used cell homogenates containing NK1R-biot, which is biotinylated in vivo in its C-terminal intracellular domain [218]. NK1R-biot was immobilized on the streptavidin-coated quartz surface by incubating the sensor surface with a cell homogenate comprising the recombinantly expressed receptors. The sensor surface was then extensively washed to remove part of the nonspecifically bound membranes. The tethered membranes showed high mechanical stability, withstanding extensive washing steps with different buffer solutions.

We determined the amount of specifically immobilized receptor using the fluorescent agonist substance P fluorescein (SP-flu) [143,154] as a marker for the NK1R-biot at the surface. As shown in Table 9.1, the presence of the biotin tag on the receptor yielded a 4-fold increase of the signal-to-background ratio, suggesting an improved immobilization specificity of cell homogenates on the streptavidin coated quartz surface. It is also remarkable that no significant improvement of the immobilization was observed if purified plasma membranes were used instead of crude cell homogenates.

biological sample	specific binding of SP-flu[a]	signal/ background ratio[b]
cell homogenates + NK1R-biot	63 ± 16%	4.2 ± 0.7
plasma membranes + NK1R-biot	54 ± 17%	2.9 ± 0.5
cell homogenates + wild-type NK1R	32 ± 5%	1.2 ± 0.2
biotin + cell homogenates + NK1R-biot	29 ± 3%	1.0

Table 9.1: Immobilization of NK1R to sensor surfaces covered with BSA/BSA-biot and streptavidin. [a] *Determined as the percentage of SP-flu removed upon addition of an excess of competitive antagonist L-732,138.* [b] *Ratio of specific binding/nonspecific binding normalized to the ratio of negative control in line 4.*

9.4.3 Binding of SP-flu to NK1R-biot on the Sensor Surface

TIRF was used to measure the binding of the fluorescein-labelled agonist SP-flu [143,154] on surface-immobilized cell membranes. The dependence of TIRF intensities versus free ligand concentration can be evaluated assuming a single binding site per receptor yielding a dissociation constant $K_{\mathrm{Ld}} = 27 \pm 9\,\mathrm{nM}$ (Figure 9.3). This is in agreement with values reported [143, 154] showing that neither the biotin tag nor the immobilization of the protein affect receptor activity significantly. According to Tota et al. [143], the receptor has a low affinity for the agonist SP-flu in the absence ($K_{\mathrm{Ld}} = 48.6\,\mathrm{nM}$) and a high affinity in the presence of its G protein ($K_{\mathrm{Ld}} = 1.2\,\mathrm{nM}$). The K_{Ld} values obtained here from our TIRF measurements indicate that the majority of NK1R-biot does not interact with G proteins. This is reasonable since the receptor was overexpressed in CHO cells in the presence of a low natural abundance of G proteins. However we cannot exclude a perturbation of the G protein binding to the immobilized receptor.

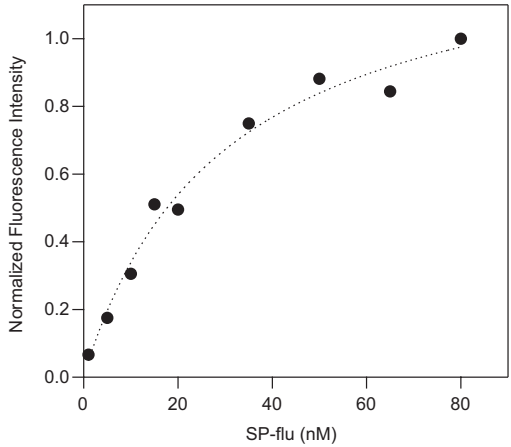

Figure 9.3: Binding of SP-flu to NK1R-biot on the sensor surface. *Binding of the fluorescent agonist SP-flu to NK1 receptors (NK1R-biot) in cell membranes on the sensor surface was measured by TIRF increasing stepwise the concentration of the fluorescent ligand in the bulk. After incubation with the highest concentration (90 nM) of SP-flu used, the sensor surface was purged with a solution of a nonfluorescent competitive antagonist (L-732,138) replacing the specifically receptor-bound SP-flu. The TIRF signal (0.011/nM) stemming from nonspecifically bound SP-flu was subtracted from the corresponding total TIRF signal, obtaining the fluorescence intensity (•) of the specifically bound ligand. Fitting a Langmuir isotherm (dashed line) to the data, shown for a typical experiment, yields a K_{Ld} value of 30 nM. Averaged data of four experiments were best fitted by a Langmuir isotherm with $K_{Ld} = 27 \pm 9$ nM.*

9.4.4 Down-Scaling Receptor Consumption

Cell membranes were immobilized on sensor surfaces by using homogenates of CHO cells, where each cell on average comprised about 1 million receptors. According to the high signal-to-noise ratio of the measured TIRF signals, experiments on membranes containing 10 times fewer receptors (100'000 receptors per cell) can be envisaged. From the normalized fluorescence intensities of Strep-flu and the specifically bound SP-flu at saturating concentrations, we estimated the molar ratio of streptavidin/NK1R-biot on the sensor surface to be 43 ± 13. This corresponds to a surface concentration of 100-400 receptors/μm^2. The measured area on a TIRF sensor was 2000 μm^2 (the cross section of the laser beam on the sensor surface), which corresponds to less than an attomole of immobilized GPCRs.

9.5 Conclusion

Although the streptavidin (or avidin)-biotin technology is well established for the immobilization of water-soluble biopolymers [227], it is used here in a novel approach for membrane proteins [202,228]. In this context, our method offers a number of interesting features summarized as follows.

Previous reports have described immobilization of purified, detergent-solubilized GPCRs, which have or have not been subjected to lipid reconstitution [202,228]. Here, it was demonstrated for the first time that biotinylated membrane proteins, here GPCRs, could be immobilized on a streptavidin-coated quartz sensor surface, using cell homogenates, without prior purification. The selective, high-affinity interaction between biotin and streptavidin allowed a template-directed purification of the receptor uniformly oriented on the support.

The NK1R-biot showed fully preserved ligand-binding activity in the tethered membranes. Due to the surface-selective and highly sensitive TIRF fluorescence detection, 1 attomol of receptor molecules was sufficient to fully characterize binding of a fluorescent agonist to the receptors. According to the measured high signal-to-noise TIRF signals, it is reasonable to extrapolate that ligand receptor interactions can be observed using tethered membranes comprising at least 10 times fewer functional receptor molecules, that is, less than 1 attomol of nonpurified receptor proteins. This opens the possibility to miniaturize further the size of the sensing regions and also to reduce the amount of required receptor proteins substantially.

The procedure is of course not limited to biotinylated recombinant membrane proteins. By artificially integrating biotinylated lipid molecules into the plasma membrane

of cells prior to homogenization, our procedure can be extended to the immobilization and functional investigation of any native or recombinant membrane receptor protein as far as a sensitive procedure is available to characterize the properties of interest. Alternatively, it is possible to use any biotinylated membrane protein for the selective immobilization of cell membranes even if other non-biotinylated membrane proteins are to be investigated. Additional methods for the formation of biotinylated surfaces are based on thiols [202] or poly(ethylene glycol) polymers [229].

This approach for the selective immobilization of native cell membranes on solid supports will be of interest for many applications of membrane protein research [174] such as investigating the function and the biochemical network of membrane proteins as well as for screening how potential therapeutic compounds might influence receptor-mediated cellular functions.

Chapter 10

Summary and Outlook

In this thesis fluorescence resonance energy transfer (FRET) and total internal reflection fluorescence (TIRF) were used for the investigation of G protein-coupled receptors (GPCR). The presented data provide new insight into GPCR signal transduction and have potential for future studies. The thesis includes all the steps from cloning of genetic constructs through cell culturing and biochemistry to the investigation of the recombinant proteins by biophysical methods.

NK1R was fluorescently labelled and shown to be functional with respect to ligand binding and calcium signaling. These fluorescent NK1R constructs can be used for several different studies such as ligand binding, trafficking, oligomerization, and protein-protein interactions. Especially the novel ACP labelling technique has been shown suitable for FRET experiments, but can also be applied for single molecule studies or fluorescence correlation spectroscopy, where low concentrations of labelled proteins are required.

It was shown that the ACP labelling was superior to the labelling with EGFP for a FRET-based specific ligand binding assay on single cells. This ligand binding assay is suitable to measure fast binding kinetics and could be also interesting for screening assays, because it can be miniaturized and there is no washing step needed.

Exploiting the advantages of the ACP labelling, mainly the multiple labelling at a desired dye ratio, it was shown by FRET studies that the NK1R does not form homo-oligomers. The observed FRET signal was strongly dependent on receptor concentration and therefore indicated that the NK1R is present in microdomains. The method used here can give further insight into the many open questions in GPCR oligomerization. Furthermore, it can be applied for other membrane proteins.

The FRET methodology described in this thesis was also used to investigate interactions between NK1R and $G\alpha_q\beta\gamma$-complexes or between $G\alpha_q$ and $G\beta\gamma$. With most

combinations, a FRET signal could be detected, but no changes were observed upon activation of the system. The reason therefore is not obvious. Using a wide-field microscope with optimal donor excitation (e.g. 430 nm for ECFP) would increase the signal to noise ratio and make it possible to detect even small changes in FRET. Furthermore, receptors and G proteins, where FRET changes upon activation have been detected before (e.g. β2AR/Gα_s and Gα_s/G$\beta\gamma$), should be used as a control.

In general, the FRET methodology established in the laboratory will give new insight into GPCR signal transduction processes. The ACP labelling or other labelling techniques allowing the precise control of DA ratios will have an impact on the quality of FRET data and e.g. questions about oligomerization can be answered more precisely.

Furthermore, a novel approach was developed to immobilize NK1R on a surface and to measure ligand binding by TIRF. The procedure is not limited to biotinylated recombinant membrane proteins. By artificially integrating biotinylated lipid molecules into the plasma membrane of cells, the procedure can be extended to the immobilization and investigation of any native or recombinant membrane protein. The method can be miniaturized and is of use for high-throughput screening assays, which is interesting for the pharmaceutical industry.

Abbreviations and Symbols

Abbreviations and Acronyms

5HT3	Mouse serotonin receptor type 3A
A	Acceptor
ACP	Acyl carrier protein
AcpS	Phosphopantetheine transferase (PPTase) from *Escherichia coli*
AcSP	SP analogue with a N-terminal acetyl group instead of the amino group
BRET	Bioluminescence resonance energy transfer
BSA	Bovine serum albumin
C-terminus	Carboxy-terminus
cAMP	Cyclic adenosinemonophosphate
Cit	Citrine (EYFP with mutation Q69M)
CoA	Coenzyme A
D	Donor
D-PBS	Dulbecco's phosphate-buffered saline
DMEM	Dulbecco's modified Eagle medium
DOPG	1,2-dioleoyl-*sn*-glycero-3-[phosphor-*rac*-(1-glycerol)]
DPPE-Cy5	N,N-diethyl-2-[4-(phenylmethyl) phenoxy] ethanamine labelled with Cy5
ECFP	Enhanced cyan fluorescent protein
EGFP	Enhanced green fluorescent protein
EYFP	Enhanced yellow fluorescent protein
FCS	Fetal calf serum
FP	Fluorescent protein
FRET	Fluorescence resonance energy transfer
GDP	Guanosinediphosphate
GFP	Green fluorescent protein
GPCR	G protein-coupled receptor
GTP	Guaninetriphosphate
G protein	Heterotrimeric GTP-binding protein
HEK293	Human embryonic kidney cells
IP3	Inositol-trisphosphate

N-terminus	Amino-terminus
NK1R	Neurokinin 1 receptor, substance P receptor, or NK1 receptor
NK2R	Neurokinin 2 receptor
NK3R	Neurokinin 3 receptor
NKA	Neurokinin A, the physiological agonist for NK2R
NKB	Neurokinin B, the physiological agonist for NK3R
PCR	Polymerase chain reaction
PPTase	Phosphopantetheine transferase
ROI	Region of interest
SP	Substance P, the physiological agonist for NK1R
TIRF	Total internal reflection fluorescence
TM	Transmembrane helix

Physical Symbols

η_{A}	Detection efficiency for the acceptor
η_{D}	Detection efficiency for the donor
κ	Factor describing the relative orientation in space of the transition dipoles between the donor and acceptor
λ	Wavelength in nm
$\Phi_{\mathrm{T}}^{\mathrm{D}}$	Quantum yield of energy transfer from the donor
ϕ_{A}	Fluorescent quantum yield of the acceptor
ϕ_{D}	Fluorescent quantum yield of the donor
σ_{Cy5}	DPPE-Cy5 surface density on vesicle
σ_{r}	Receptor surface density
τ_{DA}	Lifetime of the donor in presence of the acceptor
τ_{D}	Lifetime of the donor in absence of the acceptor
FR	FRET ratio: $F_{\mathrm{AD}}/F_{\mathrm{A}}$
ε_{A}	Molar extinction coefficient of the acceptor
ε_{D}	Molar extinction coefficient of the donor
c_{A}	Reduced acceptor concentration (acceptor surface density normalized by R_0^2
E	Efficiency of energy transfer
E_{app}	Apparent efficiency of energy transfer
EC_{50}	Half-maximal response. Molar concentration of an agonist that produces 50% of the maximal possible effect of that agonist
F_{A}	Fluorescence intensity of acceptor emission in the absence of donor (direct excitation of acceptor only)
f_{a}	Fraction of acceptor in complex with donor
F_{D}	Fluorescence intensity of donor emission in the absence of acceptor
f_{D}	Molar fluorescence of donor emission in the absence of acceptor
f_{d}	Fraction of donor in complex with acceptor

F_{AD}	Fluorescence intensity of acceptor emission in the presence of donor (consisting of fluorescence arising from energy transfer and from direct excitation of the acceptor)
F_{DA}	Fluorescence intensity of donor emission in the presence of acceptor
f_{DA}	Molar fluorescence of donor emission in the presence of acceptor
$J(\lambda)$	Spectral overlap of the donor emission with the acceptor absorption
K_{d}	Dissociation constant
k_{c}	Rate constant of internal coversion
k_{f}	Rate constant of radiative decay to the ground state
k_{isc}	Rate constant of intersystem crossing to a triplet state
k_{Q}	Rate constant of collisional quenching
k_{r}	Rate constant of vibrational relaxation
k_{T}	Rate constant of long-range resonance dipole energy transfer
n	Refractive index of the medium or number of units in a oligomeric complex
N_{A}	Avogadro's number ($6.022 \cdot 10^{23}$)
pEC_{50}	Negative logarithm of EC_{50}
r	Distance between donor and acceptor molecule
R_0	Förster Distance (distance at which FRET is 50% efficient)
R_{c}	Distance of closest approach of donor and acceptor
x'_{DU}	Mole fraction of donor labelled and unlabelled receptors together
x'_{U}	Mole fraction of unlabelled receptors
x_{A}	Acceptor mole fraction
x_{D}	Donor mole fraction
x_{mono}	Mole fraction of monomers
x_{oligo}	Mole fraction of oligomers

Bibliography

[1] B. Alberts. *Molecular biology of the cell*. Garland Science, New York, 4th edition, 2002.

[2] J. M. Berg, J. L. Tymoczko, and L. Stryer. *Biochemistry*. Freeman, New York, 5th edition, 2002.

[3] S. Takeda, S. Kadowaki, T. Haga, H. Takaesu, and S. Mitaku. Identification of G protein-coupled receptor genes from the human genome sequence. *FEBS Lett*, 520(1-3):97–101, 2002.

[4] A. Wise, K. Gearing, and S. Rees. Target validation of G protein-coupled receptors. *Drug Discov Today*, 7(4):235–46, 2002.

[5] U. Gether. Uncovering molecular mechanisms involved in activation of G protein-coupled receptors. *Endocr Rev*, 21(1):90–113, 2000.

[6] A. M. vanRhee and K. A. Jacobson. Molecular architecture of G protein-coupled receptors. *Drug Development Research*, 37(1):1–38, 1996.

[7] T. Gudermann, T. Schoneberg, and G. Schultz. Functional and structural complexity of signal transduction via G protein-coupled receptors. *Annu Rev Neurosci*, 20:399–427, 1997.

[8] K. Palczewski, T. Kumasaka, T. Hori, C. A. Behnke, H. Motoshima, B. A. Fox, I. Le Trong, D. C. Teller, T. Okada, R. E. Stenkamp, M. Yamamoto, and M. Miyano. Crystal structure of rhodopsin: A G protein-coupled receptor. *Science*, 289(5480):739–45, 2000.

[9] S. R. George, B. F. O'Dowd, and S. P. Lee. G protein-coupled receptor oligomerization and its potential for drug discovery. *Nat Rev Drug Discov*, 1(10):808–20, 2002.

[10] E. J. Neer. G proteins: critical control points for transmembrane signals. *Protein Sci*, 3(1):3–14, 1994.

[11] E. J. Helmreich and K. P. Hofmann. Structure and function of proteins in G protein-coupled signal transfer. *Biochim Biophys Acta*, 1286(3):285–322, 1996.

[12] D. E. Clapham and E. J. Neer. G protein $\beta\gamma$ subunits. *Annu Rev Pharmacol Toxicol*, 37:167–203, 1997.

[13] S. R. Sprang. G protein mechanisms: insights from structural analysis. *Annu Rev Biochem*, 66:639–78, 1997.

[14] N. Gautam, G. B. Downes, K. Yan, and O. Kisselev. The G protein $\beta\gamma$ complex. *Cell Signal*, 10(7):447–55., 1998.

[15] M. A. Wall, D. E. Coleman, E. Lee, J. A. Iniguez-Lluhi, B. A. Posner, A. G. Gilman, and S. R. Sprang. The structure of the G protein heterotrimer $G\alpha_{i1}\beta1\gamma2$. *Cell*, 83(6):1047–58, 1995.

[16] J. Wess. Molecular basis of receptor/G protein-coupling selectivity. *Pharmacol Ther*, 80(3):231–64, 1998.

[17] H. R. Bourne. How receptors talk to trimeric G proteins. *Curr Opin Cell Biol*, 9(2):134–42, 1997.

[18] B. R. Conklin, Z. Farfel, K. D. Lustig, D. Julius, and H. R. Bourne. Substitution of three amino acids switches receptor specificity of $G\alpha q$ to that of $G\alpha i$. *Nature*, 363(6426):274–6., 1993.

[19] B. R. Conklin and H. R. Bourne. Structural elements of $G\alpha$ subunits that interact with $G\beta\gamma$, receptors, and effectors. *Cell*, 73(4):631–41., 1993.

[20] E. Kostenis, M. Y. Degtyarev, B. R. Conklin, and J. Wess. The N-terminal extension of $G\alpha q$ is critical for constraining the selectivity of receptor coupling. *J Biol Chem*, 272(31):19107–10, 1997.

[21] A. Bohm, R. Gaudet, and P. B. Sigler. Structural aspects of heterotrimeric G protein signaling. *Curr Opin Biotechnol*, 8(4):480–7, 1997.

[22] G. E. Breitwieser. G protein-coupled receptor oligomerization: implications for G protein activation and cell signaling. *Circ Res*, 94(1):17–27, 2004.

[23] L. Birnbaumer. Transduction of receptor signal into modulation of effector activity by G proteins: the first 20 years or so. *FASEB J*, 4(14):3178–88, 1990.

[24] T. Gudermann, F. Kalkbrenner, and G. Schultz. Diversity and selectivity of receptor-G protein interaction. *Annu Rev Pharmacol Toxicol*, 36:429–59, 1996.

[25] J. Wess. G protein-coupled receptors: molecular mechanisms involved in receptor activation and selectivity of G protein recognition. *FASEB J*, 11(5):346–54, 1997.

[26] U. Gether and B. K. Kobilka. G protein-coupled receptors. II. Mechanism of agonist activation. *J Biol Chem*, 273(29):17979–82, 1998.

[27] S. Terrillon and M. Bouvier. Roles of G protein-coupled receptor dimerization. *EMBO Rep*, 5(1):30–4, 2004.

[28] A. E. Brady and L. E. Limbird. G protein-coupled receptor interacting proteins: emerging roles in localization and signal transduction. *Cell Signal*, 14(4):297–309, 2002.

[29] S. Klein, H. Reuveni, and A. Levitzki. Signal transduction by a nondissociable heterotrimeric yeast G protein. *Proc Natl Acad Sci USA*, 97(7):3219–23, 2000.

[30] A. Levitzki and S. Klein. G protein subunit dissociation is not an integral part of G protein action. *ChemBioChem*, 3(9):815–818, 2002.

[31] M. Bunemann, M. Frank, and M. J. Lohse. Gi protein activation in intact cells involves subunit rearrangement rather than dissociation. *Proc Natl Acad Sci USA*, 100(26):16077–82, 2003.

[32] J. M. Herz, W. J. Thomsen, and G. G. Yarbrough. Molecular approaches to receptors as targets for drug discovery. *J Recept Signal Transduct Res*, 17(5):671–776, 1997.

[33] A. Christopoulos and T. Kenakin. G protein-coupled receptor allosterism and complexing. *Pharmacol Rev*, 54(2):323–74, 2002.

[34] T. Kenakin. Efficacy at G protein-coupled receptors. *Nat Rev Drug Discov*, 1(2):103–10, 2002.

[35] R. J. Lefkowitz, S. Cotecchia, P. Samama, and T. Costa. Constitutive activity of receptors coupled to guanine nucleotide regulatory proteins. *Trends Pharmacol Sci*, 14(8):303–7., 1993.

[36] P. Leff, C. Scaramellini, C. Law, and K. McKechnie. A three-state receptor model of agonist action. *Trends Pharmacol Sci*, 18(10):355–62., 1997.

[37] T. Kenakin. Differences between natural and recombinant G protein-coupled receptor systems with varying receptor/G protein stoichiometry. *Trends Pharmacol Sci*, 18(12):456–64, 1997.

[38] J. M. Weiss, P. H. Morgan, M. W. Lutz, and T. P. Kenakin. The cubic ternary complex receptor-occupancy model. 1. Model description. *Journal of Theoretical Biology*, 178(2):151–167, 1996.

[39] J. M. Weiss, P. H. Morgan, M. W. Lutz, and T. P. Kenakin. The cubic ternary complex receptor-occupancy model. 2. Understanding apparent affinity. *Journal of Theoretical Biology*, 178(2):169–182, 1996.

[40] J. M. Weiss, P. H. Morgan, M. W. Lutz, and T. P. Kenakin. The cubic ternary complex receptor-occupancy model. 3. Resurrecting efficacy. *Journal of Theoretical Biology*, 181(4):381–397, 1996.

[41] E. Hermans. Biochemical and pharmacological control of the multiplicity of coupling at G protein-coupled receptors. *Pharmacology and Therapeutics*, 99(1):25–44, 2003.

[42] W. F. Simonds. G protein regulation of adenylate cyclase. *Trends Pharmacol Sci*, 20(2):66–73, 1999.

[43] P. C. Sternweis and A. V. Smrcka. Regulation of phospholipase C by G proteins. *Trends Biochem Sci*, 17(12):502–6, 1992.

[44] J. G. Voet and D. Voet. *Biochemistry*. Wiley, New York [etc.], second edition, 1995.

[45] G. Krapivinsky, L. Krapivinsky, K. Wickman, and D. E. Clapham. G$\beta\gamma$ binds directly to the G protein-gated K^+ channel, I_{KACh}. *J Biol Chem*, 270(49):29059–62., 1995.

[46] M. Bouvier. Oligomerization of G protein-coupled transmitter receptors. *Nat Rev Neurosci*, 2(4):274–86, 2001.

[47] E. M. Hur and K. T. Kim. G protein-coupled receptor signalling and cross-talk: achieving rapidity and specificity. *Cell Signal*, 14(5):397–405, 2002.

[48] P. R. Albert and L. Robillard. G protein specificity: traffic direction required. *Cell Signal*, 14(5):407–18, 2002.

[49] S. S. Ferguson. Evolving concepts in G protein-coupled receptor endocytosis: the role in receptor desensitization and signaling. *Pharmacol Rev*, 53(1):1–24, 2001.

[50] T. A. Kohout and R. J. Lefkowitz. Regulation of G protein-coupled receptor kinases and arrestins during receptor desensitization. *Mol Pharmacol*, 63(1):9–18, 2003.

[51] S. J. Perry and R. J. Lefkowitz. Arresting developments in heptahelical receptor signaling and regulation. *Trends Cell Biol*, 12(3):130–8, 2002.

[52] R. H. Oakley, S. A. Laporte, J. A. Holt, M. G. Caron, and L. S. Barak. Differential affinities of visual arrestin, β-arrestin1, and β-arrestin2 for G protein-coupled receptors delineate two major classes of receptors. *J Biol Chem*, 275(22):17201–10, 2000.

[53] K. L. Pierce and R. J. Lefkowitz. Classical and new roles of β-arrestins in the regulation of G protein-coupled receptors. *Nat Rev Neurosci*, 2(10):727–33, 2001.

[54] S. Angers, A. Salahpour, and M. Bouvier. Dimerization: an emerging concept for G protein-coupled receptor ontogeny and function. *Annu Rev Pharmacol Toxicol*, 42:409–35, 2002.

[55] K. D. Pfleger and K. A. Eidne. Monitoring the formation of dynamic G protein-coupled receptor-protein complexes in living cells. *Biochem J*, 385(Pt 3):625–37, 2005.

[56] P. S. Park, S. Filipek, J. W. Wells, and K. Palczewski. Oligomerization of G protein-coupled receptors: past, present, and future. *Biochemistry*, 43(50):15643–56, 2004.

[57] M. Bai. Dimerization of G protein-coupled receptors: roles in signal transduction. *Cell Signal*, 16(2):175–86, 2004.

[58] G. Milligan. G protein-coupled receptor dimerization: function and ligand pharmacology. *Mol Pharmacol*, 66(1):1–7, 2004.

[59] L. Quartara and C. A. Maggi. The tachykinin NK1 receptor. Part I: ligands and mechanisms of cellular activation. *Neuropeptides*, 31(6):537–63, 1997.

[60] L. Quartara and C. A. Maggi. The tachykinin NK1 receptor. Part II: Distribution and pathophysiological roles. *Neuropeptides*, 32(1):1–49, 1998.

[61] J. E. Krause, B. S. Sachais, and P. Blount. Tachykinin receptors. In S. J. Peroutka, editor, *Handbook of Receptors and Channels: G-Protein-coupled receptors*, pages 277–298. CRC Press Inc., 1994.

[62] M. Otsuka and K. Yoshioka. Neurotransmitter functions of mammalian tachykinins. *Physiol Rev*, 73(2):229–308, 1993.

[63] C. A. Maggi, R. Patacchini, P. Rovero, and A. Giachetti. Tachykinin receptors and tachykinin receptor antagonists. *J Auton Pharmacol*, 13(1):23–93, 1993.

[64] D. Regoli, A. Boudon, and J. L. Fauchere. Receptors and antagonists for substance P and related peptides. *Pharmacol Rev*, 46(4):551–99, 1994.

[65] S. Harrison and P. Geppetti. Substance P. *Int J Biochem Cell Biol*, 33(6):555–76, 2001.

[66] U.S. von Euler and J.H. Gaddum. An unidentified depressor substance in certain tissue extracts. *J. Physiol.*, 72:74–87, 1931.

[67] Y. Zhang, L. Lu, C. Furlonger, G. E. Wu, and C. J. Paige. Hemokinin is a hematopoietic-specific tachykinin that regulates B lymphopoiesis. *Nat Immunol*, 1(5):392–7, 2000.

[68] N. M. Page. Hemokinins and endokinins. *Cell Mol Life Sci*, 61(13):1652–63, 2004.

[69] A. M. Khawaja and D. F. Rogers. Tachykinins: receptor to effector. *Int J Biochem Cell Biol*, 28(7):721–38., 1996.

[70] E. D. Roush and M. M. Kwatra. Human substance P receptor expressed in Chinese hamster ovary cells directly activates Gαq/11, Gαs, Gαo. *FEBS Lett*, 428(3):291–4, 1998.

[71] Y. Nakajima, K. Tsuchida, M. Negishi, S. Ito, and S. Nakanishi. Direct linkage of three tachykinin receptors to stimulation of both phosphatidylinositol hydrolysis and cyclic AMP cascades in transfected Chinese hamster ovary cells. *J Biol Chem*, 267(4):2437–42, 1992.

[72] B. Holst, H. Hastrup, U. Raffetseder, L. Martini, and T. W. Schwartz. Two active molecular phenotypes of the tachykinin NK1 receptor revealed by G protein fusions and mutagenesis. *J Biol Chem*, 276(23):19793–9, 2001.

[73] K. Monastyrskaya, A. Hostettler, S. Buergi, and A. Draeger. The NK1 receptor localizes to the plasma membrane microdomains, and its activation is dependent on lipid raft integrity. *J Biol Chem*, 280(8):7135–46, 2005.

[74] K. McConalogue, C. U. Corvera, P. D. Gamp, E. F. Grady, and N. W. Bunnett. Desensitization of the neurokinin-1 receptor (NK1R) in neurons: effects of substance P on the distribution of NK1R, Gαq/11, G protein receptor kinase-2/3, and β-arrestin-1/2. *Mol Biol Cell*, 9(8):2305–24, 1998.

[75] L. S. Barak, K. Warabi, X. Feng, M. G. Caron, and M. M. Kwatra. Real-time visualization of the cellular redistribution of G protein-coupled receptor kinase 2 and β-arrestin 2 during homologous desensitization of the substance P receptor. *J Biol Chem*, 274(11):7565–9, 1999.

[76] A. M. Garland, E. F. Grady, D. G. Payan, S. R. Vigna, and N. W. Bunnett. Agonist-induced internalization of the substance P (NK1) receptor expressed in epithelial cells. *Biochem J*, 303(Pt 1):177–86, 1994.

[77] E. F. Grady, A. M. Garland, P. D. Gamp, M. Lovett, D. G. Payan, and N. W. Bunnett. Delineation of the endocytic pathway of substance P and its seven-transmembrane domain NK1 receptor. *Mol Biol Cell*, 6(5):509–24, 1995.

[78] H. Li, S. E. Leeman, B. E. Slack, G. Hauser, W. S. Saltsman, J. E. Krause, J. K. Blusztajn, and N. D. Boyd. A substance P (neurokinin-1) receptor mutant carboxyl-terminally truncated to resemble a naturally occurring receptor isoform displays enhanced responsiveness and resistance to desensitization. *Proc Natl Acad Sci USA*, 94(17):9475–80, 1997.

[79] L. Martini, H. Hastrup, B. Holst, A. Fraile-Ramos, M. Marsh, and T. W. Schwartz. NK1 receptor fused to β-arrestin displays a single-component, high-affinity molecular phenotype. *Mol Pharmacol*, 62(1):30–7, 2002.

[80] V. J. Bennett, S. A. Perrine, and M. A. Simmons. A novel mechanism of neurokinin-1 receptor resensitization. *J Pharmacol Exp Ther*, 303(3):1155–62, 2002.

[81] D. Roosterman, G. S. Cottrell, F. Schmidlin, M. Steinhoff, and N. W. Bunnett. Recycling and resensitization of the neurokinin 1 receptor. Influence of agonist concentration and Rab GTPases. *J Biol Chem*, 279(29):30670–9, 2004.

[82] M. Pfeiffer, S. Kirscht, R. Stumm, T. Koch, D. Wu, M. Laugsch, H. Schroder, V. Hollt, and S. Schulz. Heterodimerization of substance P and μ-opioid receptors regulates receptor trafficking and resensitization. *J Biol Chem*, 278(51):51630–7, 2003.

[83] M. Jordan, A. Schallhorn, and F. M. Wurm. Transfecting mammalian cells: optimization of critical parameters affecting calcium-phosphate precipitate formation. *Nucleic Acids Res*, 24(4):596–601, 1996.

[84] F. Perrin. Théorie quantique des transferts d'activation entre molécules de même espèce. Cas des solutions fluorescentes. *Ann. Phys.*, 17:283–313, 1932.

[85] T. Förster. Zwischenmolekulare Energiewanderung und Fluoreszenz. *Annalen der Physik*, 2(1-2):55–75, 1948.

[86] J. R. Lakowicz. *Principles of fluorescence spectroscopy*. Kluwer Academic/Plenum Publishers, New York, second edition, 1999.

[87] R. M. Clegg. Fluorescence resonance energy transfer and nucleic acids. *Methods Enzymol*, 211:353–88, 1992.

[88] R. E. Dale, J. Eisinger, and W. E. Blumberg. The orientational freedom of molecular probes. The orientation factor in intramolecular energy transfer. *Biophys J*, 26(2):161–93, 1979.

[89] P. R. Selvin. Fluorescence resonance energy transfer. *Methods Enzymol*, 246:300–34, 1995.

[90] P. I. Bastiaens and T. M. Jovin. Microspectroscopic imaging tracks the intracellular processing of a signal transduction protein: fluorescent-labeled protein kinase C βI. *Proc Natl Acad Sci USA*, 93(16):8407–12, 1996.

[91] P. I. Bastiaens and A. Squire. Fluorescence lifetime imaging microscopy: spatial resolution of biochemical processes in the cell. *Trends Cell Biol*, 9(2):48–52, 1999.

[92] F. S. Wouters and P. I. Bastiaens. Fluorescence lifetime imaging of receptor tyrosine kinase activity in cells. *Curr Biol*, 9(19):1127–30, 1999.

[93] M. Elangovan, R. N. Day, and A. Periasamy. Nanosecond fluorescence resonance energy transfer-fluorescence lifetime imaging microscopy to localize the protein interactions in a single living cell. *J Microsc*, 205(Pt 1):3–14, 2002.

[94] H. Wallrabe and A. Periasamy. Imaging protein molecules using FRET and FLIM microscopy. *Curr Opin Biotechnol*, 16(1):19–27, 2005.

[95] T. M. Jovin and D. J. Arndt-Jovin. Luminescence digital imaging microscopy. *Annu Rev Biophys Biophys Chem*, 18:271–308, 1989.

[96] Jr. Szaba, G., P. S. Pine, J. L. Weaver, M. Kasari, and A. Aszalos. Epitope mapping by photobleaching fluorescence resonance energy transfer measurements using a laser scanning microscope system. *Biophys J*, 61(3):661–70, 1992.

[97] Jr. Gadella, T. W. and T. M. Jovin. Oligomerization of epidermal growth factor receptors on A431 cells studied by time-resolved fluorescence imaging microscopy. A stereochemical model for tyrosine kinase receptor activation. *J Cell Biol*, 129(6):1543–58, 1995.

[98] J. Matko, A. Jenei, L. Matyus, M. Ameloot, and S. Damjanovich. Mapping of cell surface protein-patterns by combined fluorescence anisotropy and energy transfer measurements. *J Photochem Photobiol B*, 19(1):69–73, 1993.

[99] A. Miyawaki and R. Y. Tsien. Monitoring protein conformations and interactions by fluorescence resonance energy transfer between mutants of green fluorescent protein. *Methods Enzymol*, 327:472–500, 2000.

[100] W. Xue, A. L. Kindzelskii, 3rd Todd, R. F., and H. R. Petty. Physical association of complement receptor type 3 and urokinase-type plasminogen activator receptor in neutrophil membranes. *J Immunol*, 152(9):4630–40, 1994.

[101] P. I. Bastiaens, I. V. Majoul, P. J. Verveer, H. D. Soling, and T. M. Jovin. Imaging the intracellular trafficking and state of the AB5 quaternary structure of cholera toxin. *EMBO J*, 15(16):4246–53, 1996.

[102] A. K. Kenworthy. Imaging protein-protein interactions using fluorescence resonance energy transfer microscopy. *Methods*, 24(3):289–96, 2001.

[103] P. S. Uster and R. E. Pagano. Resonance energy transfer microscopy: observations of membrane-bound fluorescent probes in model membranes and in living cells. *J Cell Biol*, 103(4):1221–34, 1986.

[104] P. Nagy, G. Vamosi, A. Bodnar, S. J. Lockett, and J. Szollosi. Intensity-based energy transfer measurements in digital imaging microscopy. *Eur Biophys J*, 27(4):377–89, 1998.

[105] G. W. Gordon, G. Berry, X. H. Liang, B. Levine, and B. Herman. Quantitative fluorescence resonance energy transfer measurements using fluorescence microscopy. *Biophys J*, 74(5):2702–13, 1998.

[106] Z. Xia and Y. Liu. Reliable and global measurement of fluorescence resonance energy transfer using fluorescence microscopes. *Biophys J*, 81(4):2395–402, 2001.

[107] A. Hoppe, K. Christensen, and J. A. Swanson. Fluorescence resonance energy transfer-based stoichiometry in living cells. *Biophys J*, 83(6):3652–64, 2002.

[108] M. G. Erickson, H. Liang, M. X. Mori, and D. T. Yue. FRET two-hybrid mapping reveals function and location of L-type Ca^{2+} channel CaM preassociation. *Neuron*, 39(1):97–107, 2003.

[109] J. van Rheenen, M. Langeslag, and K. Jalink. Correcting confocal acquisition to optimize imaging of fluorescence resonance energy transfer by sensitized emission. *Biophys J*, 86(4):2517–29, 2004.

[110] T. Zal and N. R. Gascoigne. Photobleaching-corrected FRET efficiency imaging of live cells. *Biophys J*, 86(6):3923–39, 2004.

[111] L. Tron, J. Szollosi, S. Damjanovich, S. H. Helliwell, D. J. Arndt-Jovin, and T. M. Jovin. Flow cytometric measurement of fluorescence resonance energy transfer on cell surfaces. Quantitative evaluation of the transfer efficiency on a cell-by-cell basis. *Biophys J*, 45(5):939–46, 1984.

[112] A. Miyawaki, J. Llopis, R. Heim, J. M. McCaffery, J. A. Adams, M. Ikura, and R. Y. Tsien. Fluorescent indicators for Ca^{2+} based on green fluorescent proteins and calmodulin. *Nature*, 388(6645):882–7, 1997.

[113] J. P. Vilardaga, M. Bunemann, C. Krasel, M. Castro, and M. J. Lohse. Measurement of the millisecond activation switch of G protein-coupled receptors in living cells. *Nat Biotechnol*, 21(7):807–12, 2003.

[114] C. Hoffmann, G. Gaietta, M. Bunemann, S. R. Adams, S. Oberdorff-Maass, B. Behr, J. P. Vilardaga, R. Y. Tsien, M. H. Eisman, and M. J. Lohse. A FlAsH-based FRET approach to determine G protein-coupled receptor activation in living cells. *Nature Methods*, 2(3):171–176, 2005.

[115] J. Y. Vollmer, P. Alix, A. Chollet, K. Takeda, and J. L. Galzi. Subcellular compartmentalization of activation and desensitization of responses mediated by NK2 neurokinin receptors. *J Biol Chem*, 274(53):37915–22, 1999.

[116] S. Lecat, B. Bucher, Y. Mely, and J. L. Galzi. Mutations in the extracellular amino-terminal domain of the NK2 neurokinin receptor abolish cAMP signaling but preserve intracellular calcium responses. *J Biol Chem*, 277(44):42034–48, 2002.

[117] C. Gales, R. V. Rebois, M. Hogue, P. Trieu, A. Breit, T. E. Hebert, and M. Bouvier. Real-time monitoring of receptor and G protein interactions in living cells. *Nature Methods*, 2(3):177–184, 2005.

[118] C. Janetopoulos, T. Jin, and P. Devreotes. Receptor-mediated activation of heterotrimeric G proteins in living cells. *Science*, 291(5512):2408–11., 2001.

[119] I. Riven, E. Kalmanzon, L. Segev, and E. Reuveny. Conformational rearrangements associated with the gating of the G protein-coupled potassium channel revealed by FRET microscopy. *Neuron*, 38(2):225–35, 2003.

[120] L. Bertrand, S. Parent, M. Caron, M. Legault, E. Joly, S. Angers, M. Bouvier, M. Brown, B. Houle, and L. Menard. The BRET2/arrestin assay in stable recombinant cells: a platform to screen for compounds that interact with G protein-coupled receptors (GPCRs). *J Recept Signal Transduct Res*, 22(1-4):533–41, 2002.

[121] C. Krasel, M. Bunemann, K. Lorenz, and M. J. Lohse. Beta-arrestin binding to the β2-adrenergic receptor requires both receptor phosphorylation and receptor activation. *J Biol Chem*, 280(10):9528–35, 2005.

[122] M. Cebecauer, P. Guillaume, S. Mark, O. Michielin, N. Boucheron, M. Bezard, B. H. Meyer, J. M. Segura, H. Vogel, and I. F. Luescher. CD8+ cytotoxic T lymphocyte activation by soluble major histocompatibility complex-peptide dimers. *J Biol Chem*, 280(25):23820–23828, 2005.

[123] M. Zimmer. Green Fluorescent Protein (GFP): Applications, Structure, and Related Photophysical Behavior. *Chem Rev*, 102(3):759–82, 2002.

[124] G. Turcatti, K. Nemeth, M. D. Edgerton, U. Meseth, F. Talabot, M. Peitsch, J. Knowles, H. Vogel, and A. Chollet. Probing the structure and function of the tachykinin neurokinin-2 receptor through biosynthetic incorporation of fluorescent amino acids at specific sites. *J Biol Chem*, 271(33):19991–8, 1996.

[125] R. Y. Tsien. The green fluorescent protein. *Annu Rev Biochem*, 67:509–44, 1998.

[126] B. A. Griffin, S. R. Adams, and R. Y. Tsien. Specific covalent labeling of recombinant protein molecules inside live cells. *Science*, 281(5374):269–72, 1998.

[127] A. Keppler, S. Gendreizig, T. Gronemeyer, H. Pick, H. Vogel, and K. Johnsson. A general method for the covalent labeling of fusion proteins with small molecules in vivo. *Nat Biotechnol*, 21(1):86–9, 2003.

[128] N. George, H. Pick, H. Vogel, N. Johnsson, and K. Johnsson. Specific labeling of cell surface proteins with chemically diverse compounds. *J Am Chem Soc*, 126(29):8896–7, 2004.

[129] E. G. Guignet, R. Hovius, and H. Vogel. Reversible site-selective labeling of membrane proteins in live cells. *Nat Biotechnol*, 22(4):440–4, 2004.

[130] L. W. Miller, J. Sable, P. Goelet, M. P. Sheetz, and V. W. Cornish. Methotrexate conjugates: a molecular in vivo protein tag. *Angew Chem Int Ed Engl*, 43(13):1672–5, 2004.

[131] K. M. Marks, P. D. Braun, and G. P. Nolan. A general approach for chemical labeling and rapid, spatially controlled protein inactivation. *Proc Natl Acad Sci USA*, 101(27):9982–7, 2004.

[132] I. Chen, M. Howarth, W. Y. Lin, and A. Y. Ting. Site-specific labeling of cell surface proteins with biophysical probes using biotin ligase. *Nature Methods*, 2(2):99–104, 2005.

[133] L. Kallal and J. L. Benovic. Using green fluorescent proteins to study G protein-coupled receptor localization and trafficking. *Trends Pharmacol Sci*, 21(5):175–180, 2000.

[134] Joseph Sambrook and David W. Russell. *Molecular cloning a laboratory manual*. Cold Spring Harbor Laboratory Press, Cold Spring Harbor, New York, 3rd edition, 2001.

[135] M. Kozak. Point mutations define a sequence flanking the AUG initiator codon that modulates translation by eukaryotic ribosomes. *Cell*, 44(2):283–92, 1986.

[136] S. Sagan, P. Karoyan, G. Chassaing, and S. Lavielle. Further delineation of the two binding sites (R^*_n) associated with tachykinin neurokinin-1 receptors using [3-Prolinomethionine(11)]SP analogues. *J Biol Chem*, 274(34):23770–6, 1999.

[137] O. Dery, K. A. Defea, and N. W. Bunnett. Protein kinase C-mediated desensitization of the neurokinin 1 receptor. *Am J Physiol Cell Physiol*, 280(5):C1097–106., 2001.

[138] K. McConalogue, O. Dery, M. Lovett, H. Wong, J. H. Walsh, E. F. Grady, and N. W. Bunnett. Substance P-induced trafficking of β-arrestins. The role of β-arrestins in endocytosis of the neurokinin-1 receptor. *J Biol Chem*, 274(23):16257–68, 1999.

[139] Y. M. Li, M. Marnerakis, E. R. Stimson, and J. E. Maggio. Mapping peptide-binding domains of the substance P (NK1) receptor from P388D1 cells with photolabile agonists. *J Biol Chem*, 270(3):1213–20, 1995.

[140] G. Turcatti, S. Zoffmann, 3rd Lowe, J. A., S. E. Drozda, G. Chassaing, T. W. Schwartz, and A. Chollet. Characterization of non-peptide antagonist and peptide agonist binding sites of the NK1 receptor with fluorescent ligands. *J Biol Chem*, 272(34):21167–75, 1997.

[141] N. Baindur and D. J. Triggle. Selective fluorescent ligands for pharmacological receptors. *Drug Development Research*, 33(4):373–398, 1994.

[142] G. Turcatti, H. Vogel, and A. Chollet. Probing the binding domain of the NK2 receptor with fluorescent ligands: evidence that heptapeptide agonists and antagonists bind differently. *Biochemistry*, 34(12):3972–80, 1995.

[143] M. R. Tota, S. Daniel, A. Sirotina, K. E. Mazina, T. M. Fong, J. Longmore, and C. D. Strader. Characterization of a fluorescent substance P analog. *Biochemistry*, 33(44):13079–86., 1994.

[144] K. L. Martinez, B. H. Meyer, R. Hovius, K. Lundstrom, and H. Vogel. Ligand binding to G protein-coupled receptors in tethered cell membranes. *Langmuir*, 19(26):10925–10929, 2003.

[145] E. J. Adie, S. Kalinka, L. Smith, M. J. Francis, A. Marenghi, M. E. Cooper, M. Briggs, N. P. Michael, G. Milligan, and S. Game. A pH-sensitive fluor, CypHer 5, used to monitor agonist-induced G protein-coupled receptor internalization in live cells. *Biotechniques*, 33(5):1152–4, 1156–7, 2002.

[146] Y. Lill, K. L. Martinez, M. Lill, B. H. Meyer, H. Vogel, and B. Hecht. Kinetics of the initial steps of G protein-coupled receptor mediated cellular signaling revealed by single molecule imaging. *ChemPhysChem*, in press, 2005.

[147] J. Luber-Narod, N. D. Boyd, and S. E. Leeman. Guanine nucleotides decrease the affinity of substance P binding to its receptor. *Eur J Pharmacol*, 188(4-5):185–91, 1990.

[148] Y. Takeda, P. Blount, B. S. Sachais, A. D. Hershey, R. Raddatz, and J. E. Krause. Ligand binding kinetics of substance P and neurokinin A receptors stably expressed in Chinese hamster ovary cells and evidence for differential stimulation of inositol 1,4,5-trisphosphate and cyclic AMP second messenger responses. *J Neurochem*, 59(2):740–5, 1992.

[149] D. P. Geraghty and E. Burcher. Two classes of binding sites for [^{3}H]substance P in rat cerebral cortex. *Brain Res*, 601(1-2):34–40, 1993.

[150] T. Palanche, B. Ilien, S. Zoffmann, M. P. Reck, B. Bucher, S. J. Edelstein, and J. L. Galzi. The neurokinin A receptor activates calcium and cAMP responses through distinct conformational states. *J Biol Chem*, 276(37):34853–61., 2001.

[151] A. Valenzuela-Fernandez, T. Palanche, A. Amara, A. Magerus, R. Altmeyer, T. Delaunay, J. L. Virelizier, F. Baleux, J. L. Galzi, and F. Arenzana-Seisdedos. Optimal inhibition of X4 HIV isolates by the CXC chemokine stromal cell-derived factor 1 α requires interaction with cell surface heparan sulfate proteoglycans. *J Biol Chem*, 276(28):26550–8, 2001.

[152] B. Ilien, C. Franchet, P. Bernard, S. Morisset, C. O. Weill, J. J. Bourguignon, M. Hibert, and J. L. Galzi. Fluorescence resonance energy transfer to probe human M1 muscarinic receptor structure and drug binding properties. *J Neurochem*, 85(3):768–78, 2003.

[153] C. Tahtaoui, I. Parrot, P. Klotz, F. Guillier, J. L. Galzi, M. Hibert, and B. Ilien. Fluorescent pirenzepine derivatives as potential bitopic ligands of the human M1 muscarinic receptor. *J Med Chem*, 47(17):4300–15, 2004.

[154] V. J. Bennett and M. A. Simmons. Analysis of fluorescently labeled substance P analogs: binding, imaging and receptor activation. *BMC Chem Biol*, 1(1):1, 2001.

[155] J. Mellentin-Michelotti, L. T. Evangelista, E. E. Swartzman, S. J. Miraglia, W. E. Werner, and P. M. Yuan. Determination of ligand binding affinities for endogenous seven-transmembrane receptors using fluorometric microvolume assay technology. *Anal Biochem*, 272(2):182–90, 1999.

[156] M. Kneen, J. Farinas, Y. Li, and A. S. Verkman. Green fluorescent protein as a noninvasive intracellular pH indicator. *Biophys J*, 74(3):1591–9., 1998.

[157] J. Llopis, J. M. McCaffery, A. Miyawaki, M. G. Farquhar, and R. Y. Tsien. Measurement of cytosolic, mitochondrial, and Golgi pH in single living cells with green fluorescent proteins. *Proc Natl Acad Sci USA*, 95(12):6803–8, 1998.

[158] M. C. Ashby, K. Ibaraki, and J. M. Henley. It's green outside: tracking cell surface proteins with pH-sensitive GFP. *Trends Neurosci*, 27(5):257–61, 2004.

[159] Mohammed A. Ayoub, Cyril Couturier, Estelle Lucas-Meunier, Stephane Angers, Philippe Fossier, Michel Bouvier, and Ralf Jockers. Monitoring of ligand-independent dimerization and ligand-induced conformational changes of melatonin receptors in living cells by bioluminescence resonance energy transfer. *J. Biol. Chem.*, 277(24):21522–21528, 2002.

[160] J. F. Mercier, A. Salahpour, S. Angers, A. Breit, and M. Bouvier. Quantitative assessment of β1- and β2-adrenergic receptor homo- and hetero-dimerization by bioluminescence resonance energy transfer. *J Biol Chem*, 277(47):44925–31, 2002.

[161] K. Herrick-Davis, E. Grinde, and J. E. Mazurkiewicz. Biochemical and biophysical characterization of serotonin 5-HT_{2C} receptor homo-dimers on the plasma membrane of living cells. *Biochemistry*, 43(44):13963–71, 2004.

[162] B. D. Adair and D. M. Engelman. Glycophorin A helical transmembrane domains dimerize in phospholipid bilayers: a resonance energy transfer study. *Biochemistry*, 33(18):5539–44, 1994.

[163] W. Veatch and L. Stryer. The dimeric nature of the gramicidin A transmembrane channel: conductance and fluorescence energy transfer studies of hybrid channels. *J Mol Biol*, 113(1):89–102, 1977.

[164] A. K. Kenworthy and M. Edidin. Distribution of a glycosylphosphatidylinositol-anchored protein at the apical surface of MDCK cells examined at a resolution of < 100 Å using imaging fluorescence resonance energy transfer. *J Cell Biol*, 142(1):69–84, 1998.

[165] P. K. Wolber and B. S. Hudson. An analytic solution to the Förster energy transfer problem in two dimensions. *Biophys J*, 28(2):197–210, 1979.

[166] M. Rocheville, D. C. Lange, U. Kumar, R. Sasi, R. C. Patel, and Y. C. Patel. Subtypes of the somatostatin receptor assemble as functional homo- and heterodimers. *J Biol Chem*, 275(11):7862–9, 2000.

[167] X. L. Zhang, J. C. Mak, and P. J. Barnes. Characterization and autoradiographic mapping of [^{3}H]CP96,345, a nonpeptide selective NK1 receptor antagonist in guinea pig lung. *Peptides*, 16(5):867–72, 1995.

[168] M. Maruyama. Selective solubilization of physalaemin-type substance P binding sites from rat brain membranes by glycodeoxycholate and NaCl. *Brain Res*, 370(1):186–90, 1986.

[169] H. Issafras, S. Angers, S. Bulenger, C. Blanpain, M. Parmentier, C. Labbe-Jullie, M. Bouvier, and S. Marullo. Constitutive agonist-independent CCR5 oligomerization and antibody-mediated clustering occurring at physiological levels of receptors. *J Biol Chem*, 277(38):34666–73, 2002.

[170] I. Gomes, B. A. Jordan, A. Gupta, N. Trapaidze, V. Nagy, and L. A. Devi. Heterodimerization of mu and delta opioid receptors: A role in opiate synergy. *J Neurosci*, 20(22):RC110, 2000.

[171] A. Breit, M. Lagace, and M. Bouvier. Hetero-oligomerization between β2- and β3-adrenergic receptors generates a β-adrenergic signaling unit with distinct functional properties. *J Biol Chem*, 279(27):28756–65, 2004.

[172] R. R. Neubig. Membrane organization in G protein mechanisms. *FASEB J*, 8(12):939–46, 1994.

[173] R. V. Rebois, D. R. Warner, and N. S. Basi. Does subunit dissociation necessarily accompany the activation of all heterotrimeric G proteins? *Cell Signal*, 9(2):141–51, 1997.

[174] S. Heyse, T. Stora, E. Schmid, J. H. Lakey, and H. Vogel. Emerging techniques for investigating molecular interactions at lipid membranes. *Biochim Biophys Acta*, 1376(3):319–38, 1998.

[175] W. A. Clark, X. Jian, L. Chen, and J. K. Northup. Independent and synergistic interaction of retinal G protein subunits with bovine rhodopsin measured by surface plasmon resonance. *Biochem J*, 358(Pt 2):389–97, 2001.

[176] A. Waller, P. C. Simons, S. M. Biggs, B. S. Edwards, E. R. Prossnitz, and L. A. Sklar. Techniques: GPCR assembly, pharmacology and screening by flow cytometry. *Trends Pharmacol Sci*, 25(12):663–9, 2004.

[177] T. M. Yi, H. Kitano, and M. I. Simon. A quantitative characterization of the yeast heterotrimeric G protein cycle. *Proc Natl Acad Sci USA*, 100(19):10764–9, 2003.

[178] T. Higashijima, K. M. Ferguson, P. C. Sternweis, E. M. Ross, M. D. Smigel, and A. G. Gilman. The effect of activating ligands on the intrinsic fluorescence of guanine nucleotide-binding regulatory proteins. *J Biol Chem*, 262(2):752–6., 1987.

[179] P. C. Sternweis and A. G. Gilman. Aluminum: a requirement for activation of the regulatory component of adenylate cyclase by fluoride. *Proc Natl Acad Sci USA*, 79(16):4888–91, 1982.

[180] T. Higashijima, M. P. Graziano, H. Suga, M. Kainosho, and A. G. Gilman. ^{19}F and ^{31}P NMR spectroscopy of G protein α subunits. Mechanism of activation by Al_3^+ and F. *J Biol Chem*, 266(6):3396–401., 1991.

[181] R. M. Wachter and S. J. Remington. Sensitivity of the yellow variant of green fluorescent protein to halides and nitrate. *Curr Biol*, 9(17):R628–9, 1999.

[182] S. Jayaraman, P. Haggie, R. M. Wachter, S. J. Remington, and A. S. Verkman. Mechanism and cellular applications of a green fluorescent protein-based halide sensor. *J Biol Chem*, 275(9):6047–50, 2000.

[183] O. Griesbeck, G. S. Baird, R. E. Campbell, D. A. Zacharias, and R. Y. Tsien. Reducing the environmental sensitivity of yellow fluorescent protein. Mechanism and applications. *J Biol Chem*, 276(31):29188–94, 2001.

[184] J. L. Leaney, A. Benians, F. M. Graves, and A. Tinker. A novel strategy to engineer functional fluorescent inhibitory G protein α subunits. *J Biol Chem*, 277(32):28803–9, 2002.

[185] W. Liu and J. K. Northup. The helical domain of a G protein α-subunit is a regulator of its effector. *Proc Natl Acad Sci USA*, 95(22):12878–83, 1998.

[186] P. B. Wedegaertner, D. H. Chu, P. T. Wilson, M. J. Levis, and H. R. Bourne. Palmitoylation is required for signaling functions and membrane attachment of Gαq and Gαs. *J Biol Chem*, 268(33):25001–8, 1993.

[187] E. Kostenis, J. Gomeza, C. Lerche, and J. Wess. Genetic analysis of receptor-Gαq coupling selectivity. *J Biol Chem*, 272(38):23675–81, 1997.

[188] G. Venkatakrishnan and J. H. Exton. Identification of determinants in the α-subunit of Gq required for phospholipase C activation. *J Biol Chem*, 271(9):5066–72, 1996.

[189] J. Z. Yu and M. M. Rasenick. Real-time visualization of a fluorescent Gα_s: dissociation of the activated G protein from plasma membrane. *Mol Pharmacol*, 61(2):352–9, 2002.

[190] T. E. Hughes, H. Zhang, D. E. Logothetis, and C. H. Berlot. Visualization of a functional Gαq-green fluorescent protein fusion in living cells: Association with the plasma membrane is disrupted by mutational activation and by elimination of palmitoylation sites, but not by activation mediated by receptors or AlF^{4-}. *J Biol Chem*, 13:13, 2000.

[191] V. Ruiz-Velasco and S. R. Ikeda. Functional expression and FRET analysis of green fluorescent proteins fused to G protein subunits in rat sympathetic neurons. *J Physiol*, 537(Pt 3):679–92, 2001.

[192] I. Azpiazu and N. Gautam. A fluorescence resonance energy transfer-based sensor indicates that receptor access to a G protein is unrestricted in a living mammalian cell. *J Biol Chem*, 279(26):27709–18, 2004.

[193] D. S. Evanko, M. M. Thiyagarajan, and P. B. Wedegaertner. Interaction with $G\beta\gamma$ is required for membrane targeting and palmitoylation of $G\alpha_s$ and $G\alpha_q$. *J Biol Chem*, 275(2):1327–36, 2000.

[194] R. Leurs, M. J. Smit, A. E. Alewijnse, and H. Timmerman. Agonist-independent regulation of constitutively active G protein-coupled receptors. *Trends Biochem Sci*, 23(11):418–22, 1998.

[195] G. Milligan. Strategies to identify ligands for orphan G protein-coupled receptors. *Biochem Soc Trans*, 30(4):789–93, 2002.

[196] J. M. Stadel, S. Wilson, and D. J. Bergsma. Orphan G protein-coupled receptors: a neglected opportunity for pioneer drug discovery. *Trends Pharmacol Sci*, 18(11):430–7, 1997.

[197] Y. Fang, A. G. Frutos, and J. Lahiri. Membrane protein microarrays. *J Am Chem Soc*, 124(11):2394–5, 2002.

[198] A. D. Howard, G. McAllister, S. D. Feighner, Q. Liu, R. P. Nargund, L. H. Van der Ploeg, and A. A. Patchett. Orphan G protein-coupled receptors and natural ligand discovery. *Trends Pharmacol Sci*, 22(3):132–40, 2001.

[199] E. Goormaghtigh, V. Raussens, and J. M. Ruysschaert. Attenuated total reflection infrared spectroscopy of proteins and lipids in biological membranes. *Biochim Biophys Acta*, 1422(2):105–185, 1999.

[200] P. Rigler, W. P. Ulrich, P. Hoffmann, M. Mayer, and H. Vogel. Reversible immobilization of peptides: surface modification and in situ detection by attenuated total reflection FTIR spectroscopy. *ChemPhysChem*, 4(3):268–75, 2003.

[201] J. E. Baenziger, K. W. Miller, and K. J. Rothschild. Incorporation of the nicotinic acetylcholine receptor into planar multilamellar films. Characterization by fluorescence and fourier-transform infrared difference spectroscopy. *Biophys J*, 61(4):983–992, 1992.

[202] C. Bieri, O. P. Ernst, S. Heyse, K. P. Hofmann, and H. Vogel. Micropatterned immobilization of a G protein-coupled receptor and direct detection of G protein activation. *Nat Biotechnol*, 17(11):1105–8., 1999.

[203] R. Naumann, A. Jonczyk, R. Kopp, J. Vanesch, H. Ringsdorf, W. Knoll, and P. Graber. Incorporation of membrane-proteins in solid-supported lipid layers. *Angewandte Chemie International Edition in English*, 34(18):2056–2058, 1995.

[204] Z. Salamon and G. Tollin. Surface plasmon resonance studies of complex formation between cytochrome c and bovine cytochrome c oxidase incorporated into a supported planar lipid bilayer. 1. Binding of cytochrome c to cardiolipin/phosphatidylcholine membranes in the absence of oxidase. *Biophys J*, 71(2):848–857, 1996.

[205] H. Mozsolits, W. G. Thomas, and M. I. Aguilar. Surface plasmon resonance spectroscopy in the study of membrane-mediated cell signalling. *J Pept Sci*, 9(2):77–89, 2003.

[206] C. Hanel and G. Gauglitz. Comparison of reflectometric interference spectroscopy with other instruments for label-free optical detection. *Anal Bioanal Chem*, 372(1):91–100, 2002.

[207] N. L. Thompson, K. H. Pearce, and H. V. Hsieh. Total internal reflection fluorescence microscopy: application to substrate-supported planar membranes. *Eur Biophys J*, 22(5):367–78., 1993.

[208] E. L. Schmid, T. A. Keller, Z. Dienes, and H. Vogel. Reversible oriented surface immobilization of functional proteins on oxide surfaces. *Anal Chem*, 69(11):1979–85., 1997.

[209] E. L. Schmid, A. P. Tairi, R. Hovius, and H. Vogel. Screening ligands for membrane protein receptors by total internal reflection fluorescence: the 5-HT3 serotonin receptor. *Anal Chem*, 70(7):1331–8., 1998.

[210] David S. Wilson and Steffen Nock. Functional protein microarrays. *Curr Opin Chem Biol*, 6(1):81–85, 2002.

[211] L. M. Demers, S. J. Park, T. A. Taton, Z. Li, and C. A. Mirkin. Orthogonal assembly of nanoparticle building blocks on Dip-Pen nanolithographically generated Templates of DNA. *Angew Chem Int Ed Engl*, 40(16):3071–3073, 2001.

[212] F. W. Scheller, U. Wollenberger, A. Warsinke, and F. Lisdat. Research and development in biosensors. *Curr Opin Biotechnol*, 12(1):35–40, 2001.

[213] G. MacBeath. Protein microarrays and proteomics. *Nat Genet*, 32 Suppl 2:526–32, 2002.

[214] A. L. Plant. Supported hybrid bilayer membranes as rugged cell membrane mimics. *Langmuir*, 15(15):5128–5135, 1999.

[215] E. Reimhult, F. Hook, and B. Kasemo. Intact vesicle adsorption and supported biomembrane formation from vesicles in solution: Influence of surface chemistry, vesicle size, temperature, and osmotic pressure. *Langmuir*, 19(5):1681–1691, 2003.

[216] R. Naumann, S. M. Schiller, F. Giess, B. Grohe, K. B. Hartman, I. Karcher, I. Koper, J. Lubben, K. Vasilev, and W. Knoll. Tethered lipid bilayers on ultraflat gold surfaces. *Langmuir*, 19(13):5435–5443, 2003.

[217] C. A. Maggi and T. W. Schwartz. The dual nature of the tachykinin NK1 receptor. *Trends Pharmacol Sci*, 18(10):351–5., 1997.

[218] K. Lundstrom, A. Vargas, and B. Allet. Functional activity of a biotinylated human neurokinin 1 receptor fusion expressed in the Semliki Forest virus system. *Biochem Biophys Res Commun*, 208(1):260–6, 1995.

[219] K. E. Mazina, C. D. Strader, and T. M. Fong. Expression and solubilization of a recombinant human neurokinin-1 receptor in insect cells. *J Recept Res*, 14(1):63–73, 1994.

[220] S. Sugio, A. Kashima, S. Mochizuki, M. Noda, and K. Kobayashi. Crystal structure of human serum albumin at 2.5 A resolution. *Protein Eng*, 12(6):439–46, 1999.

[221] T. P. Burghardt and D. Axelrod. Total internal reflection/fluorescence photobleaching recovery study of serum albumin adsorption dynamics. *Biophys J*, 33(3):455–67., 1981.

[222] B. K. Lok, Y. L. Cheng, and C. R. Robertson. Total internal-reflection fluorescence: A technique for examining interactions of macromolecules with solid-surfaces. *J Coll Interf Sci*, 91(1):87–103, 1983.

[223] M. A. Cascieri, A. M. Macleod, D. Underwood, L. L. Shiao, E. Ber, S. Sadowski, H. Yu, K. J. Merchant, C. J. Swain, C. D. Strader, and et al. Characterization of the interaction of N-acyl-L-tryptophan benzyl ester neurokinin antagonists with the human neurokinin-1 receptor. *J Biol Chem*, 269(9):6587–91, 1994.

[224] A. Chilkoti, B. L. Schwartz, R. D. Smith, C. J. Long, and P. S. Stayton. Engineered chimeric streptavidin tetramers as novel tools for bioseparations and drug delivery. *Biotechnology (N Y)*, 13(11):1198–1204., 1995.

[225] J. P. Kraehenbuhl and C. Bonnard. Purification and characterization of membrane proteins. *Methods Enzymol*, 184:629–41, 1990.

[226] L. Lensun, T. A. Smith, and M. L. Gee. Partial denaturation of silica-adsorbed bovine serum albumin determined by time-resolved evanescent wave-induced fluorescence spectroscopy. *Langmuir*, 18(25):9924–9931, 2002.

[227] E. A. Bayer, H. Ben-Hur, and M. Wilchek. Isolation and properties of streptavidin. *Methods Enzymol*, 184:80–9, 1990.

[228] L. Neumann, T. Wohland, R. J. Whelan, R. N. Zare, and B. K. Kobilka. Functional immobilization of a ligand-activated G protein-coupled receptor. *ChemBioChem*, 3(10):993–8, 2002.

[229] N-P Huang, J. Voros, S. M. De Paul, M. Textor, and N. D. Spencer. Biotin-derivatized poly(L-lysine)-g-poly(ethylene glycol): A novel polymeric interface for bioaffinity sensing. *Langmuir*, 18(1):220–230, 2002.

Acknowledgements

It is a great pleasure to thank the following persons:

First of all, Prof. Horst Vogel for giving me the opportunity to do this thesis in his laboratory, for advice and confidence. I enjoyed the independence he gave me to pursue my project.

I especially want to thank Jean-Manuel Segura, Karen Martinez, and Ruud Hovius for the many ideas and their support throughout my work and for always being around when mostly needed.

I thank Prof. Susanna Cotecchia, Prof. Kai Johnsson, Nathalie George, Silke Mark, Jean-Baptiste Perez, Valérie Jacquier, Paulina Izewska, Daniel Abankwa, Michael Prummer, Samuel Terrettaz, Horst Pick and Cédric Reymond for the collaboration and help in different projects of my thesis.

Mme Tabet for all the help with the administrative details.

All members of the group, former and present, for the nice atmosphere which made working in this institute a pleasure.

Last but not least, I want to thank my family for love, encouragement and support (especially Mia for helping me with some of the figures).

So long, and thanks for all ...

Curriculum Vitæ

Bruno H. Meyer

Born on May 26, 1972 in Zug, Switzerland

since 2000	PhD thesis under supervision of Prof. Horst Vogel at the Institute of Biomolecular Sciences of ETH Lausanne
1993 – 1999	Environmental Sciences ETH Zurich, Diploma work: Site-Directed Fluorescence Labelling of the Na^+-dependent citrate carrier of *Klebsiella pneumoniae*
1978 – 1992	Schools in Cham and Zug, Switzerland, Matura Type B